ENGINSOFT

Newsletter

Simulation Based Engineering & Sciences

Year 15 n°1 Spring 2018

The future development of regenerative life support systems for long space missions by Melissa Project

The Engineering simulation in Lovato Electric, leader in **low voltage electrical devices**

Improving the NVH performance of a **motorbike powertrain**

Optimized production process of a **supporting plate**

Effect of Ceramic Materials on Structural Analysis of **Ball Bearings**

Performance of **road side crash barrier** with regards to vehicle crashworthiness

FMI-enabled **digital twin** for co-design of production machines

Contents

Newsletter EnginSoft
Year 15 n°1 - Spring 2018

To receive a free copy of the next EnginSoft Newsletters, please contact our Marketing office at: info@enginsoft.it

EnginSoft S.p.A.
24126 BERGAMO c/o Parco Scientifico Tecnologico
Kilometro Rosso - Edificio A1, Via Stezzano 87
Tel. +39 035 368711 • Fax +39 0461 979215
50127 FIRENZE Via Panciatichi, 40
Tel. +39 055 4376113 • Fax +39 0461 979216
35129 PADOVA Via Giambellino, 7
Tel. +39 049 7705311 • Fax +39 0461 979217
72023 MESAGNE (BRINDISI) Via A. Murri, 2 - Z.I.
Tel. +39 0831 730194 • Fax +39 0461 979224
38123 TRENTO fraz. Mattarello - Via della Stazione, 27
Tel. +39 0461 915391 • Fax +39 0461 979201
10133 TORINO Corso Marconi, 10
Tel. +39 011 6525211 • Fax +39 0461 979218

www.enginsoft.it - www.enginsoft.com
e-mail: info@enginsoft.it

The EnginSoft Newsletter is a quarterly magazine published by EnginSoft SpA

COMPANY INTERESTS
EnginSoft GmbH - Germany
EnginSoft UK - United Kingdom
EnginSoft France - France
EnginSoft Nordic - Sweden
EnginSoft Turkey - Turkey
VSA-TTC3 - Germany
www.enginsoft.com

CONSORZIO TCN www.consorziotcn.it • www.improve.it
Cascade Technologies www.cascadetechnologies.com
Reactive Search www.reactive-search.com
SimNumerica www.simnumerica.it
M3E Mathematical Methods and Models for Engineering www.m3eweb.it

ASSOCIATION INTERESTS
NAFEMS International www.nafems.it • www.nafems.org
TechNet Alliance www.technet-alliance.com

ADVERTISEMENT
For advertising opportunities, please contact our Marketing office at: l.cunico@enginsoft.com

RESPONSIBLE DIRECTOR
Stefano Odorizzi
ART DIRECTOR
Luisa Cunico
PRINTING Grafiche Dalpiaz - Trento

Autorizzazione del Tribunale di Trento n° 1353 RS di data 2/4/2008

FLASH

Simulation Engineering is a marvellous field to be working in: it is the cutting edge that allows new products to not only open gaps in the market place but attack some of the world's biggest problems. However, we must remember that we "stand on the shoulder of giants" and we rest on no greater shoulder than nature itself. It is therefore no surprise that a whole field of Biomimicry has developed to "seek sustainable solutions to human challenges by emulating nature's time-tested patterns and strategies" (Biomimicry Institute). Whether this is a honeycomb structure or the Burdock like adhesion of Velcro, many of our problems are already resolved in nature. Such natural structures can be found in SACMI's optimised support plate on page 14 or Tata's Road Side crash barrier on page 25. While the ability to create these structures are demonstrated on page 52 through the power of additive manufacturing.

Biomimicry is exemplified on page 10 by our article on the European Space Agency's (ESA) project MELISSA, supported by EnginSoft. It aims to "develop a future regenerative life support system for long term human space missions" or more simply, it is seeks to replicate earth's sustainable ecosystem in the hostile environment of space.

With Biomimicry in mind, don't forget our 34th International CAE Conference and Exhibition 8th-9th October 2018, titled "Evolving Engineering Simulation: the Age of the Digital Twin". On this occasion we will be exploring how digital twins integrate artificial intelligence, machine learning and software analytics with data to create living digital simulation models that update and change as their physical counterparts change. The digital representation provides both the elements and the dynamics of how an Internet of Things device operates and lives throughout its life cycle.

With this pervasive and enriching perspective, our annual conference is evolving with the world out there!

Stefano Odorizzi, Editor in chief

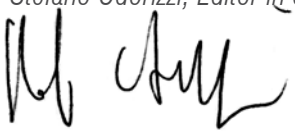

Interview with Mattia Capoferri, Electromechanical Products Designer at Lovato Electric

LOVATO Electric is one of the most important companies in the field of low voltage electrical devices. Born in 1922 in Bergamo (Italy), it has been managed by the Cacciavillani family for four generations. Almost a century of history has brought LOVATO Electric to be competitive in the distribution of electromechanical devices such as motor protection circuit breakers, contactors and switch disconnectors but also in the field of energy management, automation and control products like digital multimeters, automatic transfer switch controllers, engine and generators controllers. A worldwide distribution of the more than 10000 LOVATO Electric products is guaranteed by the 13 branches abroad and the 90 importers.

Ing. Mattia Capoferri, Electromechanical Products Designer at Lovato Electric

What is the value of your products perceived by your customers?

Behind all our products lays a solid proceeding: one of our points of strength is that everything is centered here in Bergamo, i.e. design, molding, testing, industrialization, quality dept. and production. A structure like this creates flexibility among the different departments, and allows the designers to have full control of the newborn device and all its components. This turns into the product strength and reliability that are perceived by all our customers.

What were the main reasons for introducing engineering simulation?

The constant growth of our catalogue has to fit in a very dynamic market scenario, and we must constantly be able to respond with effectiveness; this means focusing on investments that aim to reduce the time to market. In the past few years LOVATO Electric has been collaborating with EnginSoft for solving electromagnetic, kinematic and tolerance problems; the effective and helpful results obtained in these fields encouraged us to intensify our daily efforts in R&D activities. Together with the most modern rapid prototyping techniques we are now able to minimize the number of prototypes and the timing of the laboratory tests, straight reaching the best solution.

The first ANSYS software used in LOVATO Electric has been Maxwell3D, the most powerful tool for analyzing electromagnetic problems, an omnipresent physical phenomenon in all our products and deeply connected to the product performance.

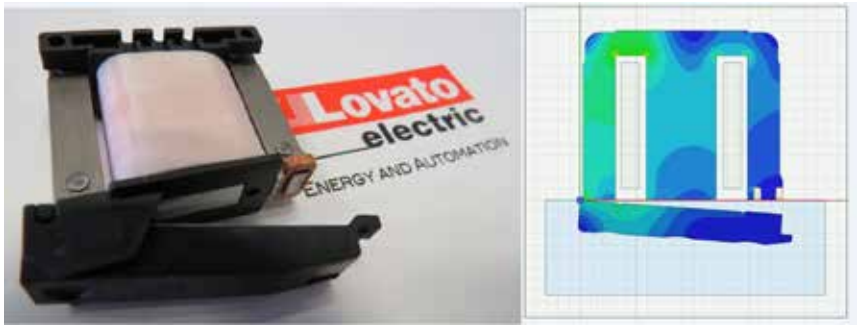

2D shunt trip release mobile and fixed core design and coil optimization; B field contours

What are the main goals reached thanks to engineering simulation?

Engineering simulation constantly travels alongside the product development process. Technically speaking, Maxwell has now made us confident in modeling the beating heart of our devices, i.e. electromagnets and coils used in contactors and motor protection circuit breakers, but also permanent magnets used in other products and also in our assembly lines. We are also developing new methodologies for the optimization of arc chambers trying to not directly model the electric arc behavior (as suggested by MHD formulations) but studying the distributions of the electric and magnetic fields, evaluating appropriate monitor quantities. With the correct inputs we are finding good matches with laboratory tests in terms of local wear: in this way we can understand a priori which configuration of arc chamber or shape of the splitting plates is going to be more efficient. One of the key improvement gained thanks to ANSYS Maxwell compared to our past approach is represented by the unsteady simulations: our operative characteristic time is of the order of the milliseconds, and now we are able to analyze in detail important phenomena of this time scale.

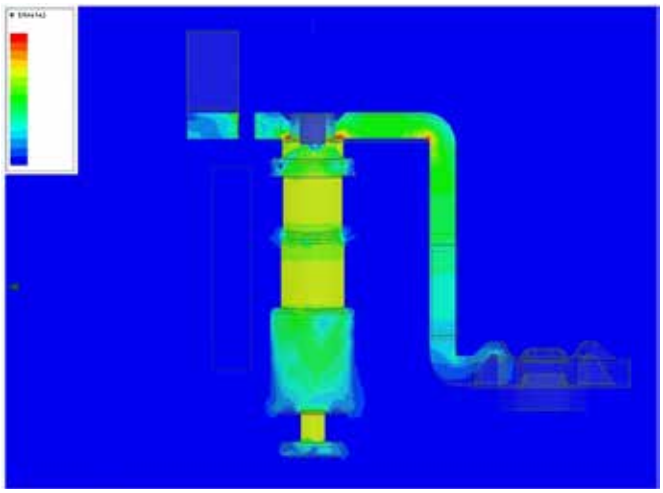

3D transient analysis of magnetotermic subassembly; B field contours

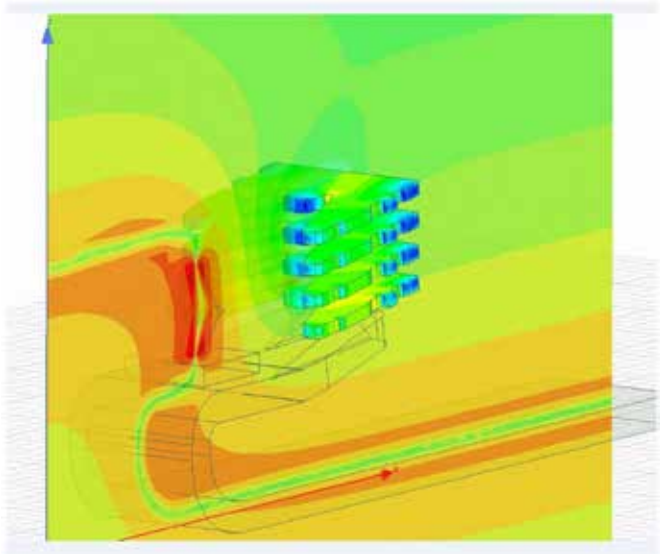

3D H and B field distribution on contacts and splitting plates in a low-voltage contactor

How do you apply engineering simulation to everyday product development?

In every new project simulation is getting an increasingly important role, and we feel confident in saying that some practices are destined to become company design standards; as a matter of fact we have some qualitative and quantitative practices depending on the design phase. We have positive feedbacks even for the process variables and lifecycle influence: our devices have to last several million cycles, during which performances drop must not occur; now, thanks to software like ANSYS Maxwell3D, we are able to simulate this long-term behavior. We have also planned to extend an internal collaboration with our lab from the perspective of spreading knowledge not only among designers and analysts.

What are your future plans for expanding the use of simulation in your Company?

We aim to a more extensive use of our current tools, enhancing the complexity of the today's model; for example we want to integrate and simulate the electronics used in some of our electromechanical devices – for example using Maxwell's Circuit Editor. This way we can handle different input signals and simulate their direct consequences on the mechanical behavior, saving also circuit boards prototyping. In parallel we are investigating other ANSYS software as well, extending our simulation power towards a multiphysical approach.

What is the added value that EnginSoft can bring to you?

We are very satisfied with the support provided by EnginSoft. For the electromagnetic CAE simulations we interface with EnginSoft offices in Florence, composed by valid people with years of experience in the electromagnetic field. The training has matched perfectly with our company's needs, and has been very effective. Anytime we need assistance, the answers are always quick and helpful. We firmly believe EnginSoft is a serious and professional partner, and we look forward to future collaborations.

Can you provide a short description of the CAE case study?

Several of our last products such as contactors, motor protection circuit breakers and shunt trip releases have all the electromagnetic components entirely designed in CAE environment. A good practice aims at an optimized geometry of the cores shape together with the winding parameters so as to guarantee the best performances of the device in terms of consumptions, heating, critical operative conditions dynamics and also costs. In order to do this we use fully parametrized models of AC/DC cores, coils and shading rings, monitoring in time dynamic and magnetic quantities using also the ANSYS Optimetrics package, that is a very powerful tool which allows us to handle every single variable of interest and study it with sensitivity analysis, DOEs and variable tuning. These methods ensure the complete understandings of the device reliability even in the most complex configurations even in the early phases of the project.

Improving the NVH performance of a motorbike powertrain

A CAE investigation of a motorbike showing an unsatisfactory NVH behavior during gear shifts: identification of the root causes and definition of the most effective design modifications

Piaggio Group is the largest European manufacturer of two-wheeled motor vehicles and the world's leaders in its sector. The Group is also a major international player in the commercial vehicle market. The product range includes scooters, motorcycles and mopeds from 50 to 1,400 cc marketed under the Piaggio, Vespa, Aprilia, Moto Guzzi, Gilera, Derbi and Scarabeo brands. The Group also operates in the light transport sector with its Ape, Porter and Quargo (Ape Truck) ranges of three- and four-wheel commercial vehicles.

The quest

The study's motivation was the assessment of the NVH behavior of a motorbike engine driveline, during its working condition, in first gear. More precisely, its behavior was considered in transient conditions during relative rotations between the first and fifth gear of the driven shaft. The study was carried out to investigate the possible causes of an undesired noise observed during road and lab tests and to identify the most effective design changes to remove it.

The solution

Physical evidence

Figure 1 shows the first and fifth gear, in the engaged condition.
The undesired noise was detected when the teeth hit the slot, during quick clutch engagement / disengagement cycles.

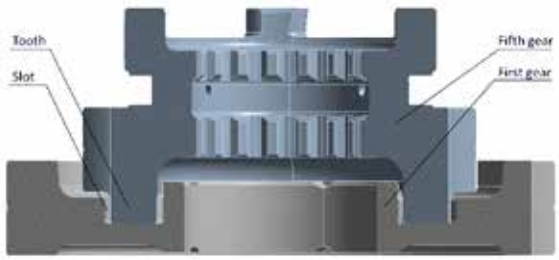

Figure 1 - Physical evidence, Engaged gears

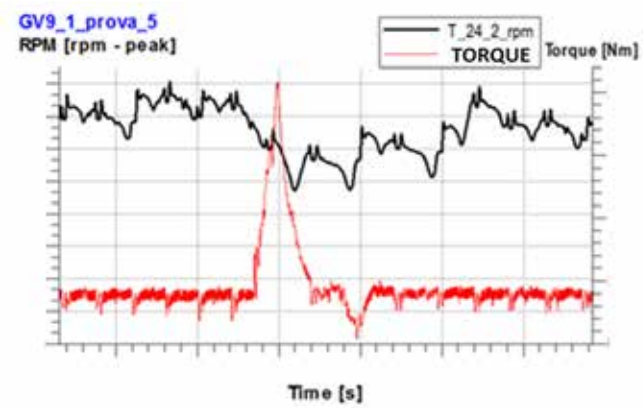

Figure 2 - Physical evidence, Torque transmitted by the driving shaft

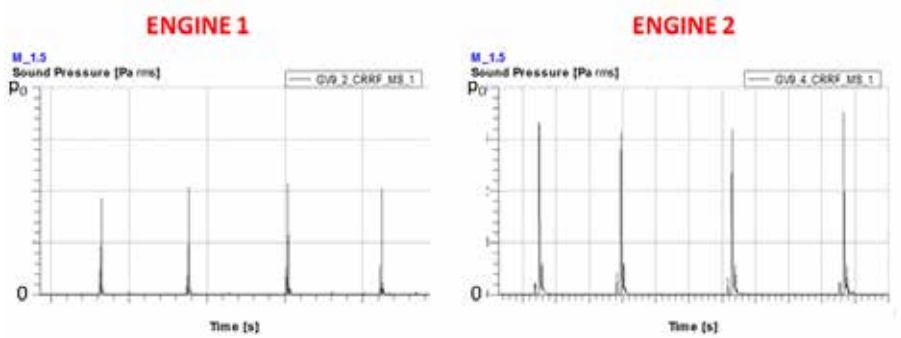

Figure 3 - Physical evidence, Comparison between two engines in terms of acoustic pressure

The phenomenon was measured in terms of acoustic pressure and of torque transmitted by a driving shaft included in the driveline. Figure 2 shows the torque time-history, which was used to validate the CAE model.

The engine under investigation ("Engine 2") was compared with another belonging to the same class, making the tooth repeatedly hit the slot. The acoustic pressure levels were measured, as shown in figure 3.

One of the main differences between the two engines is the driving shaft, which has different geometries in the two cases. Its effect was simulated by an MBS model of the powertrain.

While comparing the two engines, frequency analyses were carried out, which showed that the engine under investigation emitted noise mainly in the [300;5000] Hz.

This circumstance was taken into account to set up an FEM modal analysis of the bodies which form the engine casing; the analysis was carried out to find the cause of the worse acoustic performance of the engine under investigation, when compared with the other engine of the same class ("Engine 1").

Modelling remarks

The acoustic disturbance is the product of a sequence of causes and effects, roughly described as follows:

- the fifth gear teeth hit the slots, impulsively introducing mechanical energy into the system;
- the engine casing vibrates due to the action of the mechanical input; being the latter impulsive, all the eigenmodes can be excited; in fact, the acoustic emission interval is limited;
- the engine casing's surface velocity field, induced by the above mentioned phenomenon, is the acoustic source for the perceived disturbance, which is of course determined by the propagation through the air too.

This study covers the first two points only, by means of CAE techniques. The first point was tackled with a multibody model of the whole powertrain system, which was used to study the effects of design variants both at a component (driven fifth gear, driving shaft) and at a subsystem level (adoption of a cam coupler).

The second point was tackled with FEM modal analyses, whose results were coupled with the ISO equal loudness curves.

Multibody analysis

The model included the whole powertrain system and a dummy body, rotating around the rear wheel axis, which was used to take into account the inertial properties of the remaining part of the vehicle. The model is shown in figure 4.

On the clutch shaft, the cam coupler is visible. This subsystem was deactivated to simulate the engine's behavior in the measured configuration (see Figure 3, Engine 2); it was subsequently re-activated to measure its NVH effect.

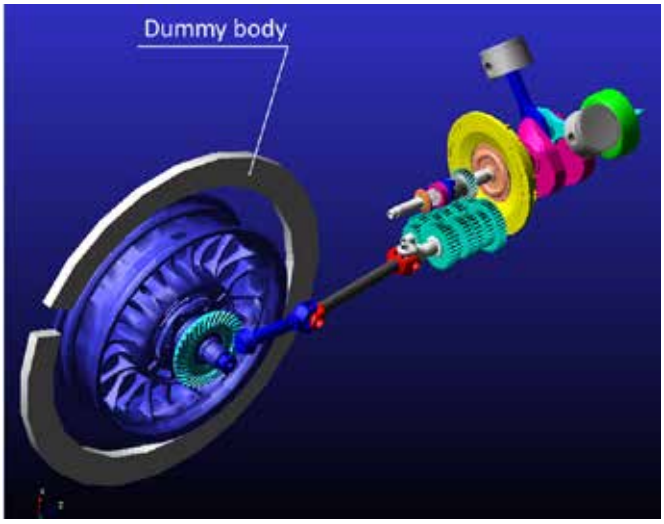

Figure 4 - Modelling remarks. Multibody analysis. The model

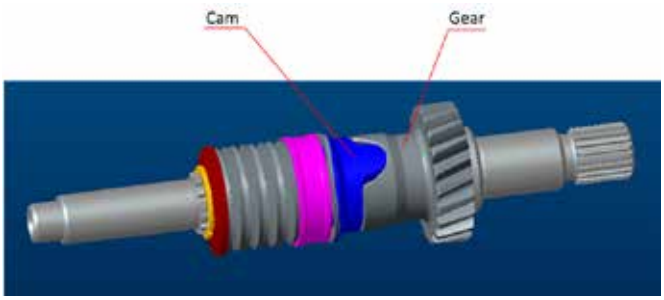

Figure 5 - Modelling remarks. Multibody analysis. Cam coupler. Interacting bodies

Clutch flexible coupler

The clutch includes a flexible coupler: a nonlinear flexible element was introduced into the model to simulate this effect.

Cam coupler

When the cam coupler (see figure 4) was activated, the interaction was modelled between the bodies shown in figure 5.

Rear wheel axle damper

A set of rubber dampers is used on the rear wheel axle.

Tyre

A tyre was introduced between the rear wheel and the dummy body (see figure 4).

Dummy body

The dummy body to simulate the remainder of the vehicle was given equivalent inertia and null mass.

Engagement between driven first and fifth gears

The description of the impacts between the two driven gears was detailed because these events trigger the cause-effect chain which determines the system's NVH behavior (see par. Modelling Remarks).
The multibody code computed the relative rotation between the two gears, starting from the configuration shown in figure 6.

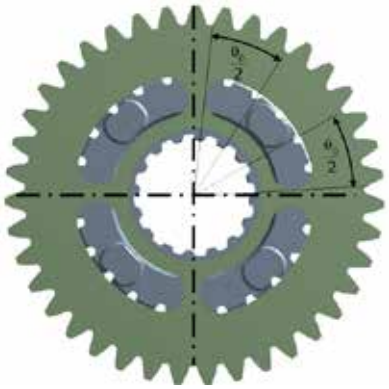

Figure 6: Modelling remarks. Multibody analysis. Engagement between driven first and fifth gears. Initial configuration

Connection between the crankshaft and the clutch shaft

Figure 7 shows the crankshaft and the clutch shaft of the multibody model (see also figure 4).

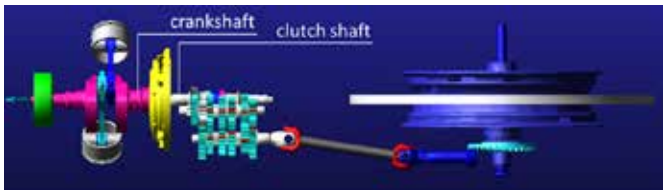

Figure 7 - Modelling remarks. Multibody analysis. Connection between the crankshaft and the clutch shaft. The crankshaft and the clutch shaft

A $\Delta(t)$ function was defined, which managed the behavior of the interface between the crankshaft and the clutch shaft:

$\Delta = 0$ - connected shafts
$\Delta = 1$ - disconnected shafts

Changing Δ between these two levels, it was possible to simulate nearly-impulsive clutch engagements, which were used during the physical tests to trigger the acoustic disturbance (see par. Physical evidence).

FEM analysis

As mentioned in par. Physical evidence, the FEM analysis' objective was to single out the eigenmodes of the engine under investigation ("Engine 2") in the frequency range which contains the significant part of the acoustic emission spectrum. The analysis was carried out to compare Engine 2 with another one ("Engine 1"), which showed a better acoustic performance.

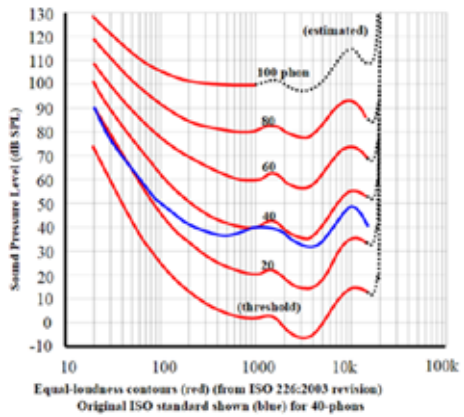

Figure 8 - Modelling remarks. FEM analysis. Equal-loudness curves

The modal data were combined with the equal-loudness curves, contained in the ISO 226:2003 standard.
The term "loudness" is used as an indicator of the perceived acoustic disturbance and its unit is the "phon". The curves in figure 8 show the points with equal loudness as a function of the frequency. For instance, the same loudness is felt listening to a 61 dB sound at 100 Hz and to a 40 dB sound at 1000 Hz.
The 40 phon curve was used to compare Engine #2 and Engine #1 (see par. Physical evidence); its ordinate was named δ and its abscissa ε.
The eignefrequencies have been classified as primary, secondary and negligible based on physical criteria that have been on purpose defined (for istance, a negligible eigenvalue has significant displacement components along neither the y nor the z direction in the standard vehicle reference frame).
The i-th primary eigenfrequency of each analyzed system was named p_i.
The i-th secondary eigenfrequency of each analyzed system was named s_i.
The following loudness indexes were defined:

$$\text{Primary index} \equiv \Gamma_p = \sum_i \frac{1}{\delta(p_i)}$$

$$\text{Secondary index} \equiv \Gamma_s = \sum_i \frac{1}{\delta(p_i)} + \sum_i \frac{1}{\delta(s_i)}$$

It's apparent how lower indexes are associated with better NVH performances in terms of acoustic source (see par. Modelling remarks).

Boundary and initial conditions

Multibody analysis

The system shown in figure 4 was excited applying the gas forces in the combustion chambers as a function of the crank angle.
Another design parameter taken into account was the shape of the driving shaft. The engine under investigation (Engine 2 in par. Physical evidence) has a driving shaft with a hollow cross section; during the experimental tests, it was compared with another engine (Engine 1 in par. Physical evidence), which has a driving shaft with a solid cross section. Thus, the effect of the adoption of a driving shaft with a solid cross section in Engine 2 was simulated. Two values of θ_0 (see figure 6) were taken into account, θ_{LOWER} and θ_{UPPER}: shifting from θ_{UPPER} to θ_{LOWER} had been proposed by the Design Department. Different sets of experimental tests have been considered: the engine speed was ω_1 during the first set and ω_2 during the second set.
The whole simulation set is shown in the table 1.
These simulations were aimed at evaluating the effect on the acoustic disturbance of the following design variants:
circumferential gap between the fifth gear teeth and the first gear slots (see figure 6): simulation #1 vs simulation #2 and simulations #3 vs simulation #4;
adoption of the cam coupler: simulation #3 vs simulation #5;
cross section of the driving shaft: simulation #4 vs simulation #6 and simulation #5 vs simulation #7.

Simulation #	Θ_0	Engine speed	Driving shaft's cross section	Cam coupler (see figure 5)
1	Θ_{UPPER}	ω_1	Hollow	Inactive
2	Θ_{LOWER}	ω_1	Hollow	Inactive
3	Θ_{UPPER}	ω_2	Hollow	Inactive
4	Θ_{LOWER}	ω_2	Hollow	Inactive
5	Θ_{UPPER}	ω_2	Hollow	Active
6	Θ_{UPPER}	ω_2	Solid	Inactive
7	ΘU_{PPER}	ω_2	Solid	Active

Table1 - Boundary and initial conditions. Multibody analysis. Simulated configurations

FEM analysis

The modal analyses of the engine casing were carried out in free conditions.

Results

Multibody analysis - Comparison with test data

The comparison was made to validate the model. It was made in terms of the torque transmitted by the driving shaft (see par. Physical evidence, figure 2) using the powertrain configuration #4 (see table 1), which was used during the experimental tests. In figure 9 the red curves show the torque time-histories.

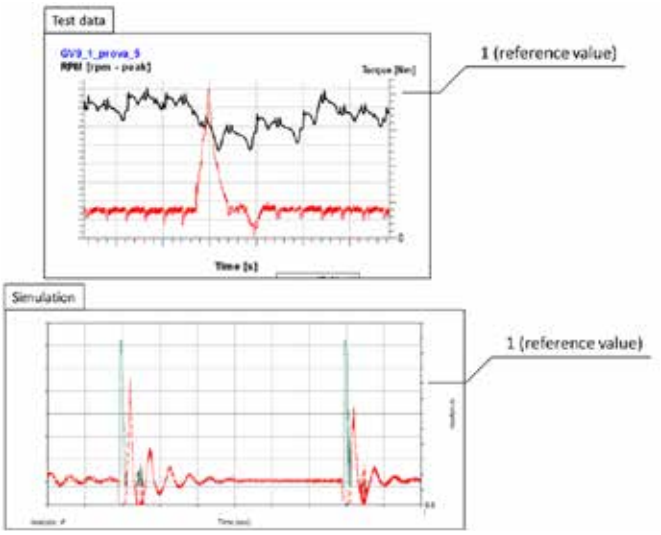

Figure 9 - Results. Multibody analysis. Comparison with the test data. Torque time-histories

Figure 9 shows that the maximum torque value in the test data is comparable with the one coming from the simulation model, which was therefore considered able to represent the physical phenomena the investigation had to deal with.

Comparison index

The simulated configurations (see table 1) were compared in terms of the RMS value η of the torque transmitted by the driving shaft.

As a result of the simulations, the most effective variants were the reduced tooth/slot gap and the simultaneous adoption of the solid cross section and of the cam coupler.

The better driveline performance with a drive shaft's solid cross section is in accordance with the test data shown in figure 3.

FEM analysis

Figure 10 shows the SPL values on the 40 phon curve at the primary and secondary eigenfrequencies for both engines which were taken into account (see par. FEM analysis of the Solution section); as mentioned, the engine under investigation is named "Engine 2" and it was compared with a similar one, named "Engine 1".

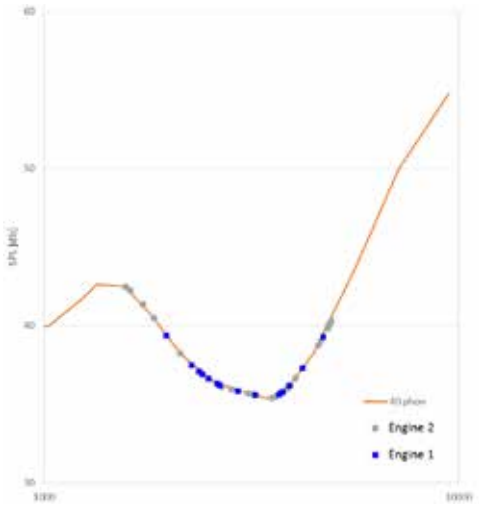

Figure 40 - Results. FEM analysis. Equal loudness curve

The overall loudness index is shown in the table 2 for each engine.

Index [1/dB]			
Secondary index		Primary index	
Engine 2	Engine 1	Engine 2	Engine 1
0.606	0.408	0.335	0.247

Table 2 - Results. FEM analysis. Overall loudness index

When the mechanical excitation (tooth/slot impacts) is the same, Engine 2 is therefore louder, as shown by the test data (see figure 3).

Conclusions

A motorbike engine had shown unsatisfactory NVH behaviour during gear shifts.

The impacts between gears was singled out as the cause.

A CAE campaign was carried out to assess the effectiveness of design variants devised to reduce the mechanical excitation due to the impacts between the gears and to analyse the behaviour of the engine casing, whose vibrations are the acoustic source.

The CAE results showed that following design variants are the most effective in terms of mechanical excitation for the powertrain system:

- reduction of the circumferential gap between the gears' teeth and the slots;
- adoption of different driving shaft's cross section and of a cam coupler.

The behaviour of the engine casing as an acoustic source was quantified by a loudness index related to the casing's eigenmodes. A comparison between different engines based on that index matched test data.

Riccardo Testi - Piaggio & C.

EnginSoft in the **ESA MELiSSA program**

EnginSoft has a long standing collaboration with ESA in the MELiSSA program. The projects developed by Enginsoft during the past 10 years are listed below:

- ALISSE - Advanced Life Support System Evaluator
- FC1 - Food Characterization Phase 1, HVAC at MPP
- SCALING - Scaling of Life Support System
- GMSS - Greenhouse Module for Space system
- HYSSE - HYdroponic Sub System Engineering
- ENRUM - ENergy Resources Utilization Mapping
- ACSA - Air and Canopy Sub – compartment Analysis
- AtSSE - Atmospheric SubSystem Engineering
- MPP –CCN5 - Operation and integration of the MELiSSA Pilot plant
- PaCMan - PlAnt Characterization unit for closed life support system – engineering, MANufacturing & testing

EnginSoft is member of the MELiSSA consortium with Dr. Lorenzo Bucchieri and is actively working in life support systems for space applications.

The MELiSSA program was started to gain knowledge for the future development of regenerative life support systems for long space missions.

The MELiSSA framework is envisioned as a micro-organism and higher plants based ecosystem, which will allow the development of technologies required for future long-term human space flight. MELiSSA is based on an "aquatic" ecosystem consisting of five distinct sections, or compartments.

The five compartments (MELiSSA loop) are here described: the first section, called the liquefying or anoxygenic fermentation compartment, collects the non-edible output from the higher plants and micro-organisms as well as the waste from consumers (i.e. astronauts). Through anaerobic processes this waste is then transformed into useful compounds, such as ammonium and volatile fatty acids.

Nearly all of the output from compartment 1 is delivered to the second section for further processing by photoheterotrophic organisms. These organisms use fatty acids, alcohols and carbohydrates along with light to produce food for the consumers. Some of the output from compartment 1, specifically the ammonium and the minerals, are not affected by the processes in compartment 2 and are instead delivered to the third section, the nitrification compartment. Through oxidization processes the ammonium is turned into nitrates. Nitrates are highly favourable sources of nitrogen for higher plants, and are used in section 4, the photosynthesis compartment, along with the minerals produced in compartment 1, to produce the bulk of the edible output for compartment 5, the consumer (astronauts/crew).

In order to allow an engineering approach, this closed loop has been organized as an assembly of compartments characterized by specific subsystem processes. Among these, the sub-system mainly responsible of the production of the human metabolic consumables is the HPC in compartment 4.

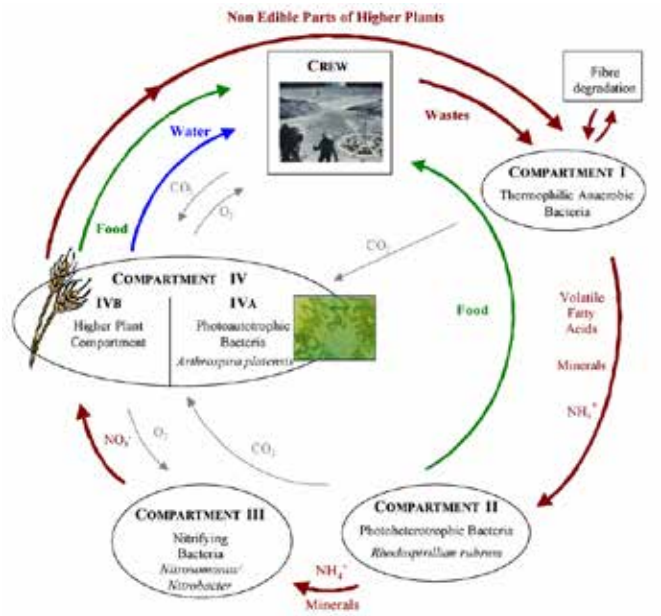

Fig. 1 - MELiSSA Loop diagram

In the framework of the MELiSSA ground system demonstration, the first objective is to demonstrate a regenerative system able to provide 100% oxygen, 100% water and 20% to 40% of the food necessary to sustain a team of rats (i.e. 1 man-equivalent). Today, the axenic microbial processes (e.g. CII, CIII, CIVa) have reached the sufficient maturity to enter in the integration phase, which is not the case of the HPC. Thus, the effort is made on this compartment.

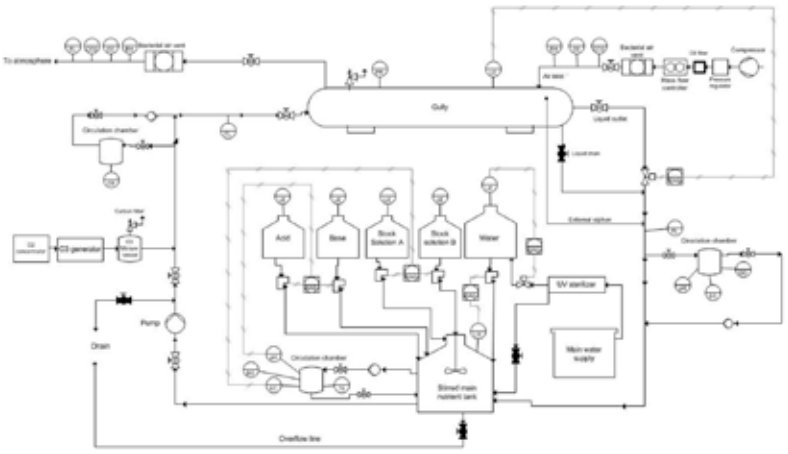

Fig. 2 - Hydroponic P&ID

PACMAN – Design Criteria

PaCMan – PIAnt Characterization unit for closed life support system – engineering, MANufacturing & testing is the newest project of a long standing collaboration between ESA and EnginSoft.

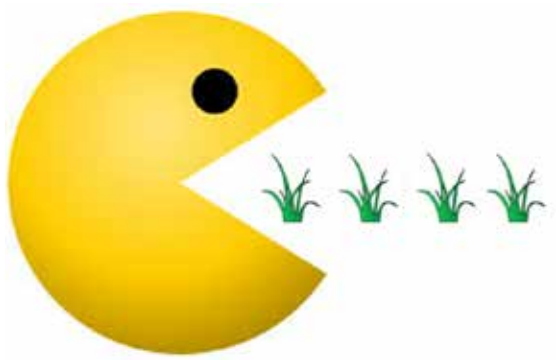

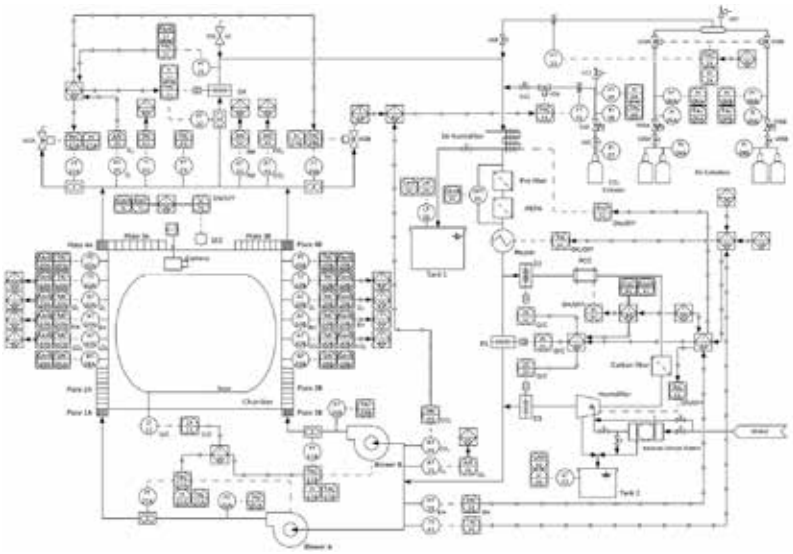

Fig. 3 - Atmospheric P&ID

The objective of the project is to design, build, assemble and test a prototype of a PCU (Plant Characterization Unit) which is conceived as a generic crop research facility and will be used extensively for scientific experiments on crop growth tests. The PCU will therefore have a design which will allow to test multi crop growth scenarios under different conditions in order to characterize the crop growth parameters. It will not be intended for food production, such units exist today (e.g., Thales) and are producing small quantities of food, however in these units it is not possible to measure the variables which are significant for plant growth, both in the root zone (rhizosphere) and aerial zone (chamber) in order to characterize the mechanistic model for plant growth.

This model has been theoretically developed by research institutions but needs several experiments to create a database which will validate and tune the model. Furthermore in the units existing today, mass balance in the rhizosphere and aerial zone cannot be discriminated since the two zones are not separate and the sub-systems are not leakage proof. Therefore it is not possible to measure exactly water production (i.e. water use efficiency), discriminating if it comes from the plants or it is just evaporation of the fluid of the hydroponic; it is difficult to measure oxygen production because of leakage, and overall the measurement system and analytics are not adequate for scientific purposes.

This project will develop a PCU with an atmospheric and Hydroponic unit with the following characteristics:

- No leakage in the PCU seen as a global system
- No leakage or mass exchange between the two sub-systems (aerial and hydroponic)
- Complete pressure management and control
- Fitting and operability of the hydroponic: cleaning disinfection
- Full control and homogeneity of environmental conditions
- Advanced measurement and monitoring system for the two separate units allowing mass balance on the atmospheric and hydroponic

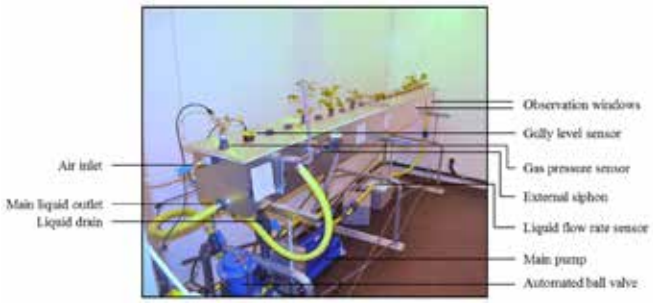

Fig. 4 - Testing of the hydroponic

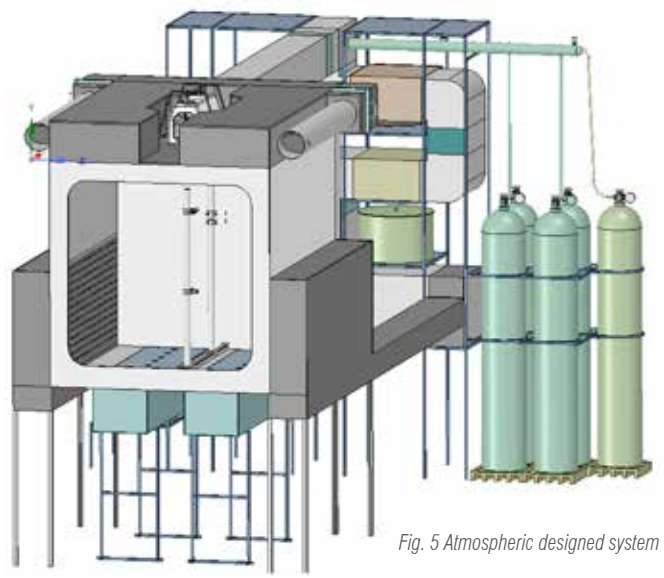

Fig. 5 Atmospheric designed system

Fig. 6 - Anti-leakage bulkhead connectors

Fig. 7 - Anti-leakage fully bolted, gasketed joints

Fig. 8 - Anti-leakage inflatable seals

The developed PCU will therefore need a design to interface the hydroponic and the aerial chamber, which will have the conflicting objective of anti-leakage, mounting operability and harvest as well as disinfection procedures.
Furthermore the engineered design will need to take into account that such units will need to be transported from the assembly workshop to the testing plant (universities in the MELiSSA consortium for example) and in future these units must be able to be transported from one lab facility to the other, thus assembly and disassembly, transportation and start-up will be taken into account in the design phase.
Following assembly, this first unit (considered a prototype) will go through functional tests mainly to verify that there is no leakage of water or gases out of the PCU or between the aerial and hydroponic subsystems inside the PCU so to be able to verify mass balances with respect to H_2O or CO_2. The functional tests will also verify the functionality of lights and filters, in addition to sensors, data acquisition system and control logic and thus the resulting composition of the atmosphere and the nutrient solution.
The anti-leakage property of the PCU and the possibility of doing mass balances with respect to water and gas will allow reliable measurements for scientific testing. Advanced monitoring of gas and liquid phase will allow further understanding of plant modelling. Homogeneous environmental conditions in hydroponic and chamber will be guaranteed. Its reduced size will help operability and functional tests with fast turnaround times. Future multiple facilities will allow parallel crop testing with different scenarios, allowing a reduction of time elapsed for trade-off studies of crop growth, hence fulfilling the characterization objective.

PACMAN - Workflow

The project is basically divided into two major steps. A first engineering step and a second manufacturing, testing and life crop test step.
Initially the PCU requirements will be set in terms of the research scenario in which it will be employed, thus meaning cleaning, disinfection, start-up, research protocol execution and finalisation. Furthermore the PCU will need to satisfy ease of maintenance in terms of availability of spare parts over a period of several years, and to be able to sustain long periods of storage.
The research scope of the PCU implies the need to measure variables of interest for higher plant compartment mechanistic modelling. These variables will be defined and selected functionality will be implemented into the PCU after a trade-off considering the project resources. Special attention shall be put on variables, which have an impact on the design of the PCU and sub-systems. Several categories can be considered both for the atmospheric and hydroponic sub-systems:

- Higher plant model variables
- Physical variables
- Measured variables
  - o Simply sampled
  - o Monitored variables
  - o Actively controlled variables and quantities

A major activity will be dedicated to design architecture solutions at predesign level. Hence based on the scenario requirements and variable hierarchy previously defined, a preliminary design with trade-off criteria which shall include manufacturability, failure tolerance, transportation issues and cost (construction and commissioning) will be proposed and engineered. Furthermore a pressure management control system will be developed in order to maintain correct pressure gradients, avoiding leakage.

At this stage, instruments and control system will be defined and selected including the on-line detection of chemical compounds. The control system will control the hydroponic sub-system as well as the atmospheric sub-system. It will define hardware and software as well as develop control laws relative to:

- Data acquisition system
- Controller
- Human machine interface

Furthermore a preliminary design will define, based on the architecture chosen, trade-off on the commercial equipment (e.g. filters, fans, condensers, pumps, valves) and propose the necessary analyses to address specific issues, such as for instance fluidic and mechanical internal interfaces as well as external interfaces.
Finally the preliminary design with trade-off criteria, a developed control system, a preliminary procurement plan and results of sensor testing, will be discussed with the Agency in order to converge towards a final design for the detailed design phase.

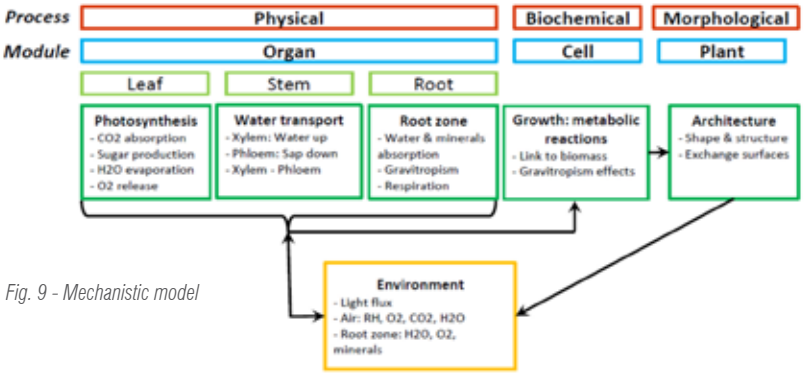

Fig. 9 - Mechanistic model


Fig. 10 - Mars Greenhouse (courtesy of NASA)

The final design will be developed with the aim to supply all necessary information for the manufacturing phase. The engineering activity will select and document all hardware and instrumentation (e.g., user manual, calibration data, materials list, components list) for further assembly and testing. A mathematical CFD model will be developed in order to predict the performance of the PCU. Particular attention shall be put on the system pressure management and internal fluid exchanges between the main sub-systems (i.e. hydroponic sub-system and atmospheric sub-system) thus controlling the pressure gradient of the whole system. Clear demonstration of the possibility to perform mass balance on the gas phase of each sub-system individually will be provided.
The final design will be reviewed based on:

- PCU detailed definition and justification of the design, including P&ID, mathematical models (e.g. CFD, control model), analysis results, breadboard test results, CAD drawings, bill of materials, commercial equipment/component list, interfaces description
- Preliminary manual of operations
- Preliminary test plan, including functional verifications, site acceptance tests, experimental tests verifying the requirements defined in Task 1, as well as associated procedures
- Procurement plan

The project will then enter its second stage.

The PCU will be manufactured and assembled, including the control system.
Before shipment to the lab, the PCU will go through a test phase WP5000 is necessary to demonstrate the full functionality of the PCU before disassembly, shipment to and commissioning in the Lab facility.
Functional test phase will require:

- Functional test plan and test procedures
- Functional test performances
- Functional test results evaluation

The PCU originally constructed, shall be partially disassembled and prepared for shipment to the lab facility. The shipment of the PCU will need to ensure its safe delivery, re-assembly, installation and verifications within the facility; hence a second functional test similar will define the full functionality of the PCU and its operational readiness.

Finally the prototype of this first PCU will be employed for life testing. The scenario is therefore to test the scientific equipment (PCU) with the final end user which will employ the PCU for its research purposes. A life test plan will be elaborated, defining the test procedures and procure the consumables necessary to validate the PCU design. The validation shall be performed over a full crop life cycle and shall include regular verifications of the level of microbial contamination. During the execution all raw data logs and "as-run" procedures shall be gathered. Finally an evaluation of the results with respect to the expected performances will be provided.
The results gathered in this final stage will allow to gain further knowledge in the mechanistic model of a plant and allow researchers to make a step further in life support systems for space exploration and a step further to the long term space missions such as mission to Mars.

For more information
Lorenzo Bucchieri - EnginSoft
l.bucchieri@enginsoft.com

Optimized production process of a supporting plate as an improvement of the product sustainability

The main goal of the described activity is the verification of an innovative production process of a steel supporting plate by using numerical simulation. The normal production process consists in different phases and processes: the laser cutting of blanks, welding, stress relieving, heat treatment and machining. The studied alternative is a sand casting process in order to obtain directly the final supporting plate. Numerical simulations were used to investigate the impact behavior of complex products in order to define the best production solution.
The new design chain represents an important simplification in order to reach a simpler, less expensive and more sustainable manufacturing process and to confirm these aspects a Life Cycle Assessment is done.

Introduction

The development of a new product is, nowadays, a multi-disciplinary work that involves structural and functional design, ergonomics, reliability, manufacturing process, quality control and assembly.
According to literature, all manufacturing process have two outputs: Geometry - macroscopic shape of the product - and Properties - all intrinsic material properties -. These two outputs completely define the performance of the product, and the design specifications that it must meet. All the manufacturing processes also involve the transformation of material from an initial condition, in term of geometry and properties, to the final needed outputs. This transformation is accomplished through the application (or removal) of energy and material. While historically the industry was focused only on the outputs and economic impact of the manufacturing process; today, the product sustainability of the production process and particularly the environmental impact is also considered.
In this project we describe, in an industrial example, a critical analysis of the Current Production, following called CP, of a steel supporting plate, the definition of an alternative production process, the simulation and optimization of the innovative process, the evaluation of the improvements in term of environmental impacts (LCA) of the proposed production process in comparison with CP.

Optimized component designs and casting processes using new engineering tools are achieved in concert with strong interactions from casting engineers and designers. This integration and human collaboration is critical for the successful speed-up of the design-process chain. Designers need strong support by casting experts to be able to take full advantage of casting performance, concerning its design and properties.
Quantitative results about casting performance provided by casting process simulation help designers to understand the impact of the process on the performance of castings in use.

Current geometry and CP description

The supporting plate is made by steel S235 JR (reference standard EN 10025-2:2014).

C% max	Si%	Mn% max	P% max	S% max	N% max	Cu% max
0,17	--	1,40	0,035	0,035	0,012	0,40
0,19	--	1,50	0,045	0,045	0,014	0,45

Table 1. Chemical composition of S235JR

The production process is constituted by 5 different steps:

- Cutting of the blanks
- Squaring and laser cutting
- Welding
- Stress relieving heat treatment
- Machining

The final component is in the Fig. 1.
The length of the welding perimeter is 30.25 m, while the component total weight is 515 kg.

Supporting plate: new geometry and new production process

The designers developed a new geometry of the plate, constituted by honeycomb structure optimized both for the final machining and the castability. The material as well has been changed moving from steel to a castable material with similar properties (gray iron). The casting process typically used for such a cast iron component is the sand casting. The weight of this component is around 625 kg (Fig. 2).

Fig. 1. Steel supporting plate

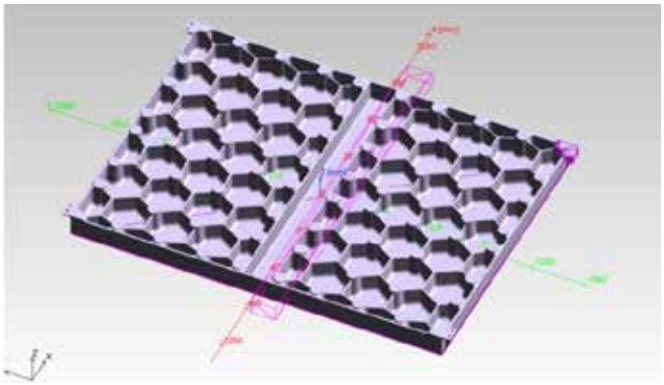

Fig. 2. New geometry of supporting plate

The optimization of the casting process to get the best component performances are done with MAGMA5 and its Optimizer.

Casting simulation is nowadays mandatory to get a reliable and robust process layout: gating, risering and chilling system. It also helps to predict metallurgy and melting practice, and offers predictions of indication like shrinkage or porosities, microstructure and mechanical properties.

Casting Process Analysis and Optimization

To simulate the casting process the geometry symmetry is considered: only one fourth of the component is simulated to speed up the optimization process.

The optimization process of a system takes into account the synergetic interaction between various parameters. A multi-objective optimization procedure returns trade-off solutions (good compromises in relation to various objectives). The optimization approach is based on automatized and parametric analysis and can reduce time-effort when many configurations and responses of a system need to be considered.

It is necessary to define parameters, objectives, constraints and responses to be monitored. The casting optimization was driven by the following aims:

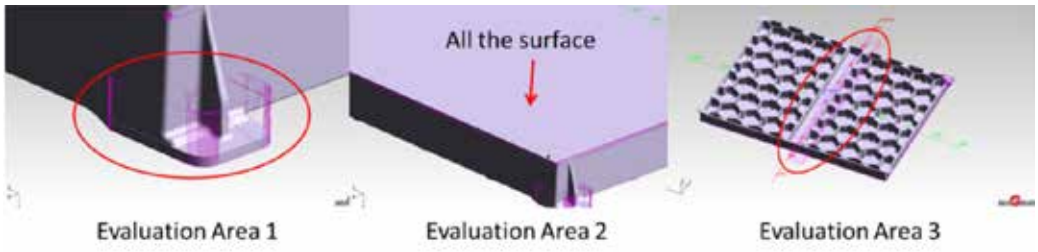

Fig. 3. Definition of the evaluation area

1. The reduction of component porosity under 10% in critical areas as the machined surface or where threated holes will be machined.
2. The minimization of the allowances, feeders and chillers used in the process to reach the maximum process efficiency.

Objectives and constraints have to be defined as follow:

- Objective 1: to minimize feeders and allowances volumes
- Objective 2: to minimize chiller volumes
- Constraint 1: maximum accepted porosity in the evaluation area 1=10%
- Constraint 2: maximum accepted porosity in the evaluation area 2=10%
- Constraint 3: maximum accepted porosity in the evaluation area 3= 10%

To define the DOE plan in order to find the optimized condition, the considered geometry input variables are:

- Diameter and height of feeders.
- Presence or absence of feeders.
- Diameter and height of chillers.
- Presence or absence of chillers. Height of allowances.

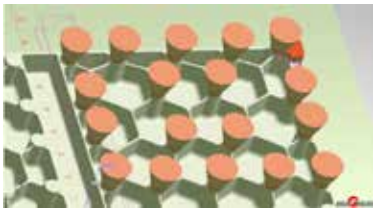

Feeder height and diameter variation

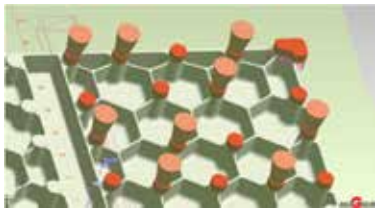

Feeder presence or absence

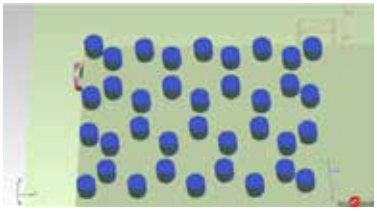

Feeder height and diameter variation

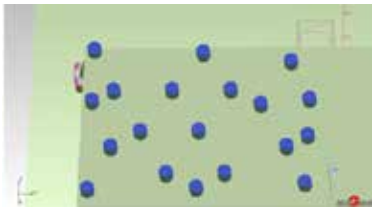

Feeder presence or absence

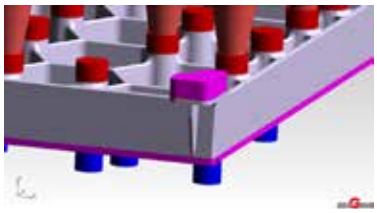

Feeder height and diameter variation

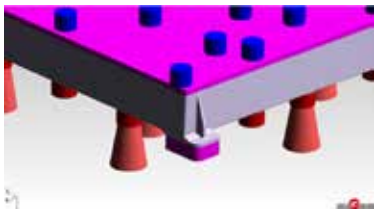

Feeder presence or absence

Fig. 4. Geometry input variations

A total of 42 independent variables were introduced in the optimization loop.
For the casting optimization a total of 1250 simulations have been done. The aim of the optimization study is the definition of the optimum casting layout generated by the DOE plan and the optimization algorithm in order to reach the objective 1 and 2 and taking into account the constraints 1, 2 and 3.

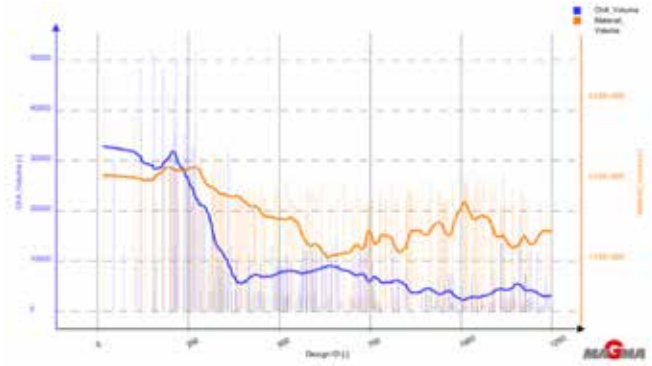

Fig. 5. Optimization history chart

In the diagram below the trend of the objectives versus the optimization run designs is defined.
The diagram shows the optimization convergence towards the reduction of both the objectives, guarantying low porosity (under 10%) in the evaluation areas.
The following 2d Scatter Chart shows the distribution of the designs vs defined objectives:

- Objective 1: to minimize feeders and extra metals volumes
- Objective 2: to minimize chiller volumes

The optimum design is the n.1106.

The 3d scatter chart shows the calculated designs vs the max porosities in the 3 different evaluation areas. The design 1106 (the optimum one) respects the constraints (porosity under 10%).
The optimum design solution has the following distribution and dimensions of feeders, chillers and allowances.

The map of porosity is analyzed in order to control the respect of the constraints (1,2 and 3): porosity value less than 10% in the evaluated areas for the optimum design.

Life Cycle Assessment: comparison between Normal Production and the casting process

Life Cycle Assessment is such a system analysis tool that can be used to assess the environmental aspects and potential impacts associated to a production system. LCA gives a holistic view of the impacts associated to a product system during:

- the whole span of life (from cradle to grave),
- from the raw material extraction through the production phase (cradle to gate)

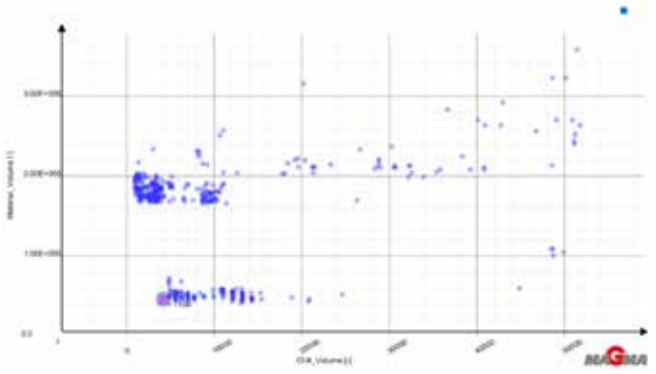

Fig. 6. 2d scatter chart

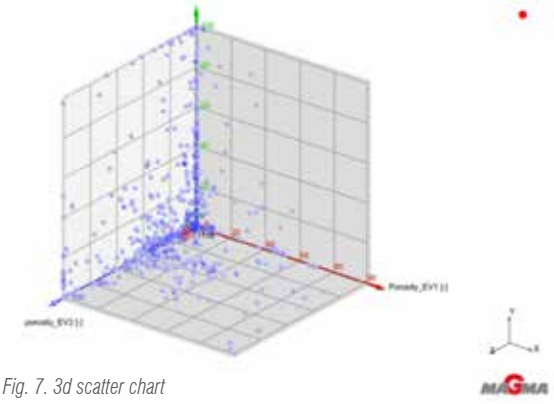

Fig. 7. 3d scatter chart

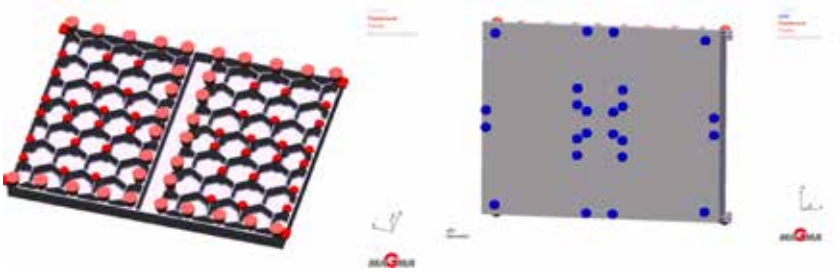

Fig. 8. Optimum design solution: feeders, allowances and chillers geometry definition

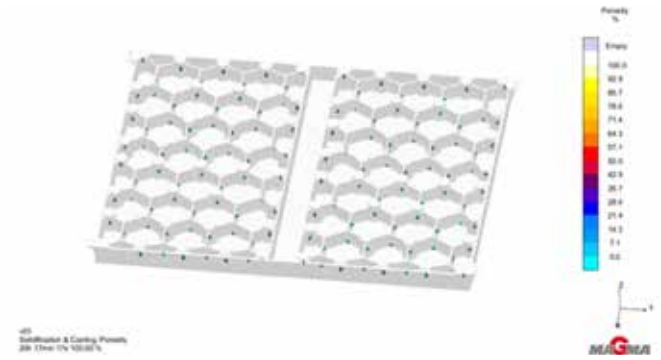

Fig. 9. Map of porosity for the optimum design component

- from the use and end-of-life phases (gate to grave) and includes the processes from the production phase only (gate to gate)

The main phases of an LCA are:
- Goal & Scope.
- Inventory Analysis.
- Impact Assessment.
- Interpretation.

The main environmental impact categories that are considered are:
- GLOBAL WARMING POTENTIAL (GWP), The Global Warming Potential (GWP) is the index that measures the warming grade of earth that is produced by the greenhouse gas and the unit of measure is kg CO_2 eq.
- ACIDIFICATION POTENTIAL (AP), the emission of NOx, SOx (from combustion of fuel) in atmosphere produces the reduction of pH in different ecosystems, with heavy consequences on organisms. The unit of measure is kg SO_2 eq.
- STRATOSPHERIC OZONE DEPLETION POTENTIAL (ODP), ozone is produced in the stratosphere and it is destroyed by different chemical reactions that transform it into molecular oxygen. ODP is the index that measures the ozone depletion and it is expressed in kg CFC-11 eq.

GaBi software is the life-cycle assessment modeling program produced by Thinkstep that EnginSoft has used in order to perform the LCA evaluation. The normal production of the steel supporting plate is constituted by several subsequent steps that are described in the table below.

The production process is constituted by 5 different steps:
- Cutting of the blanks
- Squaring and laser cutting
- Welding
- Stress relieving heat treatment
- Machining

A great simplification of the process is obtained applying the casting process, the final comment is obtained only with two steps: casting and machining (in order to eliminate the scraps). In order to make a comparison in terms of environmental impacts we can compare the consumed energy used for the Normal Production with the casting process. The length of the weld bead of the steel plate is 30,25 m and the energy necessary for the production of the welded and assembled plate is 10890MJ. To cast the steel plate the necessary energy is 2800MJ. The environmental impacts generated are proposed in the graph below.

Conclusions

The production of the steel supporting plate requests a complex process that is constituted by 5 different phases. The definition of a new geometry that can be obtained by a casting process generates a simplification of the process: only 2 steps are needed casting and machining. Thanks to the casting simulation and optimization, the production costs are reduced by 30% moving from steel welding to cast iron casting. The comparison of the LCA between the NP production and the casting process shows that the casting process is convenient also from an environmental point of view.

For more information: Giampietro Scarpa, EnginSoft
g.scarpa@enginsoft.com

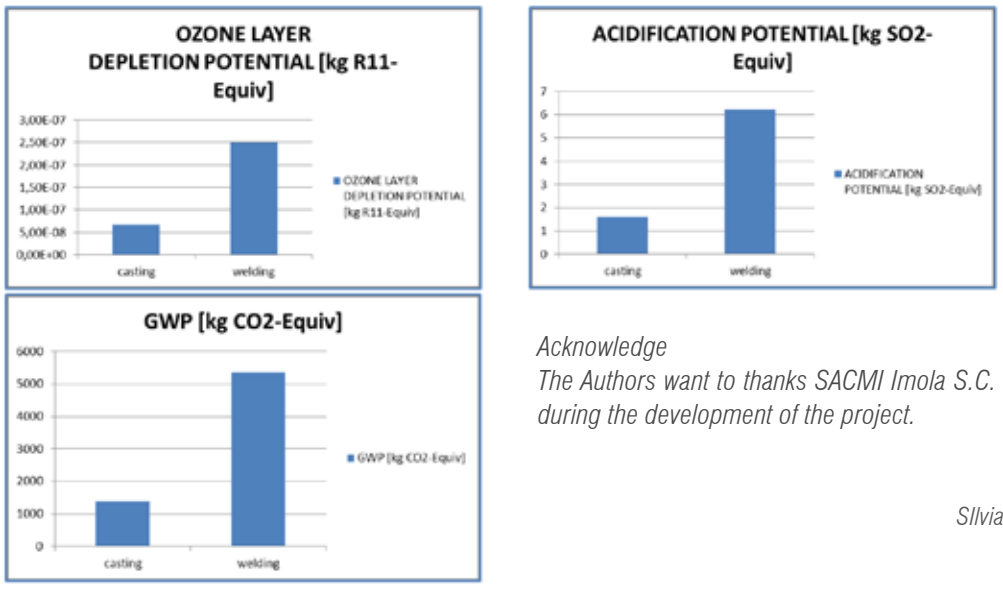

Fig. 10. Environmental impacts: comparison between Normal Production and Casting process

Acknowledge
The Authors want to thanks SACMI Imola S.C. and Enginsoft S.p.A. for the support during the development of the project.

Giacomo Bertuzzi - SACMI Imola
SIlvia Di Rosa, Giampietro Scarpa - EnginSoft

Investigating the Effect of Ceramic Materials on Structural Analysis of Ball Bearings

Structural analysis of ball bearing is done by ANSYS with using different materials in order to achieve contact pressure distribution. According to the reviews some studies were done to reach the motion, but the final displacement of ball bearing was about 6 degrees. The aim of this study is to reach the motion of ball bearing. Eventually results are obtained in 20 degrees' rotational displacement. The other aim of this study is to prove the better performance of hybrid bearings. Ceramic and steel materials are used in this study to reach this case.

Introduction

One of the most commonly used components that are used in industrial system are rolling contact bearings. They have the ability to facilitate the relative motion between two or more parts. In addition, the ability for supporting the various combinations of radial and axial loads can be mentioned as the advantages of rolling contact bearings. Bearings are usually consist of four main parts – a pair of concentric rings (the inner and outer races), rolling elements (spherical or cylindrical) and a cage or retainer as shown in Figure 1.1. Each ring is allowed to rotate while the other remains stationary.

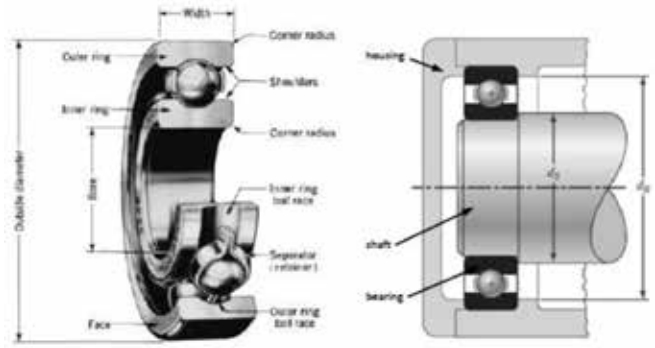

Figure 1: Single-row deep-groove ball bearing and schematic of bearing shaft assembly (Shigley, C. Mischke, Mechanical Engineering Design, McGraw Hill, 7th ed. 2003)

Contact Fatigue

Contact fatigue is a phenomenon that causes failure. This type of failure can also be found in gears, valves, and gear couplings. This phenomenon occurs in both metal alloys and ceramics.

The main difference between contact fatigue and classic structural fatigue is in the results from a contact or Hertzian stress state. Due to contact between curved surfaces, localized stress state appears. An apparent example for this phenomenon is a ball rolling over a race in a ball bearing. Motion of rolling element and contact geometry produces alternating subsurface shear stress. By continuing this motion, subsurface plastic strain builds up until a crack is generated. After the crack generated, it propagates until a pit is formed. After the surface becomes pity, the bearing starts to noisy and rough running. By continuing this situation, fracture of rolling element and catastrophic failure occurs. Fatigue spalling and high hoop stresses can cause fracture in races.

Material Evaluation

Some extensive research was carried out over recent years. Result of these works represent that silicon nitride as an extremely promising material can be used in fabricating all ceramic or hybrid steel/ceramic rolling contact bearings. Some advantages of silicon nitride over the traditional steel can be mentioned as (a) lower density, which reduces the dynamic loading at ball/raceway contacts in very high-speed applications. (b) can be used in severe lubrication and wear conditions, for example, they can respond to the requirements of short periods of oil-off operation in an aircraft engine. (c) Corrosion resistance and tolerance of contaminated lubricants.

With the advance of the space era, very demanding bearing operating conditions such as high vacuum ($<10-6$ Torr), extreme temperatures (e.g. $+230$ to -150°C), large temperature differentials, long life (both wear and fatigue life, usually 10–15 years without maintenance) and low frictional power are quite common. These ever increasingly

stringent demands present great challenges for those responsible for the development and validation of new rolling contact bearing materials.

Now, rolling bearings are made from high carbon, high chromium, and through-hardening bearing steel such as AISI 52100. For aerospace applications, they may be made from VIMVAR (vacuum induction melted-vacuum arc remelted) M50 tool steel, which can provide bearings with significantly improved fatigue and wear life. The reason of this improvement is because of lower oxygen and higher alloy contents. By considering the LP model, n = 9 assumed for single-row steel ball bearings, n =10 for single-row steel roller bearings and an average value of n = 16.1 is assumed for silicon nitride ball bearings.

Ceramic bearing design and design evaluation

As the property of silicon nitride and conventional bearing steels have huge differences, the current-used steel bearing internal geometrical parameters are not suitable for ceramic or hybrid bearings. The parameters can be considered as ball size and number, internal clearance and contact angle. In order to achieve high dynamic load capacity in steel bearings, larger diameter balls, high contact angle, and a close match between balls and raceways are used.

But in hybrid ceramic ball bearings, the direct substitution of silicon nitride balls into an proper steel bearing will result (for a given load) in a 14% higher Hertzian contact stress between balls and raceways, with a consequent reduction in the steel raceway L10 fatigue life, based on L–D theory, to about 30% of the maximum potential theoretical life.

Full scale ceramic bearing tests and field tests

Material properties, geometrical parameters and operating condition have widely effect on bearing performance and service life. According to the various studies, for a specific material and bearing geometry, full scale bearing bench tests are required to establish a database about the performance which can cover the typical operating conditions before putting a particular bearing type into practical use [6]. In order to establish exact statistical models, it is necessary to have full scale testing because variation in properties of current ceramic bearing materials in comparison to steel are more severe. Bench tests on ceramic bearings include evaluation of power loss, vibration, failure mode, heat generation. The process of endurance testing of ceramic bearings is time consuming and has usually scattered results.

Methodology

Modeling

Without considering the bearing clearance, the 3D finite element model of the 635-2RZ type of deep groove ball bearings is build. The bearing material chooses as structural steel. According to the dimensions, the model of the ball bearing is developed using SOLIDWORKS. It is imported into design modeler of ANSYS workbench 17. Due to geometrical situation, there are some limitations for each ball bearing. load ratings and limits are shown in Table 4.2.

The rolling bearings, which have the balls with different materials, have better performance in comparison with steel ball bearings. In this study, the material of balls is changed to observe the results. Mechanical properties of ceramic materials affect the performance of rolling bearing. Table 2,Table 3 and, Table 4 show the mechanical properties of used materials.

Serial No.	Parameters	Values	
Basic dynamic loading rating	C	2.3	kN
Basic static load rating	C0	0.95	kN
Fatigue load limit	Pu	0.04	kN
Reference speed	d1	80000	r/min
Limiting speed	D2	40000	r/min
Calculation factor	Kr	0.03	
Calculation factor	f0	13	

Table 1: Ball bearing calculation data

Serial No.	Material Properties	Si_3N_4
1	Density	3.20 gr/cm^3
2	Young's Modulus	300GPa
3	Bearing Strength	600 MPa
4	Poisson's ratio	0.26

Table 2: Mechanical Properties of Si_3N_4.

Serial No.	Material Properties	SiC
1	Density	3.10 gr/cm^3
2	Young's Modulus	330 GPa
3	Bearing Strength	450 MPa
4	Poisson's ratio	0.20

Table 3: Mechanical Properties of SiC.

Serial No.	Material Properties	Structural Steel
1	Density	7.85 gr/cm^3
2	Young's Modulus	200 GPa
3	Bearing Strength	2400 MPa
4	Poisson's ratio	0.3

Table 4: Mechanical Properties of Structural Steel.

Meshing

The mesh model of ball bearing is as shown in Figure 4.3. The maximum unit size of rolling body is 1mm and the minimum element size is 1.2605e-002 mm which is set in grid partition and carried on the adaptive sizing method. Automatic partition method is hex dominant. Finally, mesh produced a total of 211279 elements and 701168 nodes.

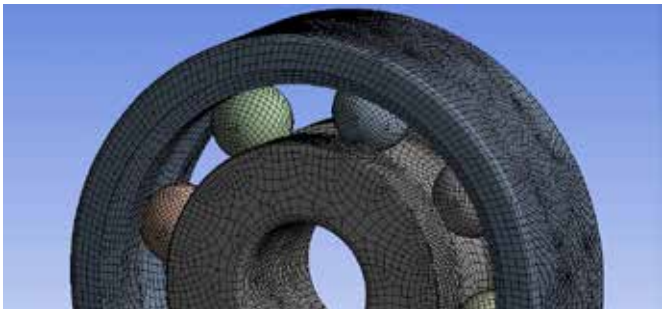

Figure 2: Mesh model of ball bearing

Contact Setup

The inner and outer raceway surfaces are chosen as target surface and correspondingly the surface of the ball was chosen as contact surface. It is necessary that to make sure the contact is rigid-flexible contact between rolling element and inner or outer ring, to choose CONTA174 as contact element type. The normal penalty stiffness (FKN) value of each contact pair was set to 0.1.

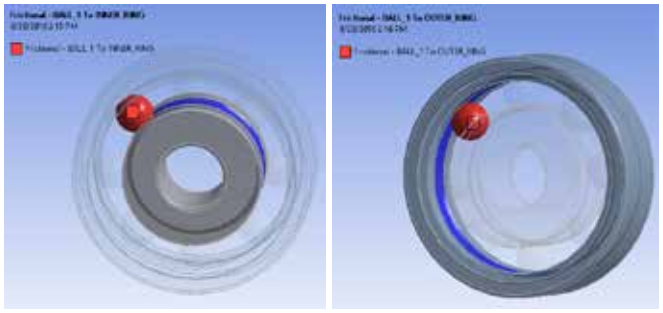

Figure 3: Contact Setup

Constraints and load applied

According to the actual working status of the bearing, constraints are applied on the outer circumferential surface to simulate the constraint of outer ring. Axial-constraint is applied on the inside and outside circumferential surface to simulate that the bearing cannot generate axial motion in the actual running process. Besides, the rolling body is constrained in axial and tangential directions and only allowed the radial elastic deformation, in order to prevent rigid body displacement in analysis. Load on the bearing includes the inertial load and displacement. Inertial load consists of gravity and rotational movement.

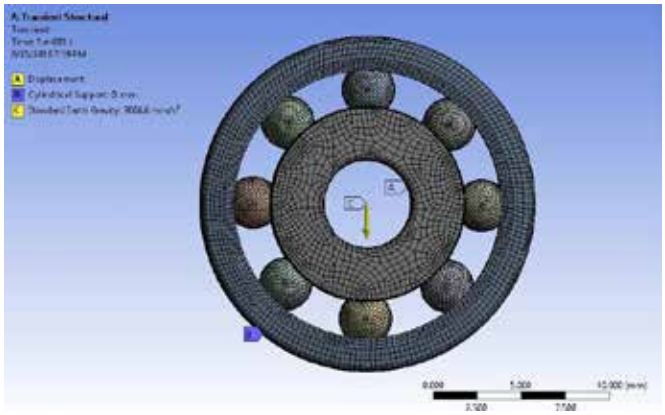

Figure 4: Constraints and boundary conditions

Analysis setting

In case of nonlinear simulation and due to contact formulation iterative solver type is selected. In addition, Newton-Raphson method is fully used.

Result and Discussion

Through the finite element simulation, contact stress and deformation distribution of the rolling elements and inner/outer raceway can be determined. Within displacement of 20 degrees with rotational speed of 860 rad/s, maximum contact stress of ball

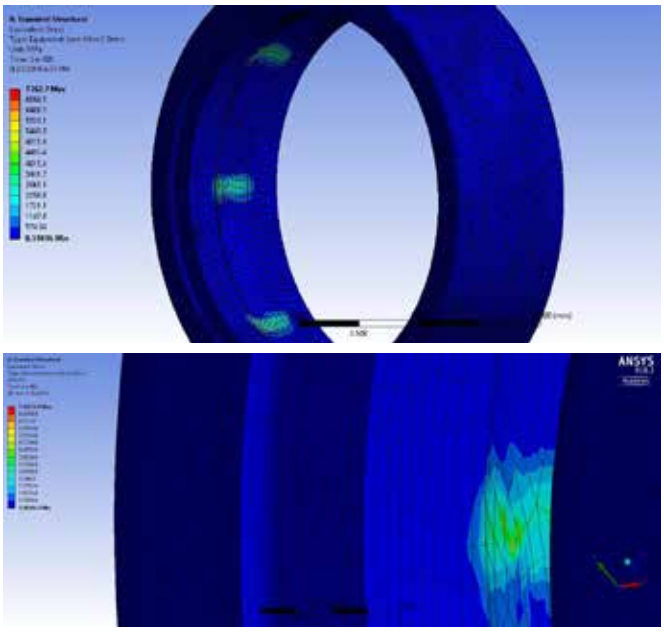

Figure 5: Equivalent Stress of outer ring (Structural Steel)

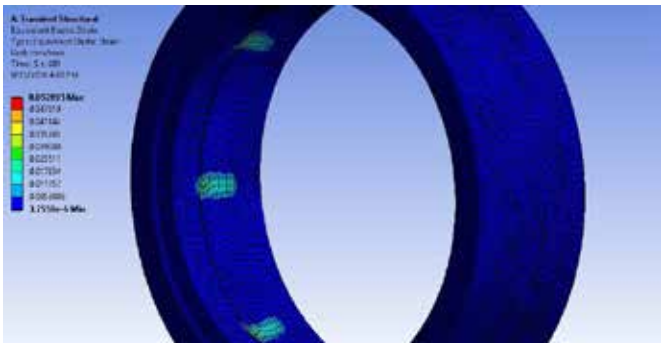

Figure 6: Equivalent Elastic Strain on outer raceway

bearing while using structural steel is 7200 MPa and maximum contact deformation is 0.15 mm. Due to geometrical complexities it was not possible to use rotational displacement as a factor of motion. After reviewing and analyzing, displacement is used for motion in cylindrical coordinates.

Maximum strain on outer raceway is about 0.052 mm/mm where the contacts occur. The Figure 6 shows the amount of strain in outer raceway.

The maximum stress and maximum strain results for balls are summarized in Table 5. The raceways were considered as structural steel and the balls material differ for each ball bearing.
The contact status changes during the simulation. Contact status affects the convergence directly. If the status changes to no contact, there would be some complexities due to convergence. On the other hand, if contact number increases, there would be too

Serial No.	Ball Material	Maximum Stress (MPa)	Maximum Strain (mm/mm)
1	Steel	2124.2	0.0099
2	Si3N4	1800.7	0.001
3	SiC	1653.9	0.00073

Table 5: Stress and Strain values for balls

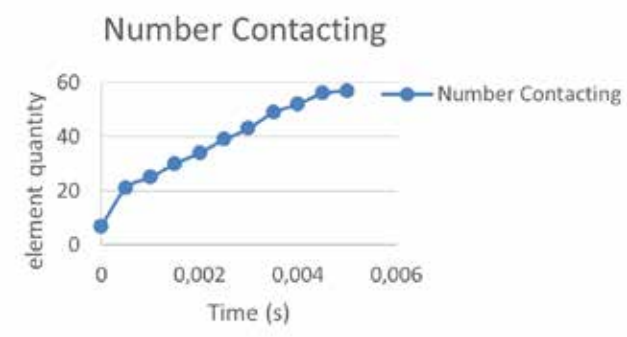

Figure 7: Contact Status

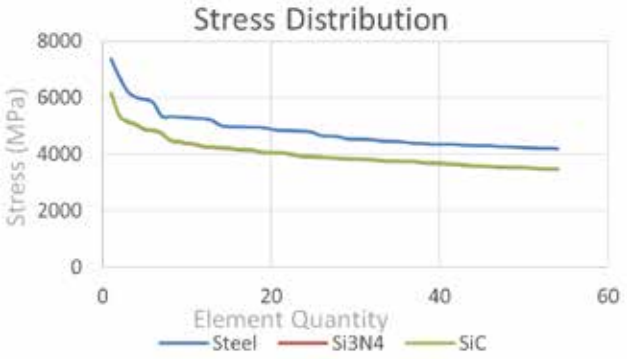

Figure 8: Stress Distribution

much penetration. This can cause difficulties in convergence too. The following graph shows the contact status during the simulation. The stress distribution was observed on all ball bearings. The Figure 8 shows the stress distribution via number of elements. In the Figure 8 the stress distribution in contact is shown.

Name	Number Contacting	Penetration (mm)	Geometric Penetration (mm)	Geometric Gap (mm)	Resulting Pinball (mm)
BALL_1 To INNER_RING	2	0	7.96E-05	1.70E-05	6.88E-02
BALL_1 To OUTER_RING	2	1.28E-15	1.50E-04	6.16E-06	6.88E-02
BALL_2 To INNER_RING	6	0	0	0	6.88E-02
BALL_2 To OUTER_RING	1	0	4.22E-05	2.07E-05	6.88E-02
BALL_3 To INNER_RING	2	0	0	0	6.88E-02
BALL_3 To OUTER_RING	4	0	0	0	6.88E-02
BALL_4 To INNER_RING	2	0	1.42E-05	1.59E-06	6.88E-02
BALL_4 To OUTER_RING	4	0	0	0	6.88E-02
BALL_6 To INNER_RING	11	8.93E-05	0	0	6.88E-02
BALL_6 To OUTER_RING	4	1.26E-15	0	0	6.88E-02
BALL_7 To INNER_RING	3	3.95E-05	3.95E-05	1.74E-06	6.88E-02
BALL_7 To OUTER_RING	14	7.88E-05	0	0	6.88E-02
BALL_8 To INNER_RING	4	6.26E-16	0	0	6.88E-02
BALL_8 To OUTER_RING	2	1.28E-15	0	0	6.88E-02
BALL_9 To INNER_RING	15	1.13E-04	1.35E-05	0	6.88E-02
BALL_9 To OUTER_RING	4	0	0	0	6.88E-02

The maximum stress occurs at contact region of ball_7 with inner ring. According to the Table 6 the initial penetration in contact of ball_7 with inner raceway is more than expected penetration.

Conclusions

Finite element analysis of a deep groove ball bearing is performed using ANSYS Workbench. According to the results, hybrid-rolling bearings can perform better than usual rolling bearing due to their mechanical properties such as Young's modulus. The higher the value of Young's modulus the more rigid the material is.

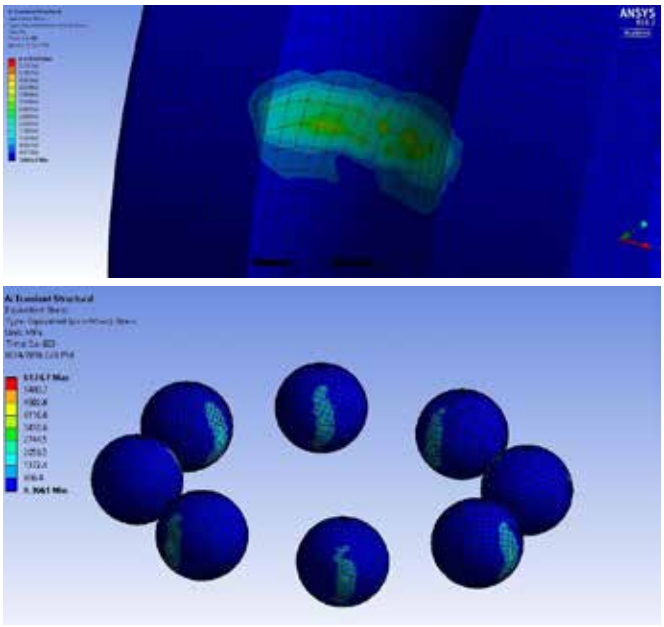

Figure 9: Equivalent Stress of outer ring and Balls (SiC)

The advantage of finite element method in calculation of contact stress distribution is that friction on the contact surface is considered. Thus, the results are expected to be more accurate than the Hertz theory. Maximum stress is observed at the outer surface of inner ring of ball bearing, Due to contact formulation and penetration of ball on raceway surface.
According to the different results obtained from the analysis, it is apparent that the Deformation and Elastic Strain induced in the SiC is less than the structural steel.

Sepehr Firouzi
Istanbul Technical University,
Department Of Mechanical Engineering,
Istanbul, Turkey

For more information:
Nasser Ghassembaglou, EnginSoft
n.ghassembaglou@enginsoft.com

Humble beginnings evolving into a highly functional equipment analysis and sizing tool

Good effort brings success or wisdom

PASS/EQUIP (previously known as PASSAT) is the pressure vessel stress analysis part of PASS (Piping and Equipment Analysis & Sizing Suite), offering smart simulation and sizing tools for every piping and equipment engineer/designer. When the development of PASS/EQUIP started 15 years ago, only specialists asked for such software and the potential market seemed to be small – mostly because the calculations, dictated by safety codes mainly based on thin shell theory, could be performed manually or in MS Excel.

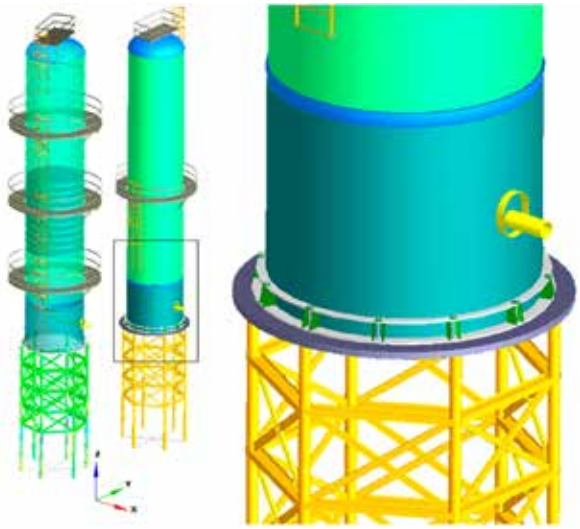

Figure 1. Column

One might think, creating a program to automate the manual or Excel calculations shouldn't be that difficult. But life had some surprises for us! As usually, when speaking with potential users the wish-list grew – fortunately for us, the number of interested users increased as well.

The development process turned out to be nonlinear. Ideas arising during the work, both from developers and users, have spawned parallel branches for the subsystems development and changed the product concept as well as approaches to the design of the user interface.

At first, it seemed that it was enough to implement calculation formulas for each type of element that makes up the vessel since the codes basically defined the requirements applicable to shells, heads, flanges, fasteners, supports, etc. separately. These formulas are mainly derived from the theory of shells and are suitable for manual calculations.

But for any column apparatus, a global analysis of complex distributed loads like wind or snow or seismic loads appeared to be required as this analysis is necessary to calculate natural frequencies. (For experts: PASS/EQUIP uses the general form of Rayleigh-Ritz method here.)

This forced our developers to understand how to correctly calculate an arbitrary construction without reducing it to a

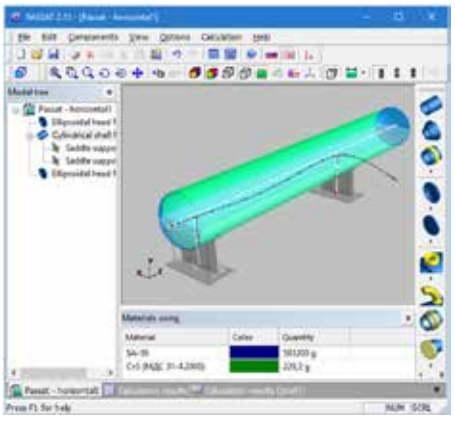

Figure 2. View of vessel model with the beam finite-elements

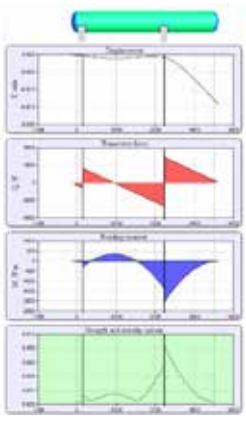

Figure 3. Report fragment with forces and moments

simplified model designed for manual calculation. So, a beam model appeared in the program to which the elements of the apparatus were "strung" on. The beam model was created as an integral part of the model, and therefore is present in all vessel types.

Hence, a natural step was to be used it in other calculations. It allows considering the influence of point and weight loads not only on the element the force is applied to, but also on the remaining elements. It helps determining the reactions in the supports, calculating the forces in the elements, determining the rigidity of the model and estimating movements, including cases of horizontal vessels with three or more supports where the task becomes statically indeterminate. For example, the program diagnoses the situation of tipping a vessel from its supports.

At the same time, an idea emerged to improve the user interface with a high-quality 3D view of the model. It was not necessary for setting the initial conditions and showing the results, but the idea radically affected the views of users and, subsequently, the program capabilities.

Users quickly concluded that (despite not being initially supported by the program's functionality) the program can be used to design a real vessel. Model creation was very simple and fast and the results looked very similar to models created in Autodesk Inventor and other mechanical CAD systems. Nothing could dissuade users when they tasted the charms of "quick vessel design". Of course, it was a computational model only, not intended for design and manufacturing purposes. But users insisted and developers did listen. As a result, the "truth of life" appeared in the form of a more detailed and realistic visualization as well as the means of exporting the model to various formats (CAD and others). Users eagerly look forward to the new features.

Of course, the developers could have known better. When a program for check calculations has some basic design functions, it starts to be considered as a design tool (the simplest example: the choice of the wall thickness from the pressure, and vice versa, the determination of the allowable thickness pressure at the stage of data input). Such "trifles" are dictated by practice, because they are convenient for the user. It turns out that they are useful in cases not predicted in advance. Thus, the development vector has changed: PASS/EQUIP is now a multipurpose product.

From the very beginning, the main ideology of the product was automation. The user only enters elements defined by their geometry and properties and then sets the loads and modes of operation. The desired calculations are done automatically. As output, a detailed report is produced with all intermediate calculations and a conclusion on the operability of the vessel. Any reasons for inoperability can easily be traced in the report.

This is very convenient for the user, but imposes serious obligations on the developer. Codes often require one to enter data that is not trivial. Sometimes the task is not trivial for a program, sometimes for a person, often for both. For example, in column apparatus analysis, calculating the support shell with holes requires to know the parameters of the weakest section. In typical cases a human may easily identify such section, but in the general case that can become very difficult. The program can do this automatically for any model.

Another example relates to the tube grids of a heat exchanger. It deals with the calculation of the maximum radius of a circle inscribed between the elements, i.e. tubes and shell. Mathematically this is the classical Problem of Apollonius. It is known that there are eight cases of the circles arrangement, producing different results. If three circles are known, the program must carry out topological analysis. Indeed, humans easily indicate them at the edge of the tube grid, however, the program requires a general algorithm. If the maximum circle is in the middle of the tube grid, one needs first to find these circles, which is difficult for a human. The computer does it better, but a preprocessing is required (for experts: the space dividing problem, for example by Delaunay criteria).

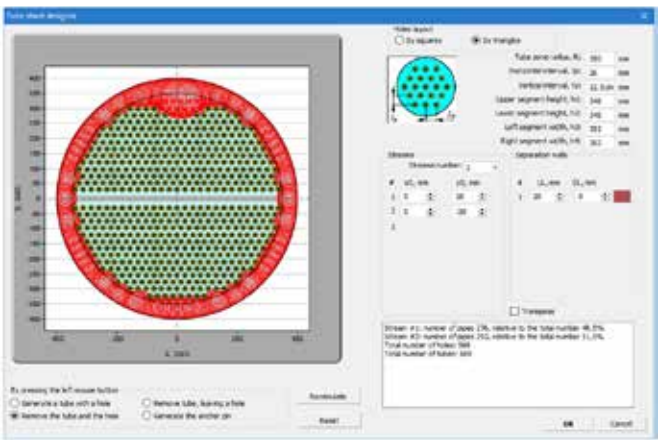

Figure 4. Tube sheet Designer

A lot of similar tasks are solved and implemented in the software. The user is not aware of them – he/she simply edits the parameters of the elements, changes the configuration of the tube grid in a special editor, moves the elements and so on.

The program is based on a powerful 3D modeling engine. It performs Boolean operations on elements to obtain the geometry required and calculates various characteristics such as areas, volumes, centers of mass and inertia.

As it can be seen above, the program now has gone far beyond the original idea of calculating individual elements according to the prescribed formulas from codes. Let's have a closer look at where we are today.

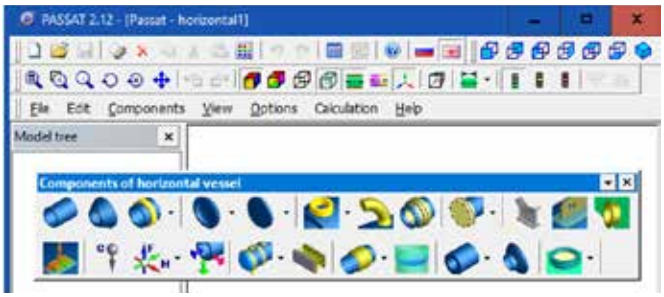

Figure 5. Elements Toolbox

To create a model of an arbitrary vessel in PASS/EQUIP a comprehensive set of elements is available. The main ones (not a complete list) are below:

- Cylindrical and conical shells
- Circular and oval nozzles (simple, inward, with reinforcement etc)
- Elliptical, semi-spherical, torispherical, with straight flange, flat with/without stiffening ribs

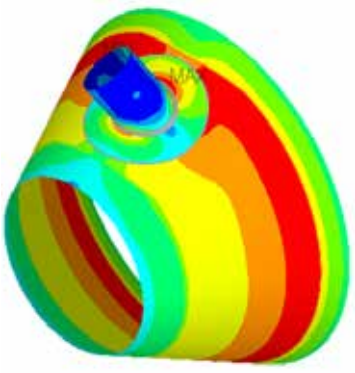

Figure 6. Nozzle-FEM

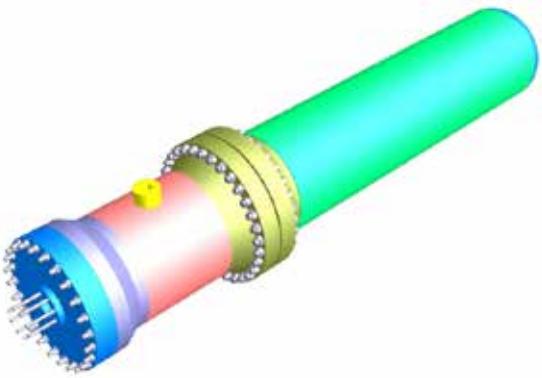

Figure 7. Reactor

- Trays, packings, ladders and service platforms for column vessels
- Supports for horizontal and vertical vessels, with/without reinforcement pads
- Supporting skirts, simple and complex (consists of cylindrical and conical sections)
- Supporting structures (pedestals)
- Flange joints
- Components of heat exchanger with fixed tube-sheets, with expanding boxes and bellows, with U-shaped tubes, with floating head

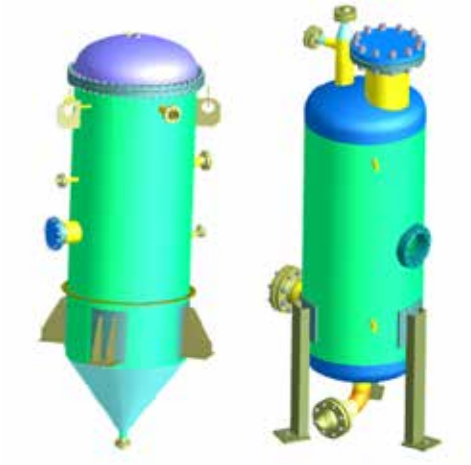

Figure 8. Vertical vessels

Calculations are performed according to various codes, the main ones being from the family of ASME VIII div.I, EN 13445-3, GOST R 52857. When possible, the program uses generalized calculation methods, such as the Rayleigh-Ritz method.

PASS/EQUIP has several configurations for different groups of applications:
PASS/EQUIP Vessel – Vessel and Column creation and analysis (seismic analysis included).
PASS/EQUIP Vessel & Exchanger – Vessel, Column plus Heat Exchanger creation and analysis (seismic analysis included).
PASS/EQUIP Tank – Vessel and Tank creation and analysis (seismic analysis included).
PASS/EQUIP Nozzle-FEM – Nozzle/vessel connection FEM analysis
PASS/EQUIP Complete – Equipment comprehensive analysis (all above).

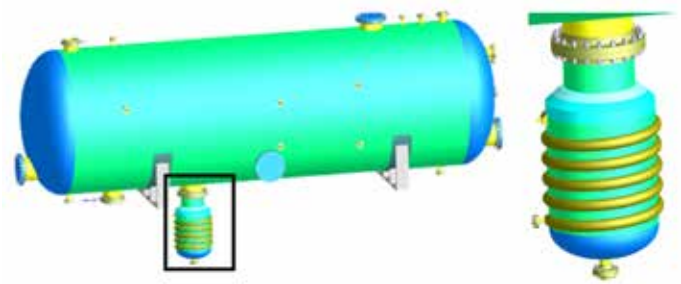

Figure 9. Horizontal vessel with heater

At the end of each calculation the program generates a report. Each report contains summary tables, comments and warnings, calculation details as well as conclusions for each element.
Reports contain multiple aspects including calculation results and analytical formulas, intermediate results and references to the code items enabling users to easily understand how these results are obtained and what causes the problems. (Some situations are not obvious for beginners. For example, improving the flange bolts can lead to worse results. The report then shows that bolts are stronger than the flange which is prohibited in the code, because bolts must not deform the flange.)
A report can be exported to the RTF format (Microsoft Word). The appearance, content and composition of the document depends on a template that can be customized by the user.

PASS/EQUIP also contains an independent module to perform stress analysis of a nozzle joint to an apparatus, Nozzle-FEM. As indicated by its name, Nozzle-FEM uses the finite element method (FEM) which makes it possible to calculate arbitrary configurations including nozzles at any angle, various gripe conditions, and a wide range of geometric parameters. The horizontal and vertical fragments of cylindrical and elliptical shells, as well as pipes (for the calculation of tees) can be considered as a main element.
The nozzle parameters (geometry and loads) can be set individually or obtained from PASS/EQUIP Vessel.
Following the PASS/EQUIP tradition, Nozzle-FEM is a tool with a high degree of automation. The user specifies geometry, materials and loads and the program calculates all the other parameters. That means, the challenges when choosing the FE, appropriate mesh set-up, selecting the calculation method and even interpreting the results are taken care of automatically!
Besides creating an analysis for the given loads, the program also determines acceptable loads on the nozzle.
The results of the calculation are visualized in 3D (dynamic display of stresses and displacements) and saved in a report similar to the PASS/EQUIP Vessel reports.

After describing the software history and capabilities, we want to conclude this article sharing some examples of real pressure vessels, calculated in PASS/EQUIP by our users. A picture is worth how many words?

Alexey Timoshkin, Andrey Krasnokutsky
PSRE Truboprovod

For more information: Livio Furlan, EnginSoft
l.furlan@enginsoft.com

Performance of road side crash barrier with regards to vehicle crashworthiness

To accomplish their endeavour of safe transportation, the regulatory institutions are constantly collecting the accidental data and investigating the causes of fatalities.
In many cases, the fatalities are due to vehicle roll over or vehicle running away from road and hitting rigid objects adjoining the road. Such incidences can be taken care of by properly restricting the vehicle by use of crash barriers. 2005 statistics from the US show that run off road crashes resulted in 31% of fatal crashes, but were only 16% of all crashes. Since the vehicle side structure has less energy absorbing structure as compared to front end, Crash barriers can further increase the injuries, if not designed properly. This paper presents study of vehicle-barrier crash pulses and vehicle kinematics with regards to various barrier profiles and properties. Further, a comparison has been presented to evaluate most suitable and lightweight design solution.

Introduction

The main purpose of Guard-rails/road-barriers/barriers is to restrict and redirect the vehicles which are running away from the road, which may result in accidents. Thus, there is a strength requirement for guard rails. But, at the same time the guard rails must not be very stiff as to cause more injuries to the occupants. To provide appropriate safety levels for impacting vehicle occupants, the safety barriers should be designed in order to absorb as much high kinetic energy as possible during the crash as well as maintain the reliability.
Thus, if there are no deformations in the vehicle or the barrier, it would result in high injuries to the occupants. Hence to make the impact softer, the barrier must absorb energy and bend to a certain limit.
The study presented in this paper is carried out with reference to the Procedure for the Safety Performance for guard-rails by NCHRP 350 using LS-DYNA FEM solver to evaluate the crashworthiness of seven different configurations of guard-rails. While doing this, analysis of various performance criteria's like OCDI, ASI, THIV etc. are calculated and the most cost-effective & viable solution among the various configurations is inferred.

NCHRP 350 Standard

NCHRP Report 350 is a consensus document of the roadside safety community. The recommended guidelines contained in NCHRP Report 350 reflect input received from a large number of researchers, hardware manufacturers, and user agencies at all levels, and other professionals in the field of roadside safety design. The report provided is a basis on which the impact performance of roadside safety features can be uniformly assessed and compared in "worst practical conditions". The crash testing guidelines present matrices for vehicular tests that are defined in terms of vehicle type, impact conditions (i.e., speed and angle), and impact location. Information is provided regarding test article installation, test vehicle specifications, tolerances on impact conditions, and critical impact locations. NCHRP Report 350 further prescribes data collection and analysis procedures, test evaluation criteria, and test documentation recommendations. The performance of a safety feature is evaluated in terms of occupant risk, structural adequacy, and potential exposure of workers and pedestrians that may be in the debris path resulting from the impact, and post impact trajectory and behavior of the vehicle.
According to NCHRP Report 350, up to seven tests are recommended to evaluate gating W-beam guardrail terminals to test level three (TL-3). TL-3 is the basic test level for passenger vehicles to which most crash-tested safety devices in use on U.S. highways have been qualified. Tests to evaluate longitudinal barriers for six test levels are presented in Table 1.

Below are the evaluation criteria

Structural Adequacy

Depending on the type of safety device and its design function, the device should be able to contain and redirect the impacting vehicle, permit controlled penetration of the impacting vehicle, or bring the vehicle to a controlled stop in a predictable manner.

Occupant Risk

In general, occupant risk relates to the degree of hazard or risk of injury to occupants in the impacting vehicle. Occupant risk is assessed in terms of

the relative velocity at which a hypothetical, unrestrained occupant impacts an interior surface of the vehicle (THIV), and the subsequent occupant ride down accelerations (AIS). Penetration of the occupant compartment is not permitted. Another element of the occupant risk evaluation is the risk of injury to occupants of the impacting vehicle, other traffic, pedestrians, or work zone personnel due to detached elements, fragments, or other debris form the test device. Vehicle stability is another aspect of the occupant risk evaluation. For all tests involving passenger vehicles, a requirement for the safety of vehicle occupants is for the impacting vehicle to remain upright (i.e., no roll over) during and after the collision.

Vehicle Trajectory

After collision it is preferable that the vehicle's trajectory not intrude into adjacent traffic lanes

Methodology

This study carries out a numerical investigation of the road barrier impact crash. The purposes of this study is to predict absorption energy and to investigate the damage level of different road barrier design after impact crash. The analysis utilizes finite element software LS-DYNA, Oasys D3PLOT which is widely used for impact simulations. The standard guard-rail design was first evaluated to know the performance of the presently installed guard-rails. Various design solutions were then proposed as a substitute to the existing design and they were evaluated under the same conditions. The design of posts and the spacing between them was maintained constant in all the cases.

In this study only one case prescribed by NCHRP 350 is taken into consideration. i.e. TL-3 test level 3 for which vehicle to barrier crash pulse and kinematics are studied with different rail configurations under same conditions. The Vehicle used is of category 820C. The velocity of the test vehicle is 100 kmph and the angle of impact is 20 degrees.

Test Level	Barrier Section	Test Designation	Impact Conditions*			Impact Point	Evaluation Criteria* (See Table 5.1)
			Vehicle	Nominal Speed (km/h)	Nominal Angle, θ (deg)		
1	Length of Need	1-10 S1-10* 1-11	820C 700C 2000P	50 50 50	20 20 25	(b) (b) (b)	A,D,F,H,I,(J),K,M A,D,F,H,I,(J),K,M A,D,F,K,L,M
	Transition	1-20# S1-20* 1-21	820C 700C 2000P	50 50 50	20 20 25	(b) (b) (b)	A,D,F,H,I,(J),K,M A,D,F,H,I,(J),K,M A,D,F,K,L,M
2	Length of Need	2-10 S2-10* 2-11	820C 700C 2000P	70 70 70	20 20 25	(b) (b) (b)	A,D,F,H,I,(J),K,M A,D,F,H,I,(J),K,M A,D,F,K,L,M
	Transition	2-20# S2-20* 2-21	820C 700C 2000P	70 70 70	20 20 25	(b) (b) (b)	A,D,F,H,I,(J),K,M A,D,F,H,I,(J),K,M A,D,F,K,L,M
3 Basic Level	Length of Need	3-10 S3-10* 3-11	820C 700C 2000P	100 100 100	20 20 25	(b) (b) (b)	A,D,F,H,I,(J),K,M A,D,F,H,I,(J),K,M A,D,F,K,L,M
	Transition	3-20# S3-20* 3-21	820C 700C 2000P	100 100 100	20 20 25	(b) (b) (b)	A,D,F,H,I,(J),K,M A,D,F,H,I,(J),K,M A,D,F,K,L,M
4	Length of Need	4-10 S4-10* 4-11# 4-12	820C 700C 2000P 8000S	100 100 100 80	20 20 25 15	(b) (b) (b) (b)	A,D,F,H,I,(J),K,M A,D,F,H,I,(J),K,M A,D,F,K,L,M A,D,G,K,M
	Transition	4-20# S4-20* 4-21# 4-22	820C 700C 2000P 8000S	100 100 100 80	20 20 25 15	(b) (b) (b) (b)	A,D,F,H,I,(J),K,M A,D,F,H,I,(J),K,M A,D,F,K,L,M A,D,G,K,M
5	Length of Need	5-10 S5-10* 5-11# 5-12	820C 700C 2000P 36000V	100 100 100 80	20 20 25 15	(b) (b) (b) (b)	A,D,F,H,I,(J),K,M A,D,F,H,I,(J),K,M A,D,F,K,L,M A,D,G,K,M
	Transition	5-20# S5-20* 5-21# 5-22	820C 700C 2000P 36000V	100 100 100 80	20 20 25 15	(b) (b) (b) (b)	A,D,F,H,I,(J),K,M A,D,F,H,I,(J),K,M A,D,F,K,L,M A,D,G,K,M
6	Length of Need	6-10 S6-10* 6-11# 6-12	820C 700C 2000P 36000T	100 100 100 80	20 20 25 15	(b) (b) (b) (b)	A,D,F,H,I,(J),K,M A,D,F,H,I,(J),K,M A,D,F,K,L,M A,D,G,K,M
	Transition	6-20# S6-20* 6-21# 6-22	820C 700C 2000P 36000T	100 100 100 80	20 20 25 15	(b) (b) (b) (b)	A,D,F,H,I,(J),K,M A,D,F,H,I,(J),K,M A,D,F,K,L,M A,D,G,K,M

Table1. Longitudinal barrier test level

Barrier Design

The current system comprised W-shaped guardrails and C-posts as shown in Figure 1.

The length of the W-beam guardrail segments was around 30 m. The C-post was 1,600 mm in length and was embedded 100 mm in the soil. The dimensions of the post were 125mm, 62.5mm, 25 mm. The distance between each post was 1905mm. The height of the barrier was 810 mm from the ground.

Three new type rails include: threi-shaped, pipe with 90mm &120m diameter, Sigma-shaped, reinforced W rail and Honeycomb structure has been investigated and compared with the existing system. All models were identical, except for the shaped of front rails. The cross section of the shaped posts are depicted in Figure 2.

Model setup and Analysis:

Vehicle Model

The vehicle chosen according to NCHRP Report 350 was a Geo Metro car (version GM-R3) from the NCAC database [4] was used in this simulation. The vehicle model is publicly accessible on the NCAC Web page. This car

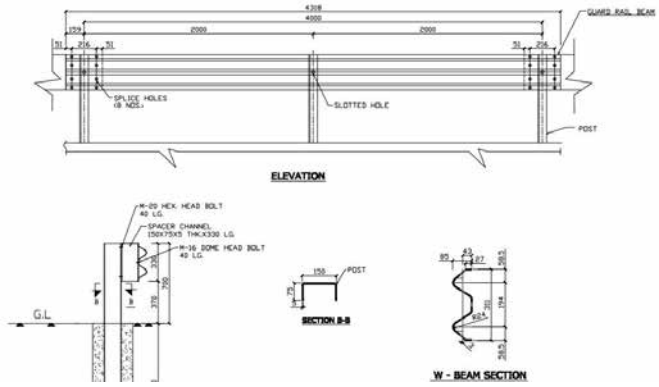

Figure 1. Standard w-shape guardrail

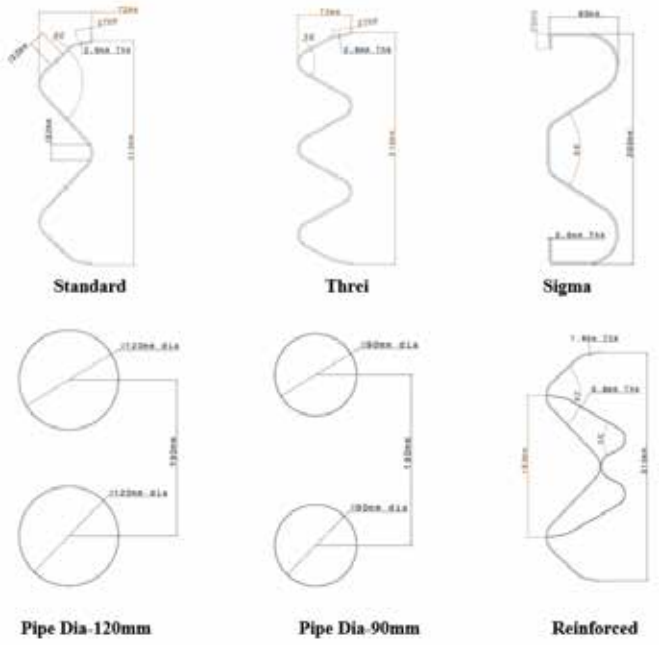

Figure 2. (a) Cross- sections of different guardrails

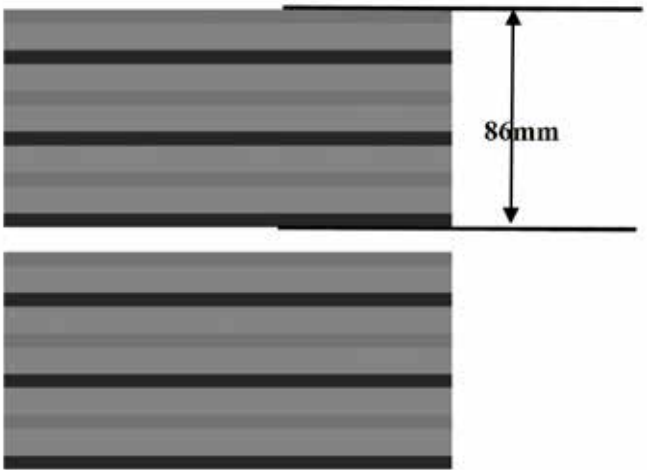

Figure 2. (b) Cross- sections of Honeycomb Structure

was useful in simulating the impact of a passenger car (900 kg) on the road safety barrier according to the TL3 test regulation for NCHRP. The car model contained 247 parts, 26,348 shell elements, and 28,737 nodes.

Barrier Model

The finite element model of road safety barrier impact were modeled in CAD software (Catia V5) and then FE model for the same was created. All the parts of the safety barrier were modeled with fully integrated shell elements with five integration points through the shell thickness to prevent hourglass mode. The bolt connections between the W-shaped segments and the posts were modeled using beam elements.

The AUTOMATIC_SINGLE_SURFACE card with a soft constraint option assigned as type 1 was used to define a contact between the components of the barrier. The W-beam guardrail component materials, such as the posts and W-beam were represented using MAT024 (a piecewise linear plasticity material model) in LS-DYNA. Table 2. Presents the properties of the material for the road safety barrier models.

Boundary Conditions

The twisting of guardrail post along the barrier axis is restricted by constraining at the extreme ends. Figure 3. Shows the constraining of rails at the end.

The study is mainly concentrated on guardrail behavior, so it is assumed that the post is fixed at ground. Figure 4. Shows the posts are contained in all degree of freedom at base.

The roadway was defined by a rigid wall card *RIGIDWALL_PLANAR having high friction value of 0.6 to simulate contact between the car and the ground. The impact test model comprised the vehicle and safety barrier. The vehicle speed was set to 100 km/h with an impact angle of 20° according to test TL-3. AUTOMATIC_SURFACE_TO_SURFACE card with soft constraint type 1 was used as a contact between the vehicle and the barrier. The coefficient of friction was set to 0.2.Figure 5. Shows one of the setup for simulations.

Material Properties	Standard	Threi	Sigma	Pipe-90	Pipe-120	Reinforced	Honeycomb
Density kg/m3	7800	7800	7800	7800	7800	7800	2610
Yield stress MPa	365	365	365	370	370	265	210
Young's modulus GPa	210	210	210	210	210	210	70
Possion's ratio	0.3	0.3	0.3	0.3	0.3	0.3	0.33
Thickness	2.6	2.6	2.6	2	2	1.8mm &0.8mm	t1-0.1, t2-0.2mm
Weight(kg)/m	14.21	16.86	17.17	13.71	16.80	13.50	7.50

Table 2. Presents the properties of the material for the road safety barrier models

Results & Discussion

The result analysis and performance evaluation of the barrier depends on the potential of the barrier to contain and redirect the vehicle, with the acceptable impact severity and working width set according to NCHRP. Figure 6-12 show the simulation kinematics of the finite element models. Those figures show the vehicle trajectory and the deformation of guardrail when the 900 kg small car impacts the safety barrier with a speed of 100 km/h at an angle of 20 degrees.

Figure 3. Constrained of rail at the end

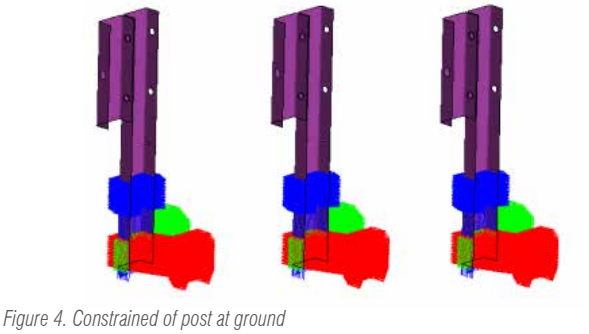

Figure 4. Constrained of post at ground

In all the cases, barriers are strong enough to prevent the vehicle from leaving the road and redirect it back on road except honeycomb. In Honeycomb guardrail, the structure seems much stiffer in terms of rate of energy absorption but stops redirection of the vehicle and sticks to the vehicle.

Figure 13. Illustrates the energy absorption obtained over time for the seven barriers with various shaped rails. The honeycomb structure shows the high energy absorption compared to others but vehicle is not getting a smooth exit as compared to other guard-rails performances. The best energy absorption is shown by reinforced rails. Also the weight to length ratio is less as compared to the standard rails.

Figure 5. Typical setup for simulation

Figure 14-20 shows the rail deformation Table 3. Shows the deflection and weight comparison of all types of the barriers under impact crash under TL-3 testing condition prescribed in NCHRP.

In NCHRP there is no criteria for measurement of rail deformation as in European regulation. By comparing the maximum deflection value to the other standards (EN1317 & AS/NZS 3845), the barriers are still within the of W3 working width range of deflection (W3<1m) with small to moderate deformation.

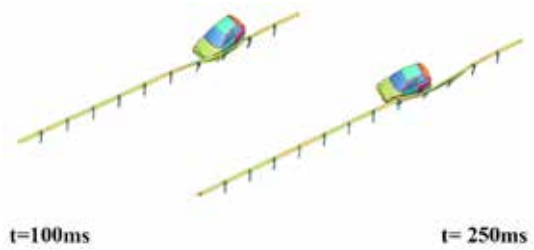

Figure 6. Performance of standard rail

Figure 7. Performance of threi shape rail

Figure 8. Performance of sigma shape rail

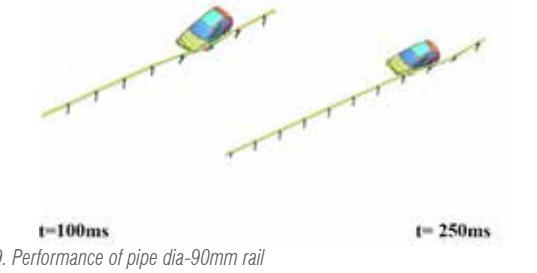

Figure 9. Performance of pipe dia-90mm rail

Figure 10. Performance of pipe dia-120mm rail

Figure 11. Performance of reinforced rail

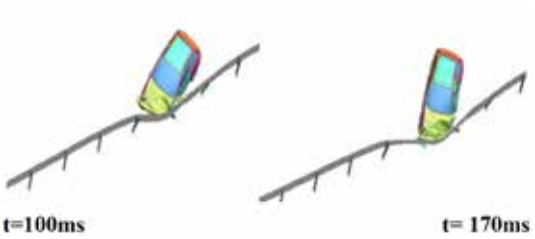

Figure 12. Absorbed energy for honeycomb type rail

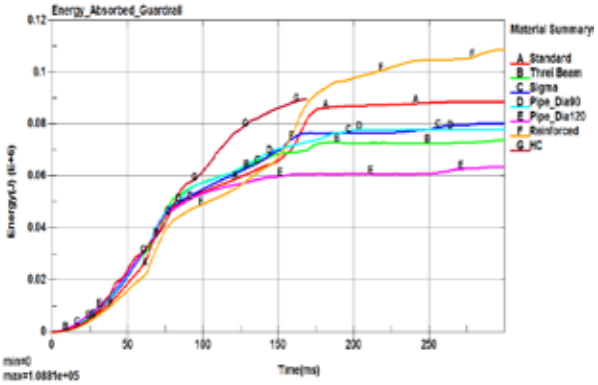

Figure 13. Comparison of energy absorbed for different guardrails

The force of the impact is distributed by the beam to the post in order to minimize the deflection, hence post also plays a vital role in rails deformations. Maximum deflection is reported for honeycomb structure and minimum is for pipe barrier with diameter 120mm whereas the minimum weight is for honeycomb structure and maximum is for sigma cross section, as seen in the Figure 21.

Honeycomb structure has a high stiffness value which is demonstrated by its good energy absorption capacity. But, the structure gets stuck in the vehicle and does not permit vehicle to smoothly exit and hence is not favorable. Thus, honeycomb structure will need a metallic envelope to be created on it, to prevent sticking and thus will not be cost effective.

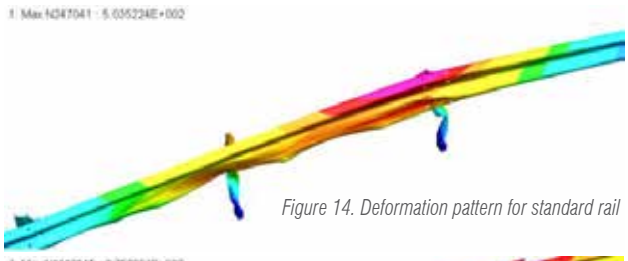
Figure 14. Deformation pattern for standard rail


Figure 15. Deformation pattern for threi rail


Figure 16. Deformation pattern for sigma rail

Figure 17. Deformation pattern for pipe diameter 90mm rail

Figure 18. Deformation pattern for pipe diameter 120mm rail

Figure 19. Deformation pattern for reinforced rail

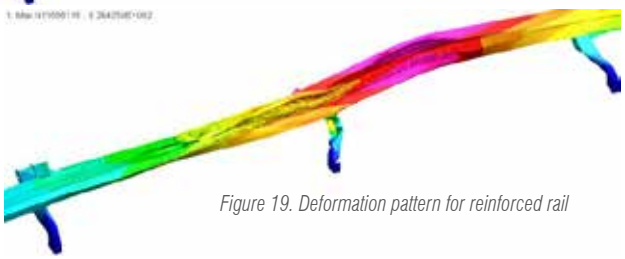

Figure 19. Deformation pattern for reinforced rail

Table 4. Shows the impact severity (ASI and THIV) of the models.
In all seven test cases, the barriers meet the NCHRP requirement. The barrier with sigma shaped rail showed the highest ASI value (i.e., 2.33), and the barrier with pipe dia-90mm shaped rails demonstrated the lowest ASI value (i.e., 0.48). The barrier with sigma-shaped rail showed the highest THIV (i.e.8.75), and the barrier with pipe dia-90mm shaped rails showed the lowest THIV (i.e. 4.81). ASI and THIV results are showing the same trend, i.e. most severe for sigma shape and least for pipe dia-90mm. Therefore the barrier with pipe dia-90mm shaped rails provide a greater safety level for vehicle occupant compared with barrier installed with other rails.

Material Properties	Standard	Threi	Sigma	Pipe-90	Pipe-120	Reinforced	Honeycomb
Density kg/m3	7800	7800	7800	7800	7800	7800	2610
Yield stress MPa	365	365	365	370	370	265	210
Young's modulus GPa	210	210	210	210	210	210	70
Possion's ratio	0.3	0.3	0.3	0.3	0.3	0.3	0.33
Thickness	2.6	2.6	2.6	2	2	1.8mm &0.8mm	t1-0.1, t2-0.2mm
Weight(kg)/m	14.21	16.86	17.17	13.71	16.80	13.50	7.50

Table 3. Deformation and weight comparison for all cross section types

Conclusions

Although the energy absorption is highest for the reinforced barrier, but the occupant injury levels depend on other factors which are accounted by the ASI and THIV values which are least for Pipe-90 barrier. The weight for the Pipe-90 barrier is just slightly above the reinforced barrier. Thus, the optimal results are registered by the Pipe-90 barrier, which demonstrates the lowest values of ASI and THIV along with low deformation value.

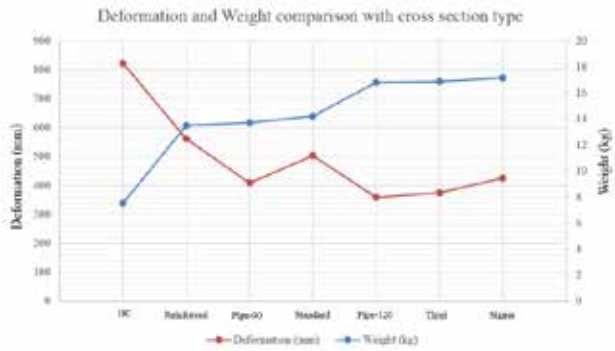

Figure 21. Deformation and weight comparison for all cross section types

Summary & Future Work

Study presents a summary for the finite-element modelling of seven different types of rails used in the guardrail system and their crashworthiness using LS-DYNA. Computational simulations have proved that, all seven different shaped rails are strong enough to prevent vehicle from leaving the road. The best performance was demonstrated by the Pipe-90 shaped rails (90mm diameter pipes) with lowest values of ASI & THIV, lower amount of deformation and light in weight.
Further study can be carried out for barriers with HSS material & can also be evaluated for mass reduction. AASHTO latest regulation can be studied for these rails, since MASH has made their criteria more stringent. Honeycomb type shows a high capability of absorbing energy, ways to eliminate sticking of vehicle into honeycomb structure can be formulated and cost effective method of manufacturing can be studied and implemented.
If facilities are available, we would also take a step towards validating the results with physical tests.

Guardrails	ASI	THIV(m/s)
Standard	1.90	6.86
Threi	1.80	5.62
Sigma	2.33	8.75
Pipe-90	0.48	4.81
Pipe-120	2.07	7.14
Reinforced	1.12	8.15
Honeycomb	1.08	6.25

Table 4. Simulation result with various guardrail shapes.

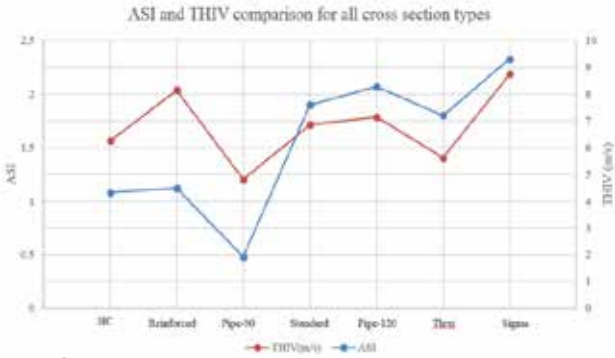

Figure 22. Simulation result with various guardrail shapes.

Deepak Patil, Prashant Topalkatti., Hrishikesh Buddhe
Tata Technologies

ANSYS and ROCKY generate savings for VALE

The largest producer of iron ore in the world uses simulation to optimize machinery, increasing production and reducing costs by 80%

ROCKY is helping us to improve various processes. The use of simulation tools can quantify the design improvements and gains; this is advantageous because mining uses large equipment that without computer simulation can cost millions for prototype development and testing. Accurate simulation results can advocate for necessary changes and updates, with the assurance of a return on investment."

Ueld José da Nobrega
Senior Engineer of Maintenance Engineering
and Industrial Automation at Vale

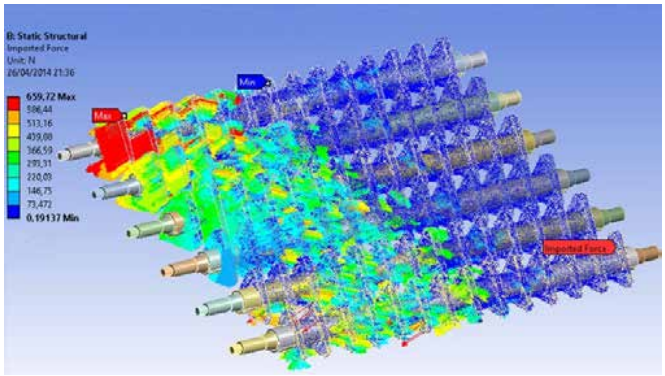

Computer simulation with ANSYS Showing Impact Force on the Rotating Disks

A major challenge in the mining industry is to develop projects that decrease required budgets and loss of raw materials by reducing equipment maintenance and wear. These costs can be minimized with the aid of computer simulation software, such as ANSYS and Rocky which are capable of modeling key variables of the processes and products, ultimately reducing failures and improving durability of the equipment.

The combined use of ANSYS software with Rocky simulation software, developed by Rocky DEM, Inc., results in efficiencies in process and equipment development in various sectors of the mining industry. Vale, the world's largest producer of iron ore, has used these coupled solutions for the past year and has achieved positive results in the Carajás iron mine, located in the state of Pará, Brazil.

"Last year and early this year we implemented some projects developed with the aid of simulation for the protection system of plants from inputs 1 and 2. The deployment of these projects cost was about US$18.2 million. In just three months the operation of each project achieved an economic return of over US$100 million," says Ueld José da Nobrega, senior engineer of the Management of Maintenance Engineering and Industrial Automation (GAAUN) at Vale. He also reports the results observed after the implementation of the projects and they were similar to those estimated in computational simulation.

PROBLEM

The solution mentioned by Ueld was developed to improve the efficiency and reduce the need for frequent grid cleaning at the hoppers' screen from plants 3 and 4. Plant 3 and plant 4 have two input lines each. They are responsible for separating the rocks by size and sift through the ore. The smaller stones and the sieved ore are sent to courtyards and storage silos, while the larger rocks return to go through the crushing mill process to achieve the proper size.

Because of the high degree of complexity, the engineering team at the Carajás plant required the use of ANSYS together with Rocky (coupled solution) in order to study the behavior and flow of rocks deposited on the grid.

With the aid of the Rocky software, they could simulate together the behavior of spherical and non-spherical particles of different sizes, measure the impact forces from the rocks on equipment, and calculate the runoff speed of ore. "The simulations are more accurate with the use of non-spherical particles, this is needed because our mineral has

Separating Equipment

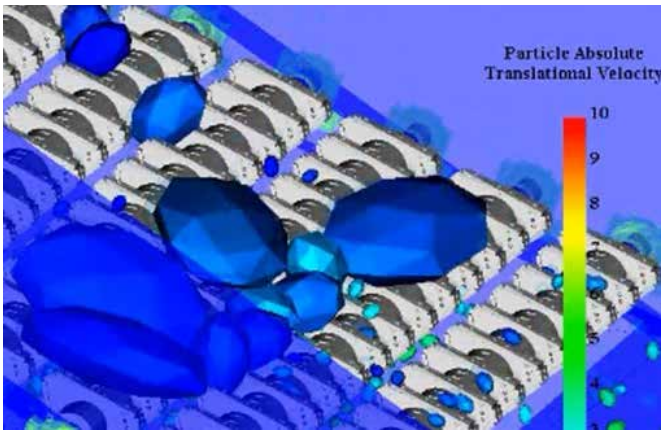

Simulation with Rocky Showing Various Size and Shape ore Falling Through and Going Over the Rotating Disks

a high content of iron," explains Ueld.

The data extracted from Rocky was used in combination with ANSYS tools to conduct structural analysis of the equipment. Engineers were able to virtually test the effect of proposed changes on the machine and how the ore would behave within the new structure. With the use of a coupled solution, Vale reduced the time spent by its staff on the development of this project by approximately 70%.

OPTIMIZATION

The solution proposed by Vale engineers was based on the operation of moving screens. They have evaluated different configurations and

Large-Scale Mining Equipment Being Directed by a Caraja's Worker

A Vale Giant Truck Being Loaded With Ore at the Carajas Iron Mine

decided to develop a new system of rotating disks, similar to the roller system widely used in coal operations.

Based on the simulation results of ANSYS and ROCKY, they defined rotational speed, tilt angle, distance and profile of the disks for operation, which changed from conventional circular shape to triangular shape.

In order to meet the new specifications, other changes had to be made to the equipment. The transmission system used in the project had to be redesigned and the support structure adapted accordingly. These changes will exceed the estimated gain of productivity in Plants 3 and 4 at Carajás, increasing production by 11.4% after the full implementation of the project.

THE BEST ORE IN WORLD!

Carajás Vale is the largest open mine in the world and is responsible for injecting into the market millions of tons of the best iron ore in the world.

The plant produces 400 thousand tons of ore a day. The flow of daily production is carried out by more than 100 off-road trucks.

ROCKY

Rocky is distributed by EnginSoft. For more information:
Massimo Tomasi - m.tomasi@enginsoft.com

Digital Twin of a production machine

FMI-enabled digital twin for co-design and virtual commissioning of production machines

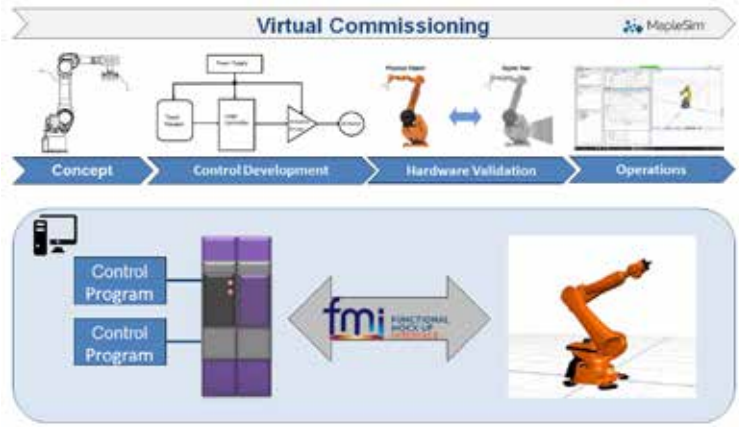

Fig.1 - FMI enabled co-design of production machines

Automated Machines manufacturers traditionally strived to remain competitive by developing ever-faster machines, to meet the increasingly demanding production cycles of their customers. In recent years however the industry need for more flexible, robust and predictable machines, has steadily grown. Last generation of machines are in fact required to provide top performances over different aspects: reliability, to avoid production downtime and minimize costly repairs; accuracy, to avoid scrap and quality issues; programming easiness and predictability during the commissioning and production ramp-up phases.

These requirements, merged with the pressure from the customer to reduce time to market, have questioned the traditional machine design processes. A new approach to machine design has emerged, that brings together two competence areas traditionally well separated in most production machines manufacturer companies: automation development and mechanical engineering. This approach allows to integrate the design efforts into a single co-design approach, from concept development to commissioning (Fig. 1).

Tools supporting FMI	FMI Version	Export	Import	Slave	Master	Notes
MapleSim	FMI_1.0	Available		Available		Modelica-based modeling and simulation tool from Maplesoft
	FMI_2.0	Available	Available	Available	Planned	

Fig.2 - MapleSim support the latest 2.0 version of the FMI standard

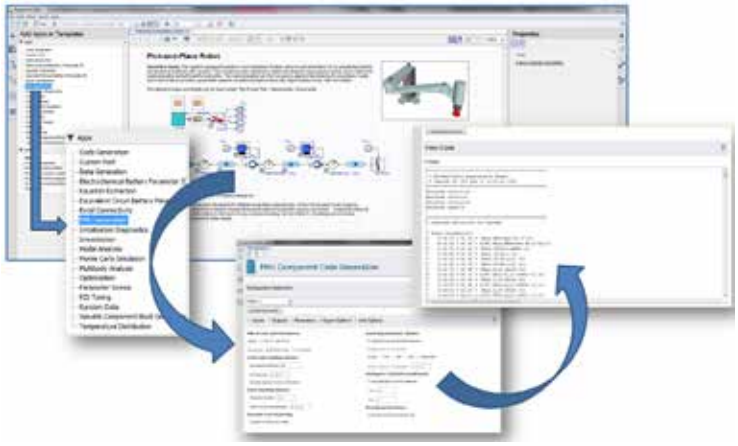

Fig.3 - Generating a FMU from MapleSim

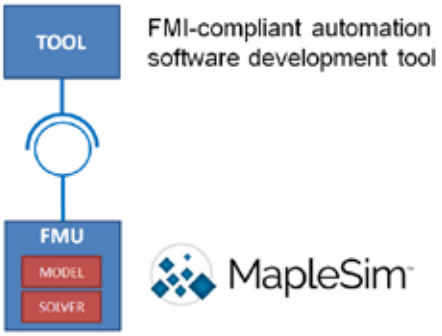

Fig. 4 - Co-design mode FMU

The key enabling technology for this innovative approach is FMI – Functional Mock-up Interface, a tool-independent standard that supports both model exchange and co-simulation of dynamic models. This technology allows mechanical engineers to effectively develop and share working machine models, at various level of details, with control developers. A modeling tool that is on the forefront of such approach is clearly MapleSim, the state-of-the-art multi-domain modeling and simulation solution from MapleSoft (Fig. 2).

MapleSim effectively exploits the latest version of the FMI standard to enable co-simulation with any FMI compliant automation software development tool (e.g. B&R Automation Studio™ and others): the co-simulation mode assumes that there are no solvers available within the target application, so the necessary solvers are provided by MapleSim and embedded together with the MapleSim machine model into an FMI compliant executable called FMU – Functional Mock-up Unit (Fig. 3 and 4).

MapleSim allows to easily develop machine models starting from importing validated 3D CAD geometries into its Model Workspace. It is therefore possible to create a high-fidelity multi-body representation of the machine, by selecting contact surfaces and adding the proper joints to the model. It is afterwards possible to add the actuation part of the model, selecting electric or hydraulic drives and all the necessary components from the rich components libraries available. Once generated, the FMU will retain and expose to the automation software development tool all the input and output parameter defined in the model, together with the solver. Together with the automation software the FMU will therefore constitute an accurate model-driven digital twin of the physical machine (Fig. 5).

The advantages provided by this co-design approach are vast. Automation software can be tested earlier in the development stages, reducing the time to market and allowing to right-size critical machine components taking into account the actual demands coming from the automation program coupled with a high-fidelity model of the machine (Fig. 6). Furthermore this approach enables virtual commissioning workflows by testing and verifying the machine functionality before the machine is physically available. Lastly the model-driven digital twin can be used during ramp-up and production to monitor the machine performance to detect changes that may provide early signals of future reliability issues and to adjust the automation program to extend the useful life of critical components subject to wear (Fig. 7).

For more information:
Giovanni Borzi, EnginSoft
g.borzi@enginsoft.com

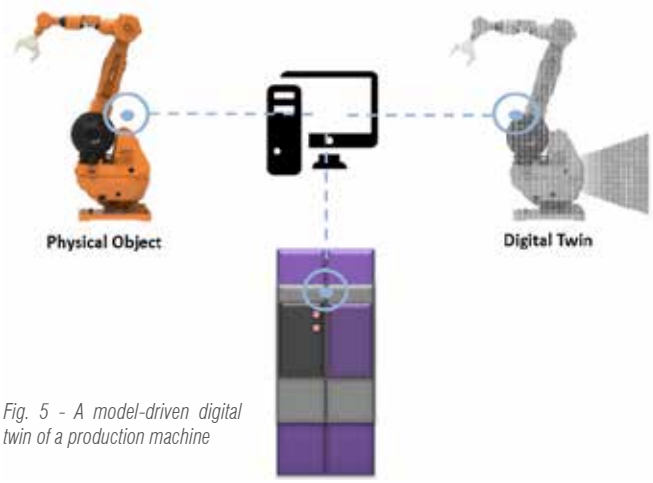

Fig. 5 - A model-driven digital twin of a production machine

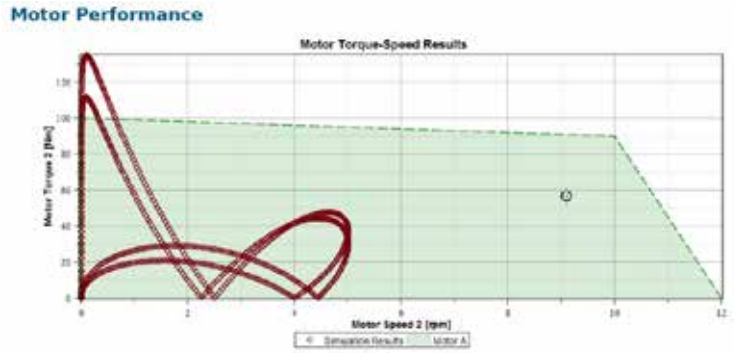

Fig.6 - Righ-sizing of a critical component in MapleSim: motor torque VS speed compared with motor specification

Numerical simulation of electromagnetic stirring in steelmaking industry

This work aims at developing a reliable and efficient strategy to simulate electromagnetic stirring (EMS) applications in steelmaking industry, especially for in-mould stirring (M-EMS) in continuous casting and for ingot casting processes. Several advanced numerical tools have been used to enhance the simulation capabilities and a coupling numerical scheme has been proposed to couple the different physics involved in the simulation. This coupling strategy has been developed in a commercial software focused on casting simulations. Finally, the model has been tested and compared to experimental and numerical results present in the literature

1. Introduction

Electromagnetic stirring is widely used in casting industry in order to control the flow of molten metal and the final properties of the piece. Stirring allows keeping the temperature uniform and avoiding segregation, leading to a better quality of the final product. In continuous casting, it also decreases the turbulence in the melt, decreasing the possibilities of a breakdown. However an efficient design is not easy since experimental data are difficult and expensive to obtain and analytical models are way too simplified to be used in industrial applications. Hence, numerical simulations are the most common tool to support the design process; the main disadvantage is the high computational cost required to perform the simulation which is strongly multiphysical. The aim of this work is to develop a set of numerical tools able to accurately model electromagnetic stirring applications with a low use of computational resources. The proposed strategy has been implemented in commercial

software (THERCAST). The fluid flow has been modelled by the variational multiscale formulation (VMS) which allows modelling the effects of small scale turbulence without explicitly tracking it, and anisotropic remeshing algorithms have been used to optimize the mesh. The electromagnetic problem has been modelled by the (A, φ) potential formulation and solved in the frequency domain. Finally a weak coupled 2-meshes-2-solvers approach has been used to model the coupled problem.

2. Mathematical model

2.1. Electromagnetic model

The (A, φ) potential model has been used to model the electromagnetic field (EMF). Thus, the evolution in time of the EMF is describes by the following system:

$$\begin{cases} \mu_0^{-1} \cdot \nabla \times \left(\mu_r^{-1} \nabla \times \boldsymbol{A}\right) = -\sigma(\partial_t \boldsymbol{A} + \nabla \phi - \boldsymbol{u} \times \nabla \times \boldsymbol{A}) \\ \nabla \cdot \left(-\sigma(\partial_t \boldsymbol{A} + \nabla \phi - \boldsymbol{u} \times \nabla \times \boldsymbol{A})\right) = 0 \end{cases}$$

where μ_0 and μ_r are the free space and material's relative magnetic permeability respectively. A is the magnetic vector potential, A is the scalar electric potential, u is the medium velocity, and φ is the electrical conductivity. The convective term can be neglected from the first equation in system (1) because the Reynolds magnetic number is Rem<<1. The system has been discretized in space by Nedelec's edge finite elements and then solved in the frequency domain. For further information about the resolution technique of the resulting complex system via real-equivalent formulation.

2.2. Mechanical model

The turbulent fluid flow has been modelled by the incompressible Navier-Stokes equation:

$$\begin{cases} \rho(\partial_t \boldsymbol{u} + \boldsymbol{u} \cdot \nabla \boldsymbol{u}) - \nabla \cdot (2\mu\varepsilon(\boldsymbol{u}) - p\boldsymbol{I}) = \boldsymbol{f}_g + \boldsymbol{f}_L \\ \nabla \cdot \boldsymbol{u} = 0 \end{cases}$$

where p, μ, f_g and f_L are the density, the viscosity, the gravity force, the Lorentz force respectively. System (2) has been solved by finite elements in a variational multiscale approach.

According to the multiscale paradigm, the variables have been split into a coarse and a fine scale. The fine scale is not solved directly, but its effects are integrated in the coarse scale resolution. The obtained formulation is both computationally light (because it does not track explicitly the small scale phenomena), and accurate (because it takes into account the effect of the small turbulence scale into the flow), thus it is suitable for highly turbulent flow simulations. For the detailed development of the weak formulation.

2.3. Coupling strategy

The coupling strategy used in this work is the so called "Two meshes two solvers approach" (2M2S). The basic principle is that the two problems (i.e. the electromagnetic and the mechanical ones) should be solved by two different software applications on two different domains with different meshes. In this work, the electromagnetic problem has been solved by using MATELEC© in a domain including the molten metal, the mould and the air surrounding the mould. The mechanical problem has been solved by using THERCAST in a domain coincident with the fluid domain. As mentioned in section (2.1), the convection of the magnetic field due to fluid's motion is negligible, so the resolution of the electromagnetic field is not affected by the mechanical problem. The Lorentz force is computed in post-process as:

$$\boldsymbol{f}_L = \boldsymbol{j} \times \mathbf{B} = -\sigma(\partial_t \boldsymbol{A} + \nabla \phi - \boldsymbol{u} \times \nabla \times \boldsymbol{A}) \times \nabla \times \boldsymbol{A}$$

The convective term has been considered in three different ways:

A. It has been neglected, since Rem<<1. The Lorentz force corresponding to the current time-step has been added as a source term in the Navier-Stokes equation. The average value of the force has been considered when the frequency $f > 2.5 \cdot I_2$, where I_2 is the second invariant of the shear rate tensor.
B. The correct value of j has been computed at each time step by solving $\nabla \cdot -\sigma(\partial_t A + \nabla \varphi - u \times \nabla \times A)$. This value has been used to compute the Lorentz force, but not for re-computing the electromagnetic field.
C. It has been considered in explicit, neglecting the divergence constraint (thus considering $\nabla \varphi = 0$). Hence, we obtain $j = -\sigma(\partial_t A - u \times \nabla \times A)$.

The techniques described in B and C use the value of u at the previous time-step, thus the time-step for the mechanical resolution has been chosen:

$$\Delta t = min\left\{\frac{h}{u}; \rho\frac{1}{\sigma B^2}\right\}$$

where h is the mesh size.

2.3.1. EM source term modelling.

The electro-magnetic influence on the fluid mechanical problem is modelled through an explicit source term in the Navier-Stokes equations, as shown in equation (1). This term is evolving in time periodically, but its variation speed may be much higher than the variation rate of the mechanical problem. If the period of this term (proportional to the period of induction T) is much lower of the turbulence characteristic time, the average value of the Lorentz force may be used. In this case, only one field has to be interpolated and stored, so the coupling interface will be light. On the contrary, if the period of the Lorentz forces is of the same scale as the turbulence period, the variation of the force within the EM period must be considered. This means that the Lorentz force corresponding to each EM time step must be stored and interpolated, leading to an increase in the requested computational effort. The highest period for which no interaction between the transient part of the Lorentz force and the turbulence appears has been based on the Kolmogorov theory and it is computed as:

$$T_{max} = \frac{1}{2.5 \cdot I_2},$$

where I_2 is the second invariant of the shear rate tensor. But this criterion is local. The transient part of the Lorentz force may interact with the turbulence, but not having a global impact or occurring in a region where the force density is so low not to change the inertia of the flow. For this reason, we propose a global criterion, namely the Ω condition to quantify the global interaction between the EM and the CFD problem. Thus, given the condition Ω_n^m, we want to verify the criterion in equation (5) on n% of the active volume, where the active volume is the region where the Lorentz force is

higher than m% of the maximum Lorentz force in any point during the whole EM period. The parameters n and m must be defined for each application.

2.4. Anisotropic mesh adaptation

The mesh of the mechanical simulation has been adapted anisotropically and dynamically during the simulation. The remeshing algorithm used in this work is based on the error estimation analysis and aims at producing the optimal mesh to discretize the input fields by minimizing the related interpolation error. For this work, we propose the following set of fields to remesh according to:

$$v = \left\{ \frac{u}{|u|}, \frac{|u|}{\max(|u|)_\Omega}, \frac{d}{\max(d)_\Omega}, \frac{|f|}{\max(|f|)_\Omega} \right\}$$

where Ω is the fluid domain, d is the boundary distance and f is the volumetric force.

3 Results

3.1 Bench test

The numerical framework described in section (2) has been tested with respect to established results; the bench case consists in a laboratory scale stirring application of Galinstan melt in a Plexiglas mould. The problem configuration and the main parameters are reported in Fig. 1 and Tab. I respectively. Thanks to the axial symmetry of the problem, only a 15°-section has been simulated. The electromagnetic simulation has been performed in a domain which includes the inductor, the melt and a air layer 1m tick from the mold external surface. The input current density has been set to I_RMS=200A and the frequency f has been varied from 50Hz to 1300Hz. The mesh (Fig. 2.a) has been refined isotropically in the melt in order to have at least 12 elements in the skin depth computed as:

$$\delta = \sqrt{\frac{\rho}{\pi f \mu}},$$

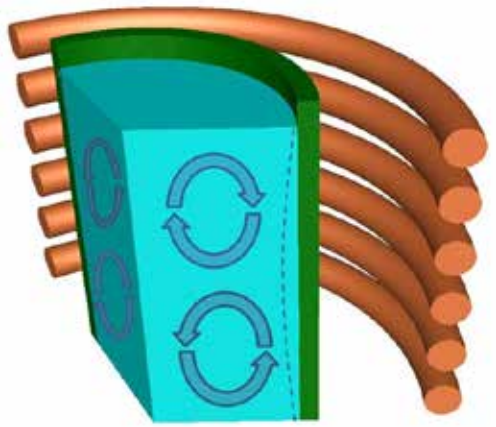

Fig. 1. Bench test configuration

The mechanical simulation has been performed in the fluid domain. No slip boundary conditions have been imposed on the solid wall boundaries and perfectly slip boundary conditions have been imposed at the symmetry planes and the free surface. The average number of elements during the dynamic mesh adaptation is 275000. A detail of the mesh used at the steady state of the mechanical simulation is shown in Fig. 2.b.

Parameter Galinstan Melt	Unit	Value
Galinstan Melt		
Density	Kg/m3	6440
Dynamic viscosity	Pa.s	0.0024
Electric conductivity	S/m	3.46·106
Radius	mm	31
Height	mm	70
Copper Inductor		
Electric conductivity	S/m	1.78·108
Number of turns	-	6
Turn diameter	mm	8
Turns distances	mm	4
Inductor radius	mm	61

Tab. I. Bench test main parameters

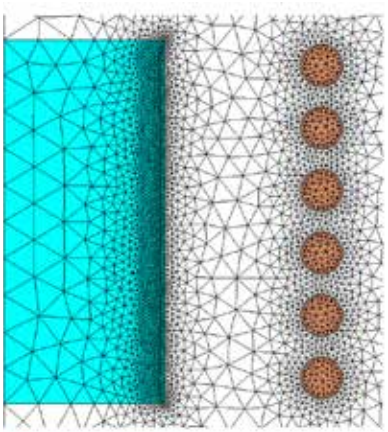

Fig. 2. Mesh of the electromagnetic simulation (MATELEC©)

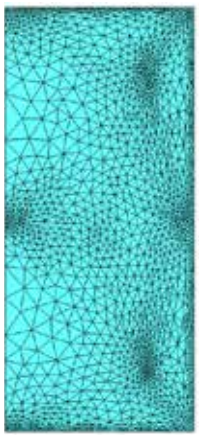

Fig. 3. Mesh of the mechanical simulation (THERCAST)

3.2 Numerical results

3.2.1 Coupling strategy

In Fig. 4, the axial velocity at the centre of the fluid cylinder is plotted. The velocity has been computed at the steady state, i.e. after 200 s and the induction frequency has been set to f=150Hz. The results have been compared to both the experimental and numerical results. In Tab. II a summary of the simulation accuracy is provided by reporting the error related to the main result variables: the maximum velocity of the fastest eddy (Ef), the maximum velocity of the slowest eddy (Es) and the position of the separation point between the eddies normalized to the maximum eddies size (Ep). In Fig. 5, the maximum recirculation velocity over the induction frequency is plotted. For lower frequencies (where experimental data are available) both VMS and k-ε are in the experimental range; however, for higher frequencies, the two solutions produce different results. In both cases the maximum velocity decreases after a peak, but the VMS solution decreases faster. Also a reference solution ($2 \cdot 10^6$ elements) confirms this tendency. Since no experimental data are available in this region, no validation can be affirmed; but the difference in results seems to be a direct consequence of the turbulence model: in VMS a better approximation of small scale turbulence is used, thus higher energy dissipation is produced at high levels of stirring force density. The

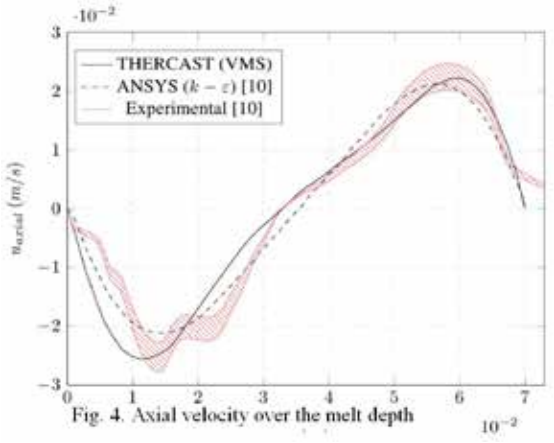

Fig. 4. Axial velocity over the melt depth

Type of error	ANSYS (k-ε)	THERCAST (VMS)
Ef	16%	1.4%
Es	5.2%	1%
Ep	7%	0.4%

Tab II. Error related to Fig. 4

three different coupling techniques described in section (2.3) have been tested; in Fig. 6, the error of the maximum axial velocity obtained by the different coupling schemes is shown. The error has been computed with respect to the coupling strategy B, which is the most accurate one from the theoretical point of view. Strategy A results to be more accurate than C. In both cases, the error has two peaks: one at low frequency and one at the frequency corresponding to the maximum velocity produced. This is due to the fact that the mechanical effect of the convective term (i.e. $u \times \nabla \times A$) depends on two different factors: by increasing the frequency the velocity tends to increase(which increases the effect of the convective term), but the skin depth decreases, dumping the electromagnetic penetration (which decreases the effect of the convective term).It is also remarkable that the approach A leads to an overestimation of the velocity because the braking effect is neglected, while approach C leads to a underestimation of the velocity since the braking term is considered without accounting for the self-balance due to the creation of an electric field $\nabla\varphi$. In Tab. III, the time analysis for each coupling scheme is proposed. Let's consider strategy A as the reference. The

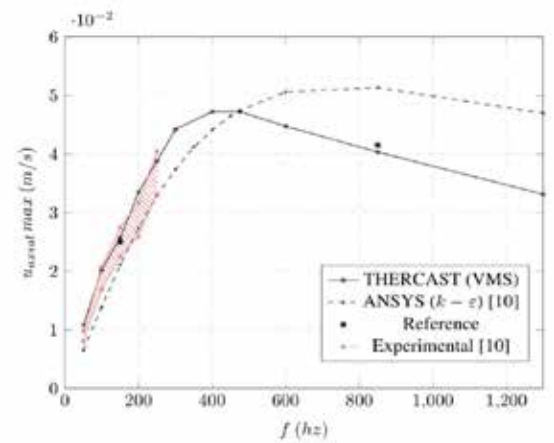

Fig. 5. Maximum axial velocity over induction frequency

resolution of Navier-Stokes equation is the most expensive part of the computation, in particular due to the long physical time to be simulated before reaching the steady state. Approach B, which is the most accurate, is about 50% more expensive than A, since the value of the electrical current has to be computed at each time step by solving the second equation in System (1). Approach C is the less accurate and it is slightly more expensive than A, since the convective term of the Lorenz force has to be computed at each time step.

4 Conclusions

The coupling strategy between electromagnetic and fluid mechanical simulations has been investigated. Several numerical tools (e.g. VMS, anisotropic remeshing, edge finite elements) have been adopted to achieve a good modelling of both the turbulent flow and the magnetic field produced by the stirrer. The results have been compared to experimental and numerical benchmarks present in the literature; finally, different coupling strategies have been tested in order to determinate the most effective one in terms of accuracy and computational effort. Neglecting the mechanical effect (as well as the electromagnetic influence) of the magnetic field convection is the most efficient choice leading to a small velocity overestimation (Err<2%) and remarkable computational time decrease (-35% with respect to the mechanical modelling of the convection term).

L. Marioni - Transvalor, MINES ParisTech
E. Hachem, MINES ParisTech
F. Bay - MINES ParisTech

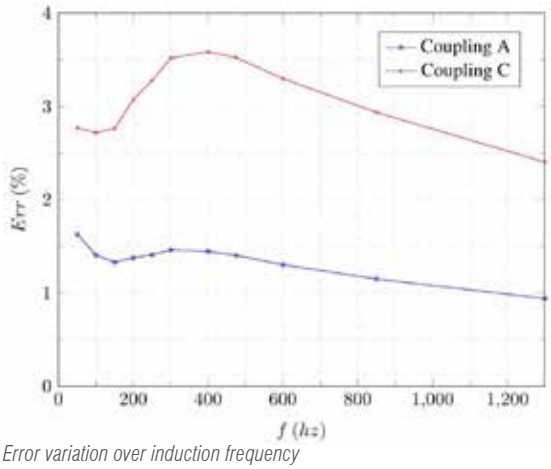

Fig. 6. Error variation over induction frequency

	A	B	C
Navier-Stokes resolution	87.3%	56.6%	87%
Maxwell resolution	3.6%	2.4%	3.6%
Remeshing	8.8%	5.7%	8.7%
Coupling Interface	0.3%	35.3%	0.7%
Total Time	Ref.	+54%	+0.3%

Tab III. Computational effort comparison between different coupling strategies

For more information on Simulation Techniques applied in Steelmaking Indusrty please contact EnginSoft Process Simulation Competence Center: Marcello Gabrielli, EnginSoft m.gabrielli@enginsoft.com

Structural Optimization of the “Tulip” Housing of a Tripod Type Inner CV Joint for the power transmission in a Formula SAE sport car

This research project aims at fully exploiting the potential of Additive Manufacturing technologies in the redesign of a key component of the power transmission of the Formula SAE car of the University of Padova. The most suitable geometrical configuration is identified through Genesis GTAM, which is a topological optimizer with advanced algorithms for several manufacturing processes (including Additive Manufacturing). The geometry is then refined by performing a standard optimization, where the modeFRONTIER optimizer drives a parametrized FEA model created in ANSYS Workbench. Mass minimisation, while maintaining both static and fatigue strength, are the objective and the constraints, respectively. Further to the design phase, the component is additively manufactured. Finally, the prototype will be tested at the test bench at the University of Padova by applying the spectrum loading acquired on the track.

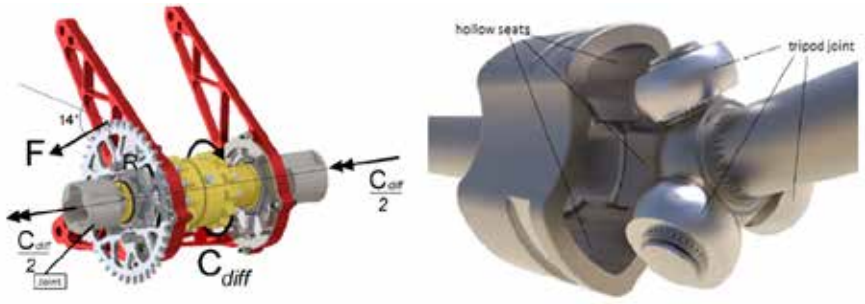

Figure 1 –Loads applied to the joint when it is coupled with the differential and constraint system of the joint-tripod assembly

Introduction

Although the proposed approach is general and applicable to any mechanical component, this study focuses on the shape optimization of the tulip housing of a tripod type CV joint. Two of these joints are mounted on the rear axle of a Formula-SAE sport car to transfer the power from the gearbox to the wheels. The

project has started from the component, which was designed for the last season (2017 model car).
As shown in Figure 1, the CV joint consists of a tripod joint, made of three balls lodged on bearings, which is inserted into a "tulip" shaped housing. This scheme of constraints allows to decouple the bending and shear stresses between the joint and the axle. As a result, the two halves of the joint and the shaft are mainly subjected to pure torsion load.

The baseline joint, which was mounted on the 2017 Formula-SAE UNIPD car, was made of Ti6Al4V titanium alloy and manufactured by additive process. However, the shape of the existing components has not been optimized to exploit the opportunities given by additive manufacturing. This recent manufacturing approach has almost no constraints, giving the designer the possibility to define free-forms that could not be obtained with any other traditional method. The goal of this project is to demonstrate that through advanced design tools it becomes possible to really exploit this freedom, leading to a significant improvement of the parts. In particular, two different optimization techniques are applied in sequence.
The project started with a wide research about the mechanical properties and behavior of additively manufactured specimens (which are still quite uncommon in literature). Material data, together with load specifications, are the fundamental pieces of information for a reliable structural optimization.

The best shape for the tulip housing is searched by means of the GTAM software, developed by VR&D. GTAM is a structural topology optimizer that plays with Finite Element Models to obtain given objectives, while respecting given constraints. In order to carry out this task, GTAM is connected to a FE model of the tulip housing, fully built in ANSYS Workbench. The optimization is run with the aim to minimize the component mass, while satisfying the material strength and providing a reasonable torsional stiffness. The topology optimizer creates parts where the shape given to the material is tailored to the stress flows, so that that less participating material portions are removed. At the same time, the algorithm forces the shape to be easily engineered for later manufacturing.
Once the shape is defined, a second optimization process is used to refine the result and further improve the structure layout. The output of GTAM is engineered and transformed into a parametric CAD in ANSYS Workbench. Parameters are applied to some fillet radii, wall thicknesses, draft angles and so on. Such CAD is finally used to create a new FE model, which is completely manageable by a multi-objective optimizer such as modeFRONTIER, developed by ESTECO. Once again, the optimization process is asked to reduce the overall mass, while satisfying all stress and stiffness constraints. The difference with the topology optimization is that modeFRONTIER does not change the shape, but adjusts the shape that was previously identified by GTAM.

The new tulip housing will be printed by Sisma SpA using a Ti6Al4V titanium alloy. At the end, the component will be also tested in laboratory, by applying the load histories of a track lap recorded in field in a previous work.
In the following paragraphs, all design phases will be described.

Analysis and simulation of the actual joint configuration

The idea of pursuing a great mass reduction, by exploiting the advantages of additive manufacturing process, implicates the search of a well-supported literature background for the mechanical characterization of additively manufactured components. Several studies focus on the process parameters optimization, while fewer ones investigate the fatigue strength of AM specimens. In particular, a study performed by M. Benedetti et Al investigates the effects of surface roughness on the fatigue life of Ti6Al4V "as-built" specimens. This study individuates 400 MPa (maximum stress value) as fatigue limit. In another paper, H. Gong et Al individuate 350 MPa for specimens in "as-built" conditions and 400 MPa for "stress relieved" as built surface conditions. All of the literature sources suggest using 400 MPa as high cycle reference fatigue strength, for the chosen titanium alloy. The fatigue criteria will be on the maximum principal stress. The maximum torsional load to apply is derived from road data acquisitions carried out with the 2017 Formula SAE car. The worst situation occurs in first-gear, at maximum acceleration, when the tire suddenly loses and then retrieves adherence on the asphalt. The highest torque used for design purposes is 475 Nm.
Boundary conditions and material properties referenced in the analysis phase are given in Table 1.

Design parameters	
Endurable stress	400 MPa
Maximum torque	475 Nm

Ti6Al4V (additive) properties	
E	106000 MPa
UTS	1270 MPa
Yield Stress	1129 MPa
Hardness HV	384
Fatigue Limit	400 MPa

Table 1 – Summary of material properties and structural design parameters

Static-Structural analysis with ANSYS Workbench

The mechanical analysis starts with a proper defeaturing of the initial geometry. This task is performed with the CAD tool included in ANSYS Workbench. This phase is important to speed up the structural calculations and to provide a suitable starting point for the optimization tasks as well. The simplification of the geometry consists in filling the shaft, removing the teeth at the end of the shaft, and filling the exterior grooves. These operations lead to

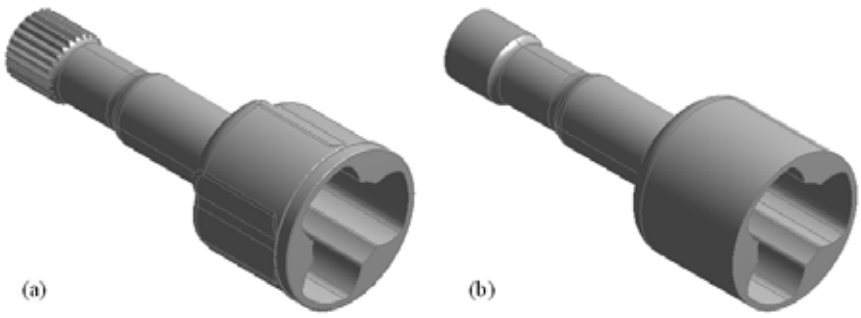

Figure 2 – (a) original CAD model of the joint, (b) defeatured model for both FE analyses and optimization phases

a less detailed geometry and provide a larger continuous material volume for the topology optimization program GTAM, to achieve a more detailed and less constrained solution.
The Figure 2 shows on the left side the original CAD geometry of the component made available by the team of the Formula-SAE project of the University of Padova and on the right side the simplified model prepared for the analysis phase.
After the geometry simplification is completed, material properties and boundary conditions reported in Table 1 are assigned to the part (Figure 3). The torsion moment is applied through the "moment" function of ANSYS Workbench, which applies a number of tangential forces on all surface nodes so that the overall moment is 475 Nm (i.e. the design value). Three "Fixed supports" are set on the contact surfaces between the tulip housing and tripod; the patches are created measuring the hollow seats on the used component.

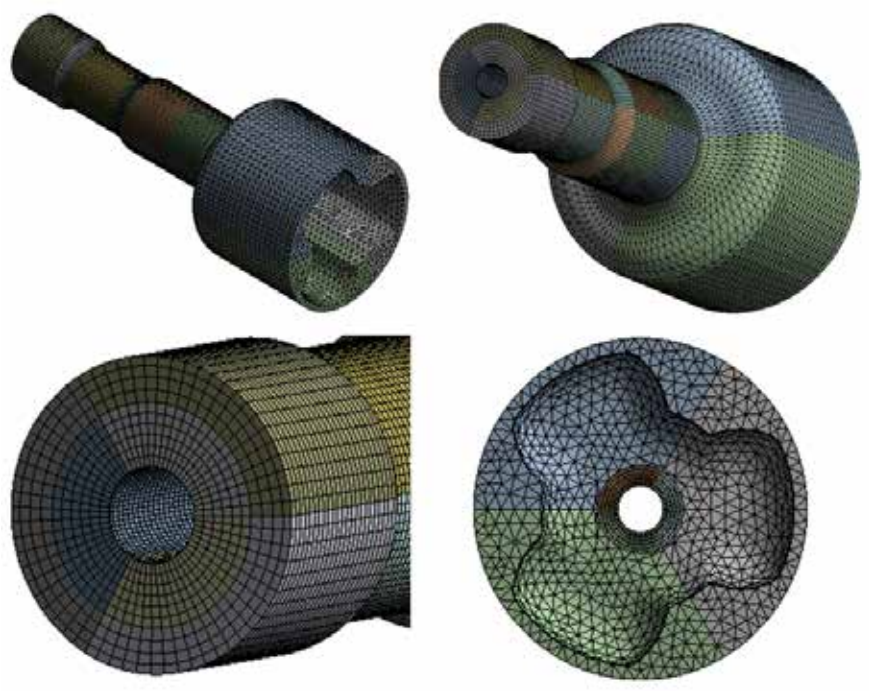

Figure 4 – Component split and accurate meshing (sweep method on most parts)

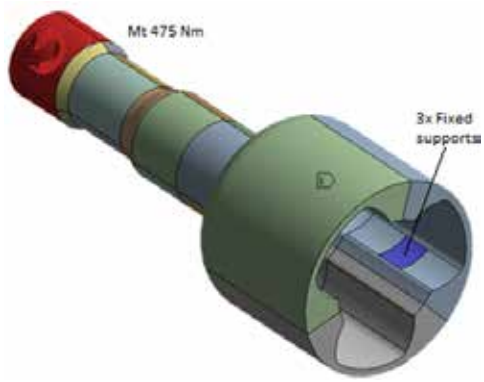

Figure 3 – Boundary conditions for the static-structural model in ANSYS Workbench

In order to guide the meshing phase, the component is split in different sub bodies. First, the shaft is sliced into constant diameter sections. Then, all pieces are split by three, exploiting the 120 degrees symmetry of the joint. This strategy provides an increased number of edges and faces to apply a larger number of mesh controls. Moreover, all smaller pieces, with exception of the tripod seat, can now be discretized by means of swept mesh, which is definitely the most convenient choice. A 1 mm global size control is set on the shaft bodies, while the tulip housing is meshed with tetrahedrons (quadratic) elements using a size of 2 mm. The final FE model consists 343284 nodes and 104424 elements; the mesh is shown in Figure 4.

The results of the static analysis are shown in Figure 5. The quantities extracted from the FE model are the maximum principal stress and the directional displacement, with reference to a cylindrical system, which is coaxial with the shaft. The Y displacements in this reference system coincide with the tangential displacement of the joint, which make it possible to extract the angular deformation of the joint:

$$\alpha\,[deg] = 2\frac{UY}{d}\frac{180}{\pi}$$

where UY is the displacement on the surface and d = 27.94 mm is the diameter of the extremity. The torsional stiffness can be evaluated easily as follows:

$$Kt(joint) = \frac{Mt}{\alpha}$$

Where Mt is the torque applied and α is the torsional deformation. The joint is connected to the transmission shaft, whose torsional stiffness is given by:

$$Kt(axle) = \frac{G \cdot Jp}{l}$$

where G = 40610 MPa is the shear modulus of the Titanium alloy of the transmission shaft, Jp = 22596 mm⁴ is the polar moment of inertia of the shaft section, and l = 470 mm is the length of the shaft. The calculation leads to an overall shaft stiffness of Kt(axle) = 34.07 Nm/deg.

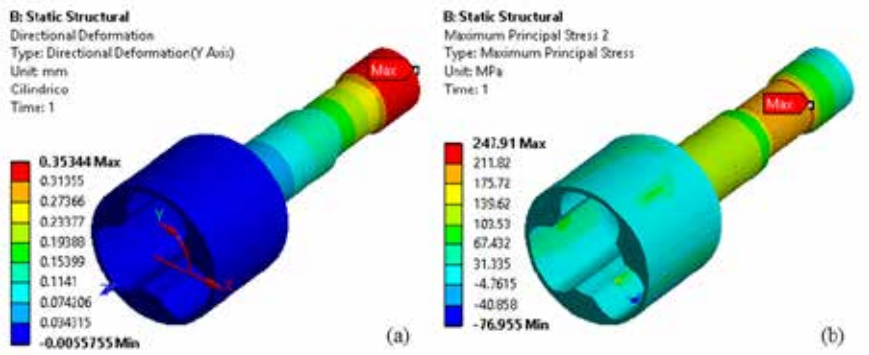

Figure 5 – FE results: (a) Hoop displacements in the cylindrical coordinate system, (b) Maximum principal stress

Table 2	
Maximum principal stress	248 MPa
Maximum directional displacement (UY)	0.35 mm
Joint stiffness Kt (joint)	325 Nm/deg
Shaft stiffness Kt (axle)	34.1 Nm/deg
Fatigue Limit	400 MPa

Table 2 – Summary of the numerical results obtained from the simulation in ANSYS Workbench

Table 2 clearly shows that the tulip housing of the CV joint is about 10 times stiffer than the transmission shaft. Since the two components are connected in series, the overall stiffness of the transmission is mainly governed by the shaft. Therefore, the stiffness of the joint is not a relevant parameter to be considered in the optimization process, at least within certain limits. It will be evaluated for completeness of the design and just to monitor the overall structural response.

Topology optimization with GTAM

Topology optimization aims to determine the optimum morphology of the component by removing those elements which are not necessary for the application. The algorithm of the topology optimizer searches for maximum (or minimum) of an objective function F(x) built from a design variable x. In particular, the design variable can be the normalized density x of each Finite Element in the mesh, which can assume any value in the continuous range [0;1]. When x = 0, the element no longer exists, whereas, when x = 1, the element is fully dense.

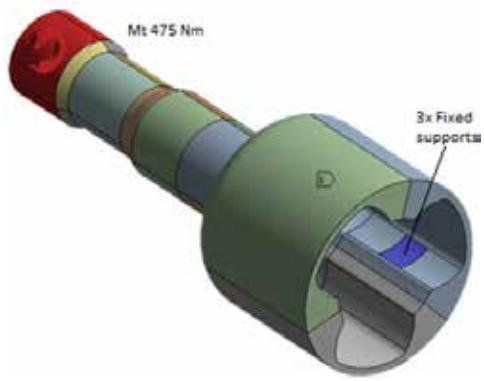

Figure 6 – Regions (domains) specified for the topology optimization phase

Topology region	Objective	Constraint 1	Constraint 2
1	Minimize Strain Energy	Final mass > 30% of initial mass	Maximum Principal Stress < 400 MPa
2	Minimize Strain Energy Minimize Mass	Maximum Principal Stress < 400 MPa	--
3	Minimize Strain Energy, Minimize Mass	Maximum Principal Stress < 400 MPa	--
4	Minimize Strain Energy	Final mass > 10% of initial mass	Maximum Principal Stress < 400 MPa

Table 3 – Definition of objectives and constraints for each topology region in GTAM®

The design variable x can be used to build a complex objective function that combines both the density and the Young's modulus of each element in the design space (design based method).

$$E(x) = E_{min} + (E_0 - E_{min})\, x^{RV1}$$

$$\rho(x) = \rho_0\, x$$

where: E(x) is the Young's modulus of the element, E_0 is the initial Young's modulus, E_{min} is the minimum value for the Young's modulus, RV1 is a real user defined value (typically $2<RV1<3$), p(x) is the actual element density, p_0 is the initial density, and x is the topology design variable ($0 \leq x \leq 1$) that governs both the density of the element and the Young's modulus.
The minimization (or maximization) of the objective function $F(E(x),p(x))=F(x)$ is performed by satisfying a number M of constraints that depend on the chosen manufacturing process and any other boundary condition that is set a priori.
$g_j(x) \leq 0 \quad j=1,M$

$g_j(x)$ is a constraint inequality be respected.
The definition of the optimization problem in GTAM is fully assisted by the graphical interface, which is completely integrated in ANSYS Workbench. In particular, the user is requested to set the following entities:

- Topology region: Volume (domain) for the optimizer, defined by a body in ANSYS Workbench;
- Objective: Function to be minimize or maximize;
- Constraint: Inequality representing a limit for the optimizer that must be respected.

For our project, we have defined the topological optimization on 4 different regions, by assigning different objectives and constraints for each of them. Since the mesh is continuous between the bodies, the result will be coherent and consistent in any case. The chosen domains are shown in Figure 6, while the optimization criteria are summarized in Table 3.
The load case for the topology optimization is the same previously used for the static structural analysis. In addition to loads and external constraints, the optimization problem requires to define further constraints. In particular, it is necessary to prevent the optimizer from changing the geometrical features that govern the assembly possibility of the system. For this reason, some "frozen regions" have been specified. The first constraint has been placed over the external surface of region 3, to keep the bearing mounts. The second constraint has been defined over the hollow seats of the zone 4, to keep the interface with the tripod joint. A further constraint has been defined inside the spline pin, to avoid the creation of an undesired internal shoulder at the junction between spline pin and tulip housing.
The default settings of the optimizer are set into the "analysis setting" panel of GTAM (max 15 iterations with a soft convergence rule). Simulations have been completed after 48 hours of CPU time (on a simple Windows workstation).

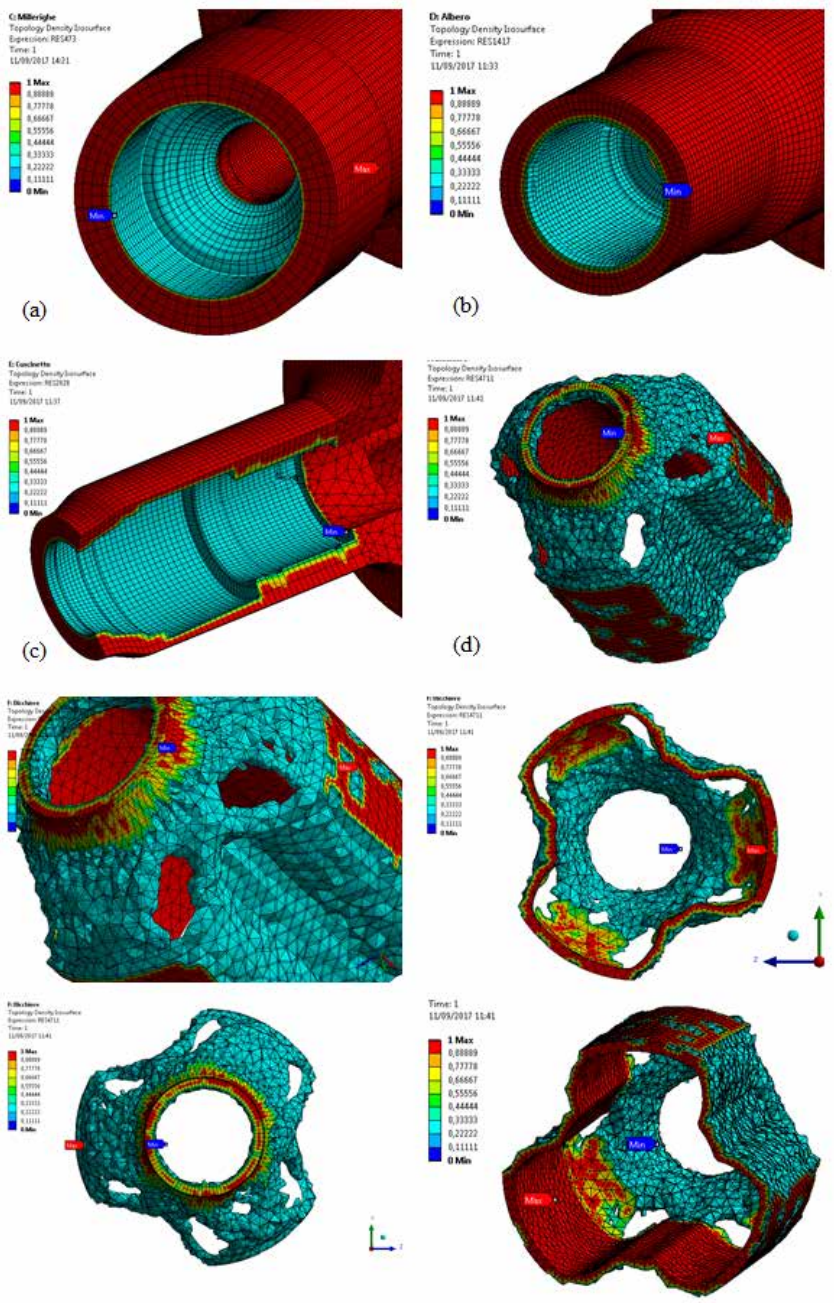

Figure 7 – Results of the topology optimization: (a) is the spline pin zone, (b) zone (2), (c) zone of the external, (d) tripod joint seat

The results of the topology optimization can be presented by using the "density iso-surface" command, selecting the capped iso-surface mode and setting a cut-off value of 0.3 for the element density. The Figure 7 highlights in red the full material zone and the frozen surfaces, while other colors show the elements with normalized density $x > 0.3$.
The volume of material "saved" by the optimizer can also be exported through the "export coarsened surface" command. However, since the optimization is based on activation and deactivation of mesh elements, the exported object will be an irregular STL file. This aspect highlights the need of well refined mesh to allow a better quality of the result.
While running the preliminary simulations, the sensitivity of GTAM to load boundary conditions could be appreciated. If the torque is applied through four lumped forces, then the optimizer identifies four main ribs where stresses coming from points of load application are conveyed. On the contrary, if the torque is distributed over the entire surface (which is more realistic, because the toothed joint is designed for this purpose), then the result complies with axial symmetry.
The final result of the topology optimization indicates how the part has to be shaped to better use the material capabilities. At the moment, the technology is not yet capable of generating a real CAD file from the saved elements. Therefore, the user must build a new CAD from scratch by combining the outputs of GTAM and any other remark given by the manufacturer of the real component (which has to be involved at this stage).

Although consistent in an engineering sense, the results given by the topology optimizer are very difficult to be foreseen in advance. The mass reduction has been achieved with a strong reduction of thicknesses. In particular, in zone (1), GTAM draws an internal cone with decreasing diameter going from outside to inside. This is clearly caused by the increasing torsional moment transferred by the external teeth to the shaft. In zone (2) and (3), the great reduction of material is mainly due to a reshape of the internal profile of the hole. However, the most impressive solution is in zone (4), where the minimization of the mass leads to the creation of holes, having circular symmetry. In order to keep adequate resistance of the part, GTAM places some cross shaped reinforcements between the holes, creating an amazing new geometry. The final shape of the component can be built only through an additive manufacturing process.

Parametric optimization with modeFRONTIER

Since the topology optimization does not deliver a CAD model, it must be reconstructed by hand. The level of detail given by GTAM's output was not enough fine to size some geometric entities such as transition radii, thicknesses and angles. Therefore, it was decided to keep these quantities as free parameters in the new CAD, in order to make a further refinement step possible. The final optimization task has been driven by modeFRONTIER software, developed by ESTECO, which is a general-purpose multi-objective optimizer. Once connected with ANSYS Workbench, modeFRONTIER adjusts the specified parameters (i.e. the geometrical unknowns) to either minimize or maximize given performance indexes (i.e. mass), while fulfilling assigned constraints (i.e. maximum stress). For our specific needs, the Multi-Objective-Genetic-Algorithm was chosen from modeFRONTIER's library. This algorithm starts from a population of designs generated by an initial Design of Experiments and then generates new populations of designs whose

performances move towards the assigned criteria [10]. At the end of the process, modeFRONTIER generates a family of optimal solutions (depending on the number of objectives), which are called all together Pareto's Frontier.

Geometry reconstruction phase and parametric model creation

The original CAD model of the joint is modified using the GTAM solution as a guideline. The rough STL file exported from GTAM is imported into ANSYS Workbench Design Modeler as a reference geometry. The new CAD is then built by sketching over the imported mesh, as shown in Figure 8.

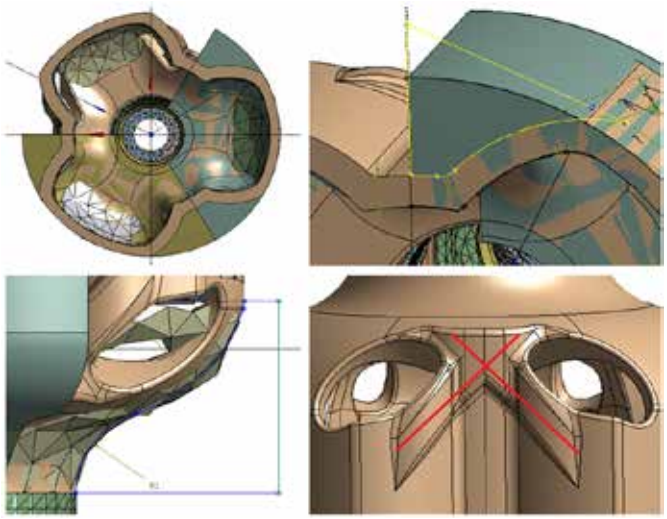

Figure 8 – Engineering geometry definition starting from the GTAM output to create the new parameterized geometry

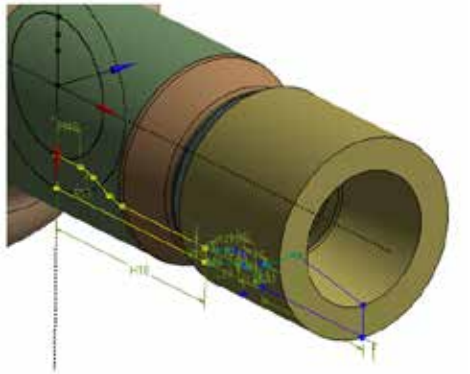

Figure 9 – Reconstruction of the geometry of zones (1), (2), (3) and definition of the parametric sketch in Design Modeler

While the region (4) requires advanced CAD techniques to copy the free-form geometries, the remaining part of the component can be rebuilt by revolving a parametric sketch of the inner hole (Figure 9). This is indeed the zone where modeFRONTIER will optimize the unknown parameters. The region (4) is excluded from the refined optimization phase because the output obtained from GTAM is considered to be already structurally efficient and because of the need for reducing the time involved in free-form parametric CAD definition. The parameters included in the refinement are shown in Figure 10 and summarized in Table 4.

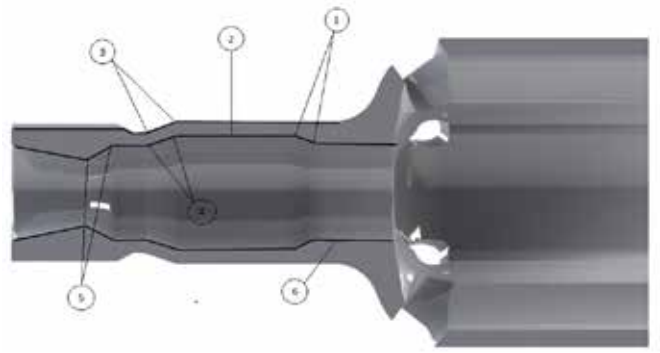

Figure 10 – Optimization parameters for modeFRONTIER

ID N°	Parameters	Min	Max	Step
1	R external bearing zone	3	12	0.5
2	Thickness external bearing zone	2	3.5	0.25
3	R ext external bearing zone	1	9	0.5
4	R int external bearing zone	1	6	0.5
5	R blend spline pin	1	5	0.5
6	L horizontal length inside zone (3)	1	10	0.5

Table 4 – Parameters and design space for the optimization phase with modeFRONTIER

The optimized solution of the component was agreed with Sisma SpA, in order to meet all of the manufacturing limitations. First, all 90° shoulders are removed, because building direction is axial. Second, the component is shortened with respect to its initial length (170 mm), because the working volume of the MySynt100 machine is 100 mm in width and 130 mm in height. To achieve this mandatory criterion, the connection between the spline pin and the external bearing rolling surface is removed. However, the final model still maintains the geometrical features of the original one, since the removed part has a uniform cross section. The shortened model height is about 127 millimeters, with a maximum cross section of 61 millimeters (base diameter).

Optimization settings and results

The output variables extracted from the FE model to manage the optimization are the Maximum Principal Stress (to be minimized and constrained to not exceed 400 MPa), the overall mass (to be minimized) and the tangential displacement (to monitor the torsional stiffness). The connection of modeFRONTIER to ANSYS Workbench is straightforward, since modeFRONTIER includes a dedicated node that automatically recognizes input and output parameters of ANSYS Workbench.

Output Parameters	Objective	Constraint
Maximum Principal Stress	Minimize	< 400 MPa
Mass	Minimize	----------

Table 5 – Summary of objectives and constraints for the optimization phase

Once input variables (geometrical parameters) and output variables (objectives and constraints) are set, the optimization process can be started. First, a population of designs is generated to train the

Genetic Algorithms to the sensitivity of results with respect to the input parameters. The size of the Design of Experiments is calculated with a rule of thumb:
DOE size = 2 × (N inputs × N objectives) = 2 × (9 × 2) = 36 -> 35

DOE designs are generated through SOBOL algorithm, which is a pseudo-random algorithm of filling the variable's space with a given number of designs. The optimization process has been entrusted to a MOGA II algorithm, which creates many generations of designs with same size of the DOE. In each generation, the algorithm capitalizes the information from the previous generations and move towards the requested objectives. Although the maximum number of generations was set to 100, significant results become available after 20 generations (610 designs evaluated); calculation time was 50 hours on a regular workstation. As expected, not all the generated designs were valid: only a percentage of about 35% met the imposed stress constraint. However, a significant Pareto Front was outlined, making possible to choose an optimal solution (see Figure 11 and Table 6).

ID 593	Input var.	Value	Output var.	Value
1	R blend external bearing zone	12 mm	Stress (max)	397 MPa
2	Thickness external bearing zone	3 mm	Mass	0.251 kg
3	R ext external bearing zone	9 mm	Stifness (max)	392.5 Nm/ deg
4	R int external bearing zone	3 mm		
5	R blend spline pin	2.5 mm		
6	L horizontal lenght inside zone (3)	1.5 mm		

Table 6 – Parameters of the optimum design after the modeFRONTIER optimization phase

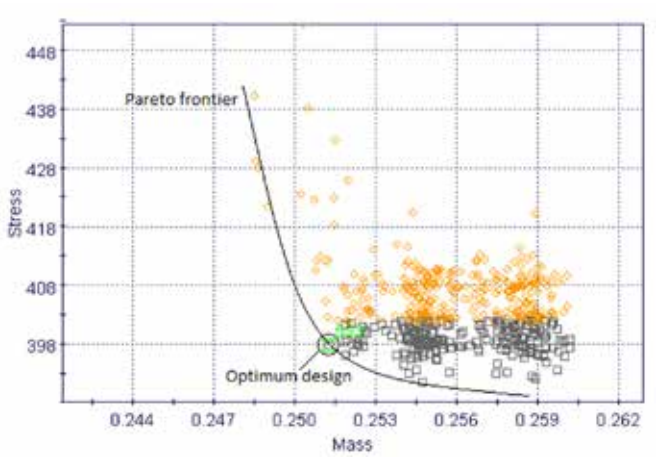

Figure 11 – Scatter plot of the two objective Mass minimization and Stress minimization. Pareto Frontier is well outlined and the optimum design n°593 is highlighted.

GTAM and modeFRONTIER proved to be complementary tools: the first to identify the shape from scratch, the second to refine the optimization starting from an engineered design. Moreover, both tools are easily integrated with ANSYS Workbench, implying a fast set up and solution of the optimization tasks.

In this project, the innovative design approach has led to an impressive 43.6% mass reduction of the component, while complying with all of the maximum stress constraints. The optimized design solution will be additively manufactured and tested in the laboratory, by applying the load history from telemetry data acquisition in the track. In case the tests confirm the numerical results, the methodology described in this paper sets new frontiers in the design of automotive components, even for the most demanding applications.

Conclusions

Topology and parametric optimization techniques, sinergically combined, have been found to be suitable for weight reduction of components manufactured by additive processes. These advanced design methods, which relies on optimization algorithms and Finite Elements models, make possible to fully exploit the design freedom that is implicitly made available by additive manufacturing processes.

Riccardo Morandini, Giovanni Meneghetti
University of Padova, Department of Industrial Engineering
Fabiano Maggio, Federico Andrea Bologna - EnginSoft
Adriano Bernardi - Sisma

For more information:
Federico Andrea Bologna, EnginSoft
f.bologna@enginsoft.com

Figure 12 - Results of the topology optimization

Optimizing a perfect race engine.

ESTECO Academy Design Competition winner

modeFRONTIER enabled Michael Bambula of the University of Florida to run the workflow, integrate third-party software, automate the design exploration process and perform post-process analysis

The winner, Michael Bambula of the University of Florida, presented a top-notch design project, in which he achieved significant performance improvements (64.2 hp @16500 rpm) while developing a complete model for a Moto3 bike and realistic simulations that also considered the specifics of the race track. Organized in partnership with Aprilia Racing and Gamma Technologies, the competition was open to teams of undergraduate and graduate engineering students. The challenge was to improve the design of a 4 stroke single cylinder engine through multidisciplinary optimization (using modeFRONTIER) and 1-D simulation of the engine system with GT-SUITE. The competition award included an internship opportunity at the APRILIA Racing team, which counts several World Championship Awards.

The goal of the project was to maximize engine power. Due to the constrained engine architecture, an optimization of the Intake/Exhaust system was performed. Gamma Technologies supplied a set of simulation tools (GT-Suite) to develop the 1-D model of the high-performance engine.

Various aspects of the base engine architecture were constrained such as Bore, Stroke, Con Rod Length, Engine Speed, Max Valve Diameters, Max Valve Lift, Max Throttle Diameter, Max Compression Ratio, Non-variable Cam Timing, and Naturally Aspirated. Considering these constraints, the optimization of the cylinder filling (Wave Dynamics) was seen as the logical design direction.

modeFRONTIER workflow was used to automate the design exploration process and integrate Excel and GT-Suite for computing lifts value intake and exhaust valve lift profiles and simulating the engine power output.

During the development of the 1-D Engine Model there were inherently many unknowns, therefore Michael made assumptions supported by rigorous research. The design variables related to the intake/exhaust system were automatically found by modeFRONTIER to optimize the output results: sum of engine power across engine speeds speeds from lowest to highest respectively (11500 rpm to 17500 rpm). “modeFRONTIER ran 1000 different designs that varied the input parameters.

The Hybrid Algorithm did an amazing job at finding the optimum solutions based on the objective of maximizing the engine power” said Michael Bambula, University of Florida Racing Team.

“The analysis went beyond just determining the most powerful engine”, continued Bambula, “in fact the final objective, aimed at determining whether a certain design is sufficient for motorsports, was to compare it to lap times. This is why it was decided that the final group of optimum results from modeFRONTIER would be simulated in OptimumLap software considering, among other assumptions, a Moto3 motorcycle model traversing the Phillip Island Grand Prix Circuit in Australia”.

MICHAEL BAMBULA (KYLE BEGGS TEAM, UNIVERSITY OF FLORIDA)

Michael Bambula was born in Fürth, Germany and initially moved to the Bahamas and then to South Florida with his twin brother Alex and mother Karin. He completed his Bachelors of Science in Mechanical Engineering with a focus on Energy Systems at the University of Central Florida in Orlando, Florida. During his time there he was heavily involved in the Formula SAE team; helping to design Brakes, Drivetrain, and Powertrain systems. He eventually managed the team in the 2014 - 2015 season to 2 national competitions. Michael is currently pursuing his Masters of Science in Mechanical Engineering with a focus on Thermal Sciences and Fluid Dynamics at the University of Florida while working in the Systems Analysis Team at Cummins Inc.

Cone-Meter Performance Optimization Through a CFD-Experimental Approach

V-cone flow meters are widely adopted due to their many advantages, as a wide rangeability and a low sensitivity to vibration, and are suitable for many types of fluids and two-phase flows. The actual reference standard prescribes geometric, installation and operating procedures for V-cone meter measurements in ducts and calibration instructions with specific ranges of main geometric and operating parameters. To overcome the limitations of the standard and better adapt the geometry to the requirements of an industrial application, a design optimization of a V-cone meter has been done through a combined numerical and experimental approach. The numerical model has been validated against wind tunnel tests on a scale model. A CFD analysis on the modified-to-standard configuration leaded to the calibration relation of the measuring device. Results have shown a good accuracy of the calibration formulas and an appreciable rangebility of the cone meter in the proposed configuration.

Introduction

The cone-meter, better known as V-cone, is a differential pressure device originally introduced by McCrometer Inc. and has been increasingly adopted for flow rate measurement in industrial application. It consists of a bi-conic shape body coaxially inserted within the pipe, its obstruction generating a reduced cross section and a consequent pressure decrease. In the standard configuration, pressure tappings are located upstream by the device, flush on pipe wall, and downstream on the back face of the cone (Figure 1). Limited pressure losses, applicability to a wide range of working fluids (even two-phase), good resistance to wear and high turndown ratio have been promoting V-cone applicability to many industrial scenarios. Moreover, moderate perturbation is generated on the main flow as a consequence of cone meter installation and limited effect of upstream elbows has been observed.

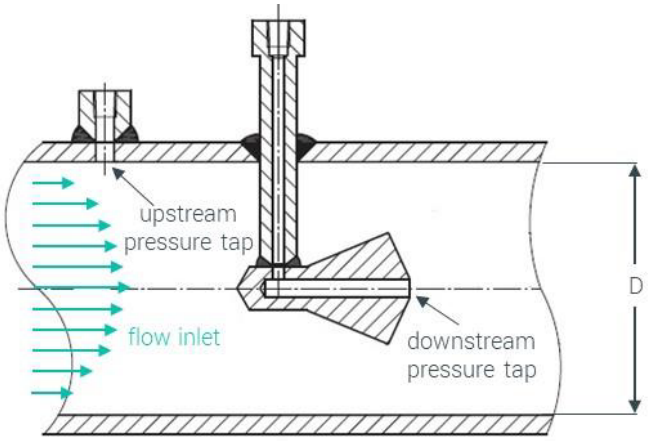

Figure 1 - Geometric scheme representative of a standard cone-meter

Guidelines on device geometry and method of use has been recently issued through standard ISO 5167-5:2016, this prescribing also the instrument formulation and its range of applicability in terms of main dimensional and operating parameters, i.e. pipe diameter D, diameter ratio β and Reynolds number Re. Alternative geometries of the cone meter are also admitted by the reference standard whether appropriate calibration is handled.

BONO ENERGIA S.p.A. is adopting V-cone within its product portfolio for flow measurement in many operating conditions, including small to large Re, single and two phase flows, different kind of fluids. V-cone appears to be a suitable choice for flow measurement according to these prerequisites, but some amendments has been envisaged to the standard configuration. Specifically, the downstream pressure tapping will be flush mounted on the pipe wall and the device geometry will be optimized according to the installation and usage needs. A proper calibration is therefore necessary in such new configuration.

At this scope, ASTARTE has been asked to design, test and calibrate the new cone-meter by means of a coupled numerical/experimental approach. The commercial CFD code Ansys Fluent has been used for the definition of a numerical procedure to be applied for the calibration of the modified layout. In this framework, as a first step, a campaign of fluid-dynamic simulations on the cone-meter in the standard configuration has been performed in order to replicate the experimental tests reported by the international literature [6], and according to the same procedure adopted by the standard for cone-meter calibration. Once the numerical procedure has been validated, the same CFD model was applied to the modified layout and the corresponding calibration curves have been obtained.

Furthermore, several tests have been conducted in the low-speed wind tunnel of the Cagliari University, at the Department of Mechanical, Chemical and Materials Engineering (D.I.M.C.M.). The results confirmed the validity of the calibration curves of the new cone-meter configuration, and comparison with CFD data, showed the good accuracy of the numerical model. The present approach allowed to obtain a validated numerical tool to be applied for calibration and analysis of cone-meters in different layout and operating conditions, together with a significant reduction of experimental activities.

Numerical calibration of the modified cone-meter

The mass flow rate (q_m) in a pipe can be measured through a cone-meter by relating the pressure readings of the upstream and downstream pressure tappings (Δp) and the inflow density (ρ_1) with the discharge coefficient (C) and the expansion factor (ε):

$$q_m = \frac{C}{\sqrt{1-\beta^4}} \varepsilon \frac{\pi}{4} (D\beta)^2 \sqrt{2\Delta p\, \rho_1}$$

The reference standard indicates how to evaluate the parameters ε and C for the standard positioning of the upstream and downstream tappings and for pipe diameters below 500mm. More in the detail, ε is a correction factor used to take into account for the compressibility of the fluid. It can be derived from the upstream pressure p1 and the pressure drop Δp, by means of an empirical equation (Eq. 2) which includes the two coefficients a and b:

$$\varepsilon = 1 - (a + b\beta^4)\frac{\Delta p}{k p_1}$$

Test #	Diameter (inch)	β	Mass flow rate (kg/s)	Re	Pressure outlet values adopted in CFD simulations (kPa)	
1	6	0.75	1	$0.5{\cdot}10^6$	min	max
2	6	0.55	1	$0.5{\cdot}10^6$	30	250
3	6	0.45	1	$0.5{\cdot}10^6$	30	250
4	6	0.45	0.5	$0.25{\cdot}10^6$	30	250
5	4	0.55	0.66	$0.5{\cdot}10^6$	0	250
6	4	0.55	0.33	$0.5{\cdot}10^6$	0	150
7	4	0.65	0.66	$0.5{\cdot}10^6$	-10	80
8	4	0.65	0.33	$0.5{\cdot}10^6$	0	100
9	3	0.75	0.5	$0.5{\cdot}10^6$	-10	150

Table 1 - Operating conditions of the calibration tests

Reference data

For the standard cone-meter, the a and b values have been estimated on the base of numerous flow rate measurements (a_{EXP}, b_{EXP}) with constant Re, obtained through an experimental test campaign with air (Table 1):
a_{EXP}=0.649; b_{EXP}=0.696

Nevertheless, Eq. 2 is valid for any kind of fluid provided that the corresponding isentropic coefficient k is known and $p_2/p_1 \geq 0.75$ is satisfied.

However, the geometric and installation conditions defined by the standard are not consistent with the configuration proposed by BONO ENERGIA S.p.A. A campaign of CFD simulations have been performed within the present work, on the same operating conditions of the reference tests reported in Table 1. The scope was to define and validate a numerical model able to fully replicate the experiments and to represent the basis of a numerical procedure for the cone-meter calibration in the new proposed configuration.

Numerical study

The CFD simulations have been performed by means of the commercial code ANSYS Fluent on a 2D axisymmetric domain representative of an axial section of the standard cone-meter. Two straight pipe sections, 10 x D long, have been also included upstream and downstream of the instrument, thus reducing the influence of the boundaries on the flow field close to the device. The supporting structure of the cone has been omitted to the benefit of a geometrical model simplification. The influence of such simplification on the solution accuracy has been then evaluated by comparison against experimental data. Figure 2 shows a schematic representation of the typical geometrical domain and of the main boundary conditions adopted.

The upstream and downstream straight pipe sections have been discretized by means of a totally structured computational grid with rectangular cells, while a hybrid mesh has been adopted for the geometrical region close to the cone-meter. This latter one has been subdivided in a structured region near the pipe wall, to better solve the boundary layer, and in an inner unstructured region with triangular cells (Figure 3).

A steady state CFD simulation has been performed for each of the reference tests of Table 1, with the corresponding mass flow rate of air (ideal gas at 300K) at the inlet. A pressure outlet condition has been imposed at the domain exit, whose value has been changed within the ranges reported in Table 1. The 2D axisymmetric form of the governing equations has been solved, while the Realizable k-ε model has been

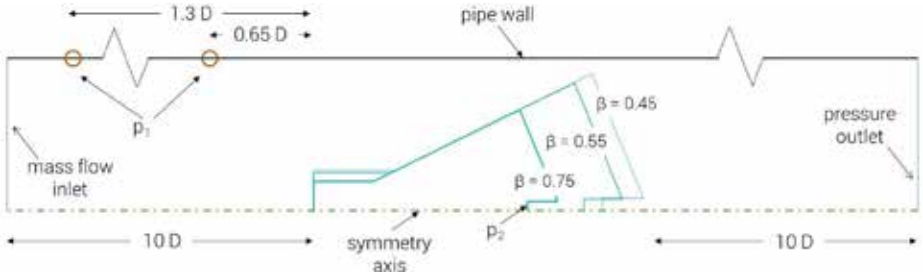

Figure 2 – Geometrical domain and boundary conditions

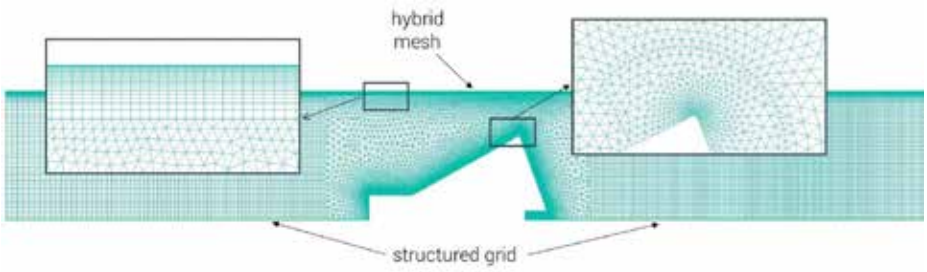

Figure 3 - Typical computational grid

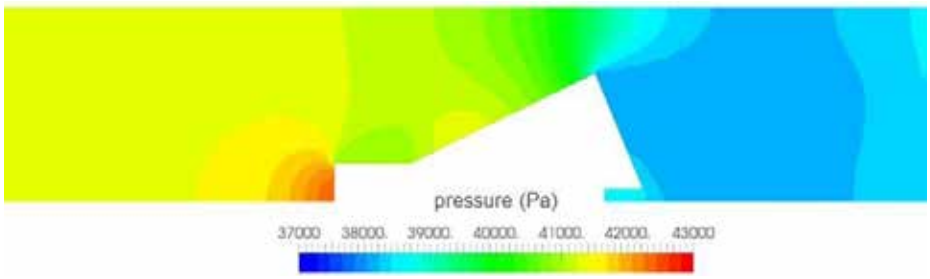

Figure 4 - Pressure field surrounding the cone-meter predicted by the simulation of the test 1 (D = 6in, β = 0.75, p_{out} = 40 kPa)

adopted for the turbulence together with the Enhanced Wall Treatment, to better estimate the flow on the wall.
A typical pressure field generated by the presence of the cone-meter in an unperturbed flow stream is reported in Figure 4, as predicted by the simulation of the test 1 (D = 6in, β = 0.75, p_{out} = 40 kPa). Potential flow effects are generated from the interaction between the air flow and the device, which lead to a static pressure decrease already before the geometric reduced cross section.

According to the experimental procedure of the cone-meter calibration, the term C·ε in Eq. 1 has been estimated from the results of each simulation at the different operating pressures, and tabulated as function of $\Delta p/k \cdot p_1$. After a grid sensitivity analysis, the comparison between the numerical and the experimental C·ε curves demonstrated the good accuracy of the CFD result and confirmed the possibility to use the simulations as alternative to the experiments for instrument calibration. As an example, the diagram of Figure 5 a) reports the CFD results of test 1, which are in fair agreement with the corresponding experimental measurements (also reported) for the entire interval of pressure considered.
The results provided by the CFD simulations allowed a numerical calibration of the device, and the evaluation of the coefficients a and b of Eq. 2, by means of a fitting procedure:
a_{CFD}=0.694; b_{CFD}=0.655

The ε values for β = 0.75 (test 1) evaluated by means of a_{CFD} and b_{CFD} are compared in Figure 5 b) with those obtained using the coefficients from experimental calibration (a_{EXP} and b_{EXP}). As can be observed, the two corresponding trends are well aligned, with a relative difference that, within the pressure range considered, reaches the maximum value of 0.18% (at $\Delta p/k \cdot p_1$ = 0.0323).

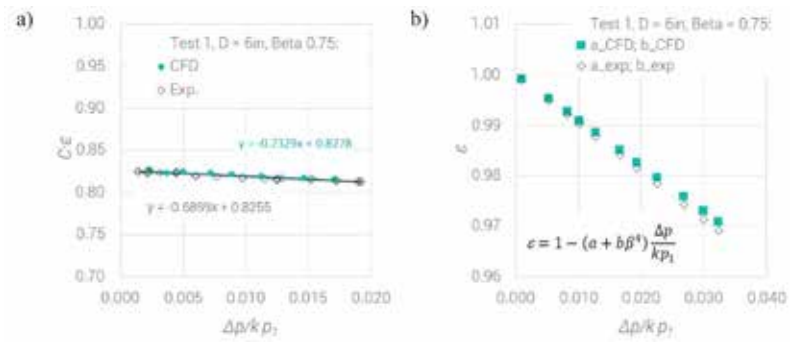

Figure 5 - Test 1, comparison between numerical results and experimental data at the different operating pressure: a) trend of C·ε; b) ε values from formulation

Validation of the procedure on the modified cone-meter

Once the numerical calibration has been built on the reference data, the same procedure has been performed on the modified layout of the cone-meter developed according to BONO ENERGIA S.p.A. requirements. As a result, the values of the coefficients a_{CFD} and b_{CFD} for the new configuration have been obtained, as well as the curve of the discharge coefficient C at different Re (up to $2 \cdot 10^6$). Wind tunnel experimental tests on an in-scale model of the new cone-meter with β = 0.65 have been performed at the Fluid-dynamic laboratory of the Mechanical, Chemical and Materials Department (D.I.M.C.M.) of University of Cagliari. The scope of the tests was to provide further data for the validation of the numerical models defined in the previous phase of the work and to verify the accuracy of the calibration curves obtained through the numerical procedure.

Experimental tests

The test rig consisted of an axial fan connected to a 2500mm long straight pipe (test section, D = 214mm) through a squared flow straightener (h = 550mm), a convergent section and a squared-to-circle joint, Figure 6. The fan was powered by an electric motor with inverter (ABB mod. ACS 300), whose frequency was varied in order to regulate the flow rate of air toward the test section. The cone-meter has been installed within the test section, 1000mm distant from the inlet and aligned to the pipe axis. The body of the cone has been obtained by turning of a unique plastic (PVC) bar, while its support has been made of brass and tightened perpendicularly to the cone noise (Figure 7 a)).

All the pressure tappings of the cone-meter have been placed along the upper generatrix of the pipe. Also, two pressure taps have been mounted in the convergent section of the flow straightener (figure 6), with the scope of evaluating a pressure difference to be correlated to the mass flow in the tunnel. In order to do this, the wind tunnel has been run without the cone-meter, calculating the mass flow rate from the measurement of the velocity profile at the outlet of the duct, by means of an aerodynamic probe. The pressure difference in the convergent section of the straightener has been measured with a Betz micromanometer (with a resolution of 0.2mmH2O), while the pressures in the test section of the wind tunnel have been acquired at the frequency of 1000Hz, using a Validyne P55D differential transducer connected to a National Instrument data acquisition board.
The experimental tests have been conducted at ambient conditions characterized by an atmospheric pressure of 761mmHg (101458.3Pa) and a temperature equal to 20°C. As illustrated before, the air mass flow rate has been regulated by varying the output frequency of the inverter, until the achievement of the target value.
During each test, the pressures has been acquired upstream and downstream of the cone meter as well as close to the outflow section of the wind tunnel, these readings enabled evaluating the pressure difference and loss due to the

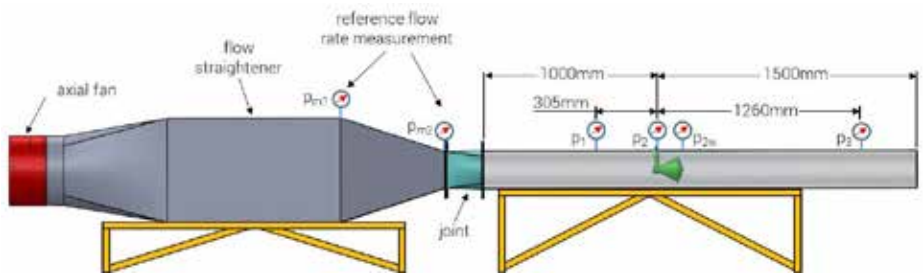

Figure 6 - Experimental rig layout

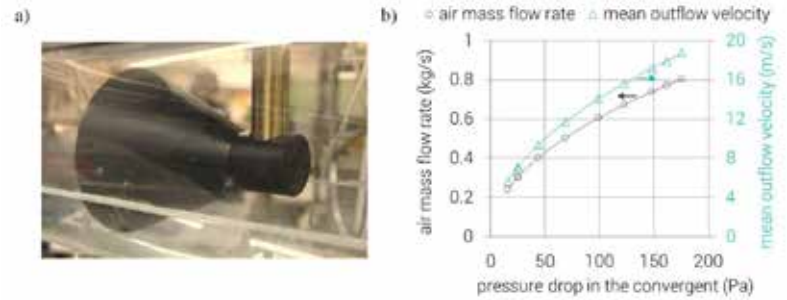

Figure 7 – a) in scale model of the cone-meter used in the experimental tests and b) calibration curves of the wind tunnel

presence of the device. Each measurement consisted of 1s acquisition time, so that the final value arose from the average of 1000 samples.

Accuracy evaluation with experimental data

CFD simulations have been performed reproducing the same conditions of the experimental tests, as reported in Table 2, by adopting a numerical domain which replicates the dimensions of the wind tunnel test section and includes the in-scale model of the cone-meter. Accordingly, computational mesh design undertakes the same settings exploited for the numerical calibration procedure. For each simulation, the corresponding experimental mass flow rate of air has been imposed as boundary condition at the inlet.

Table 2 also reports the main results of the measurements. The mass flow rates have been evaluated through Eq. 1, with the pressure drop measured trough the cone-meter and ε and C obtained from the numerical calibration of the instrument in the new configuration. The comparison between the measured mass flow rate and the effective values shows how the maximum error is equal to 1.6%, observed at the lower mean flow velocities (below 8m/s). The good accuracy of the results constituted a valid confirmation for the developed numerical calibration procedure which, therefore, could represent a better cost-and-time-effective alternative to the experimental testing.

A further comparison between numerical and experimental data is shown in the diagram of Figure 8 a), where the values of the upstream pressure p_1 are reported as function of the squared inflow velocity. Both experimental test and numerical simulations provided upstream pressure values which linearly increase with the squared inlet velocity, according to the governing equations for incompressible flows. Moreover, there is a good correlation between experimental and numerical data within the entire range of velocity observed. Figure 8 b) reports the evolution of the pressure drop through the cone-meter (Δp_{12}) and the pressure loss (Δp_{loss}) for the different inflow velocity, both of them reported to the absolute inlet pressure p_1. The good agreement between the experimental data and the numerical results is confirmed and the global trend of the two variables is aligned with the behavior of a standard cone-meter with $\beta = 0.65$.

Conclusions

A combined numerical/experimental approach has been adopted for the set-up of a calibration procedure for cone-meter in non-standard geometrical configuration and operating conditions. At this scope, a specific numerical model has been developed and validated against experimental data. The CFD model has been applied for the calibration of a new V-cone layout which may better fit the installation and operating needs of BONO ENERGIA S.p.A.. The resulting calibration curves allow to estimate the flow rate with an accuracy higher than 98%, as measured in a devoted experimental campaign conducted in the low-speed wind tunnel of the Cagliari University, at the Department of Mechanical, Chemical and Materials Engineering (D.I.M.C.M.).

The developed numerical tool is therefore applicable for calibration and analyses of cone-meters in different layout and operating conditions, allowing a significant reduction of experimental activities.

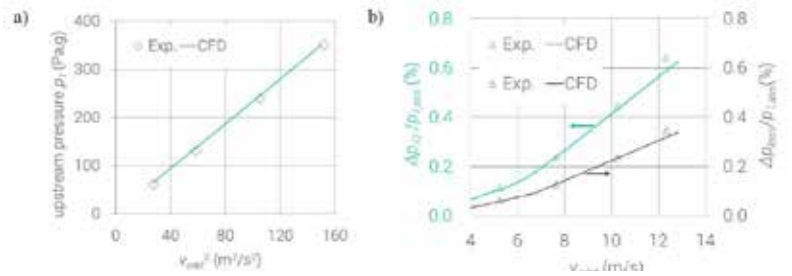

Figure 8 – comparison between experimental data and numerical results: a) upstream pressure as function of the squared velocity inlet and b) pressure drop through the cone and pressure loss as function of the velocity inlet

Test #	Inverter frequency	Δp in the convergent	Mean flow velocity	Re	Mass flow rate		
					effective	measured	rel. error
	Hz	Pa	m/s	-	Kg/s		%
E-1	50.0	76.7	12.3	$1.74 \cdot 10^5$	0.533	0.537	0.7
E-2	41.3	53.0	10.3	$1.45 \cdot 10^5$	0.443	0.443	0.03
E-3	30.6	29.4	7.7	$1.08 \cdot 10^5$	0.331	0.326	-1.6
E-4	21.4	13.7	5.2	$7.41 \cdot 10^4$	0.227	0.223	-1.6

Table 2 - Operating conditions of the experimental tests and mass flow measurements

Marco Bertoli, Giorgio Melis, Francesco Cambuli
Astarte Strategies S.r.l.

Antonio Landi - Bono Energia

Gianluca Marongiu, Francesco Cambuli
University of Cagliari, Mechanical Chemical and Materials Engineering Department (DIMCM)

ANSYS 2018 : The software development metrics and EnginSoft's role

The annual meeting of ANSYS took place in Orlando, Florida, last January, hosting all the local delegates of the company and all the Channel partners contributing to the ANSYS business.
As usual the event focused its attention on the percentage results concerning the management of the past year, as well as on some business strategies, not only from an economic point of view but also in relation to the influence of the technological evolution on the company productivity.
The software marked positive results in 2017 and, although no precise numbers were communicated, the overall selling value almost reached a billion of dollars in Europe and North America, with an increase of 15% on the new business.
Such increase is referred to different geographic areas and to specific application areas: summarizing, it can be highlighted that the Mbu (Mechanical business unit) achieved a 11% as average global value, the Fbu (Fluid-dynamic business unit) a 24% and the Ebu (Electronics business unit) even a 34%.
Such differences are related to the historical introduction of the different applications, proving how the most recent ones, as the electronic part, have better growing rates than the most mature ones.
The interesting "leit motiv" of the conference has been velocity: it refers to the drastic reduction of mesh generation time, to solution availability and results accessibility even with huge files; it also considers the users' needs, providing fluid and immediate analyses combined with accessible comprehension.
The main question arisen during this meeting has been: where is the software development going? The replay can be summarized in 4 main issues:

- New release (the 19th is going to be available this month) with a great improvement in terms of capabilities for each application field. The main enhancements will positively affect fracture mechanics, acoustics, user's interface, general dynamics and many more.

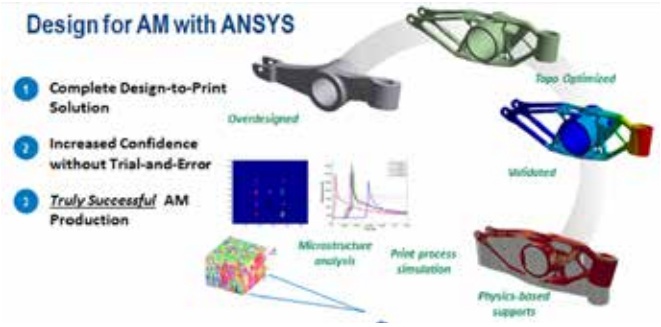

Ansys Additive: Additive manufacturing (3D printing) is a technology that produces three-dimensional parts layer by layer from a variety of materials. Its design with Ansys offers a complete design-to-print solution and an increased confidence without trial-and-error, allowing a truly successful AM production

Ansys Discovery : ANSYS Discovery Live is a new multiple physics simulation platform that combines several key ingredients to produce a software tool that engineers can use to do almost instantaneous virtual prototypes of the behaviour of their designs directly from their solid models

- ANSYS Additive
- ANSYS Discovery
- ANSYS Digital Twin

The role of EnginSoft has been once more confirmed as prominent within ANSYS business, reaffirming its involvement as ANSYS Elite Channel partner to determine the success of the code, its applications and supporting the assistance and training of its users.

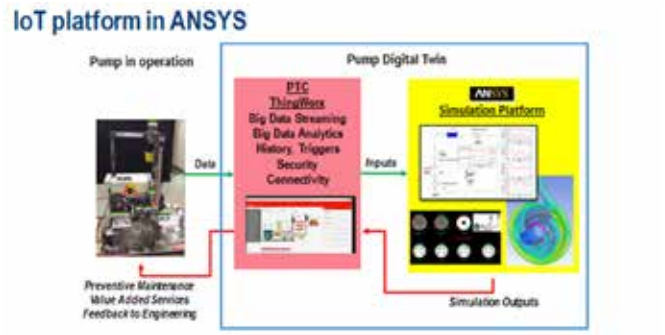

Ansys Digital Twin: Engineering simulation has traditionally been used for new product design and virtual testing, eliminating the need to build multiple prototypes prior to product launch. Now, with the emergence of the Industrial Internet of Things (IIoT), simulation is expanding into operations. The IIoT enables engineers to communicate with sensors and actuators on an operating product to capture data and monitor operating parameters. The result is a digital twin of the physical product or process that can be used to monitor real-time prescriptive analytics and test predictive maintenance to optimize asset performance. The digital twin also provides data that can be used to improve the physical product design throughout the product lifecycle.
By using ANSYS physics-based simulation in conjunction with analytics, companies can make confident predictions about future product performance, reduce the cost and risk of unplanned downtime and improve future product development processes.

ANSYS Discovery AIM: what's new in the Release 19

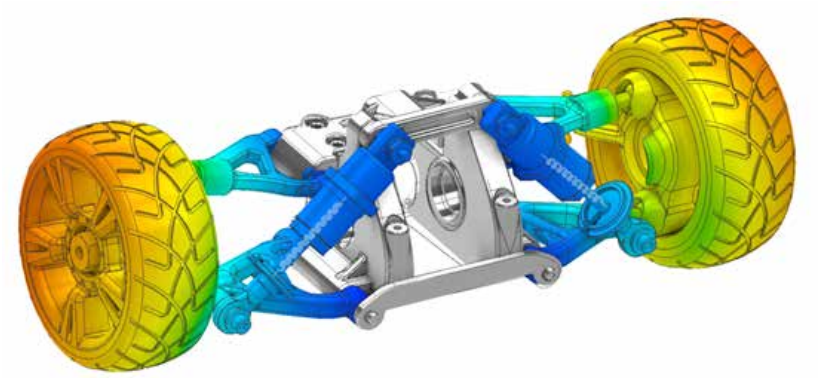

Most of the cost of developing a product is determined by the choices made at the beginning of the design process. What would happen if we got used to digitally exploring design choices already in the early stages of development? The "anticipated" simulation allows to make more informed decisions, to avoid carrying out impracticable projects and to reduce the costs of prototyping and laboratory tests.
For this reason ANSYS has developed Discovery AIM, a simulation software designed to the use in the early design phases.
AIM combines geometric modeling, having integrated the Discovery SpaceClaim tool, with multiphysical FEM analysis and optimization. So it can be qualified as a complete simulation tool.
The presence of guided and intuitive workflows makes this tool easy to be used, and greatly reduces learning time (and consequently staff training costs). Discovery AIM allows the user to perform fluid dynamic, structural, modal, thermal and electromagnetic analysis, as well as combinations of these physics.
A topological optimization tool is also available starting from the latest versions. In R19 new types of constraints are available, in particular it is possible to impose the symmetry, both mirrored and radial, of an object to be optimized.

It is also possible to monitor the optimization process live, displaying the progressive result of the analysis in the graphic window, iteration after iteration.
Discovery AIM is a fast growing product, which ANSYS enriches with a lot of new features every release. For example, in R19 it is possible to define a porous medium, also orthotropic, thus being able to simulate fluid dynamic analysis through perforated filters or membranes.
As regards the structural part, contact modeling has been improved, in particular the management of small sliding for the Bonded and No Separation contacts has been enhanced.
It has also been implemented the possibility to insert Spring connections, very useful in the simulation, for example, of mechanical suspensions. The interaction between the Discovery family of products and ANSYS Mechanical is increasingly promoted: in R19 it is possible to import, in addition to geometry and mesh, also named selections, coordinate systems and materials defined with AIM directly in the Mechanical.
The ANSYS perspective is in fact to promote the integration between the various technologies, making them more and more complementary.

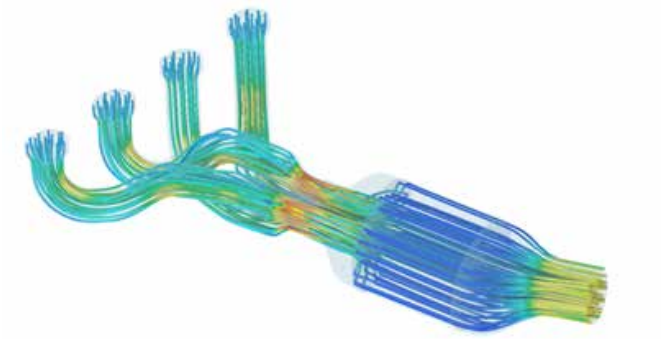

Finally, AIM R19 presents the opportunity to transfer the geometry on which you are working on Discovery Live, the new technology born in the ANSYS house.
And it is also possible to generate an analysis through Discovery Live and transfer it to AIM for a more in-depth study of the configuration.
In fact, this year the AIM standalone license includes both the geometry management product, Discovery SpaceClaim, and the new Discovery Live product.
It is definitively set up a new family of completely innovative products at ANSYS.

For more information:
Maria Cristina Mancino, EnginSoft
m.mancino@enginsoft.com

ANSYS acquires 3DSIM to become the new landmark in AM simulation

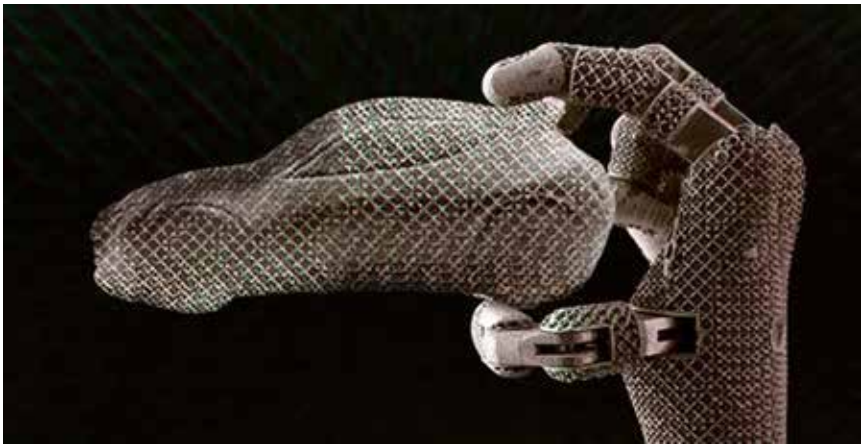

On November 2017 ANSYS Inc. has announced the acquisition of 3DSIM company, now the world leader software technology for Simulation-Driven Additive Manufacturing (AM) will be available in the ANSYS portfolio, becoming the only end-to-end AM simulation workflow in the world today. Starting from the new release ANSYS 19.0, thanks to this new agreement, many innovative features are available for engineers, designers and AM machine operators.

Additive manufacturing – Pros & Cons

The AM processes allow to adopt completely new types of design features changing the way of thinking about product development, thanks to the nature of the layer-upon-layer material addition. It's now possible to realize very strange geometries as well, achieving extreme lightweighting according with optimized external geometry profiles and internal organic lattice structures. It was difficult or sometimes impossible in the past with conventional manufacturing processes, now it's possible to do it, but all these new technological opportunities have to be managed and exploited through an efficient Design for Additive Manufacturing (DfAM).

To create an optimal AM components is the new challenge for designers and engineers, in particular when we talk about metal AM. This industry has been inspired by polymer AM in terms of design, but several additional "pitfalls" have to be recognized and avoided, for instance support structures removing or distortion compensation. For polymeric parts, support removing is quite easy, but it is more difficult for metal parts. Therefore, support material saving and thermal distortion control will play an essential role in metal AM design. Actually the most common metal AM techniques used are powder bed laser sintering technology – where a metal powder is melted with a laser to build up a particular shape. ANSYS's 2018 solutions are focused on laser powder bed fusion, but future improvements will expand ANSYS AM products to simulate additional metal and polymer AM processes.

Return of Investments

The ANSYS AM simulation workflow has a fundamental role to increase productivity and to reduce development time and costs. Quantifying the return on investment is really immediate: on average, usage of AM machine costs more than €100/hour for

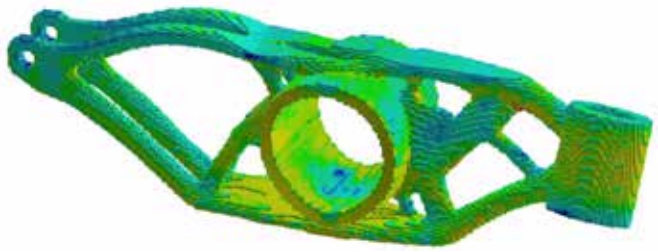

Thermo-structural simulation of a metal AM part

ANSYS simulation workflow for metal AM parts

machine time (including materials, operator time, etc). Trying to get an AM metal component, 2-10 failed builds could be there, wasting 20-60 hours (or more) into the build. That's €2.000-€6.000 per build, €4.000-€60.000 (or more) to get 1 geometry to print correctly. For large platform machines, a single build can take 2-3 weeks. A single failed platform can waste €50.000 - €100.000, and causes a company to miss a time-based milestone. ANSYS Additive Print & Suite saves users by dramatically reducing failures.

Traditional CNC machined vs. 3D printed part

ANSYS AM Simulation Solutions and development roadmap

ANSYS Additive Print and ANSYS Additive Suite are the new solutions available for the customers.

These tools enable customers to face up the entire AM process chain, including topological optimization, part validation, build setup, support generation, build failure prevention, microstructure prediction and much more. It's reliable because in ANSYS platform the user can read and manage the scan vectors directly from machine manufacturers and calculates the thermal history for every scan vector in the entire part.

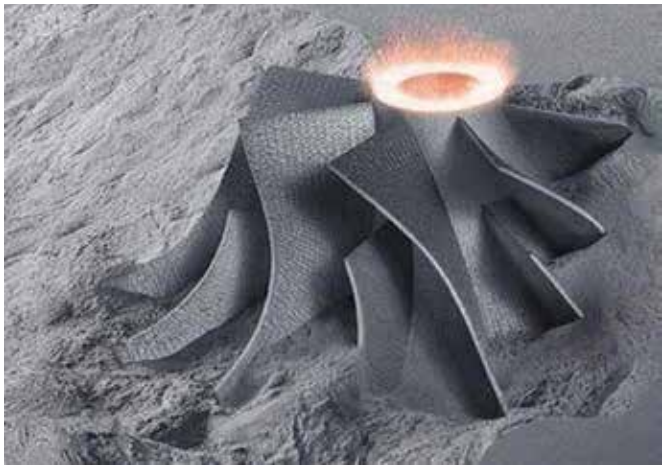

AM process - Laser Powder Bed Fusion

ANSYS Additive Print is a stand-alone solution developed specifically for AM machine operators and design engineers who design parts to be manufactured via AM. Easy-to-use, fast and very powerful, ANSYS SpaceClaim is included and it allows users to visualize and clean up their geometry and properly orient the part to be printed. Here the main ANSYS Additive Print features:

- Final shape of the printed part
- Layer-by-layer distortion, shape and stress visualizations
- Automatic prediction of optimal support structures
- Automatic distortion compensated STL files
- Blade Crash and build failure prevention

ANSYS Additive Suite is the most comprehensive solution for Enterprise-Level customers interested in understanding AM, completely embedded in ANSYS Mechanical environment.

The suite contains:

- Topology & Lattice Optimization - for studying more effective shapes to reach weight reduction and lattice density optimization.
- SpaceClaim - CAD environment to create, import and prepare CAD geometry. Moreover, faceted data toolkit is available to work with STL files, to repair and clean-up optimized parts, to ensure direct interface with AM machines.
- Mechanical – thermo-structural analysis and design validation.
- Mechanical Additive Process Simulation (MAPS) - native feature in ANSYS Mechanical for predicting part shape distortion and stresses from the AM build process.
- Additive Print stand-alone - see description above.
- Additive Science - standalone application for material design/ investigation and for setting optimal machine parameters. This application has been developed for metal AM experts, material scientists, powder bed machine manufacturers, metallurgists in aerospace, biotech, and automotive OEMs and large suppliers focusing on AM.

All the features will be released according to a development roadmap in ANSYS 19.0, 19.1 and 19.2.

For more information:
Fabio Rossetti, EnginSoft - f.rossetti@enginsoft.com

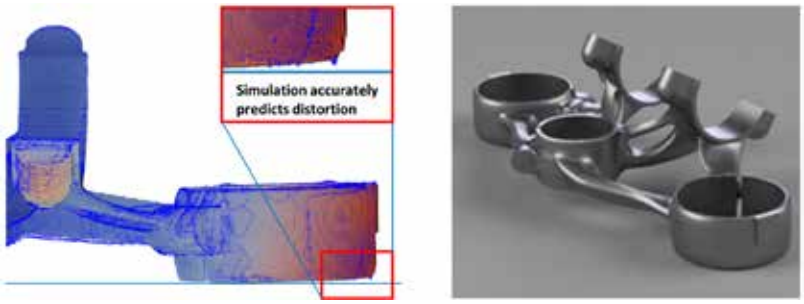

Bike stem geometry (Provided by GRM Consulting and BCIT) – Distortion compensation analysis

ANSYS CFD R19.0

ANSYS 19.0 fluid dynamics includes new features and functionalities for different type of problems, with the main focus on accuracy, in particular for the physics that were too complicated or time consuming with the previous releases. Additionally, a single license is introduced for Ansys Chemkin Enterprise (combustion and reacting flows)

ANSYS FLUENT

Ansys Fluent introduces new capabilities and overall improvements at different levels.

Meshing Mode

A new option is available for the import of geometry from SpaceClaim. If the Share Topology is present, import will produce one object per part, otherwise import will produce one object per body.

Fluent User Interface

Enhancements for the graphical interface introduce the possibility to filter tree contents for a rapid selection of the needed tools; the boundary zones can now be displayed from the tree. All the preferred graphical configurations (colours, mouse button, etc.) can be stored in the User Preferences Menu or in an external file.
A new client application is included with the possibility to connect to an interactive or batch solver session on a remote machine. From the remote session you can extract simulation data and visualize results using contour/vector plots, monitor solution convergence using residual and monitor plots, modify under relaxation factor, start/pause/interrupt the calculation or send any text command to the server.

Solver Enhancements

Numeric default changes tend to improve the convergence with the symmetry boundary conditions and for cases with specified shear condition; transient simulation with rotating domains are now accelerated through improved predictor. A new dedicated boundary condition is Mass-Flow-Outlet that improves usability for turbo flow modelling and avoids confusion for the user (previously you had to use Mass-Flow-Inlet with the Outward Normal specification). For cases that use the algebraic multigrid (AMG) scheme, an aggressive option is now available, which optimizes the solver for better convergence using higher multigrid coarsening rates.

Physics

The overset meshes are now available with the Multiple Reference Frame (MRF), user-defined scalars, mixture multiphase model with non-granular flows and/or cavitation, evaporation and condensation.
The VOF-to-DPM Model Transition is fully supported and it provides a connection between the Eulerian VOF model and the Lagrangian DPM.

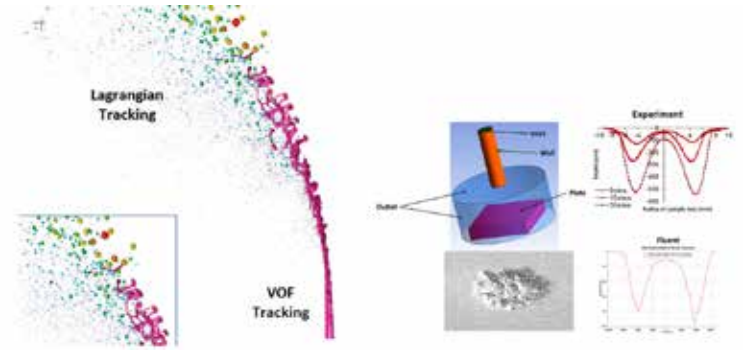

In simulation of liquid sprays, roughly spherical liquid structures in the VOF solution can be converted automatically into Lagrangian particle parcels. With the definition of transition criteria and dynamic mesh adaption, detailed simulations of primary atomization are possible for gas turbines and internal combustion engines.
The erosion models are now coupled with dynamic meshes in order to account for changes in the shape and position of walls.

For more information:
Michele Andreoli, EnginSoft
m.andreoli@enginsoft.com

ANSYS CFX

Ansys CFX is the flagship product for turbomachinery CFD simulations and is recognized for its outstanding accuracy, robustness and speed. New features and enhancements are described below.

Harmonic analysis for 100X faster results

Previously, to optimize performance, the flow for every turbomachinery blade in every row had to be painstakingly calculated — a prohibitively expensive undertaking. ANSYS 19.0 introduces harmonic analysis to solve these time-intensive problems in the frequency domain, avoiding the need to march in time. It's now possible to calculate as few as one or two blade per row to obtain up to a 100X accelerated, full wheel solution — with significant reductions in hardware requirements. Harmonic analysis is not an approximation — the results match the transient full wheel solution.

Blade Flutter enhancements

With ANSYS 19.0, you can now apply complex vibrational modes from a cyclic modal analysis to CFX flutter analysis. This reduces the

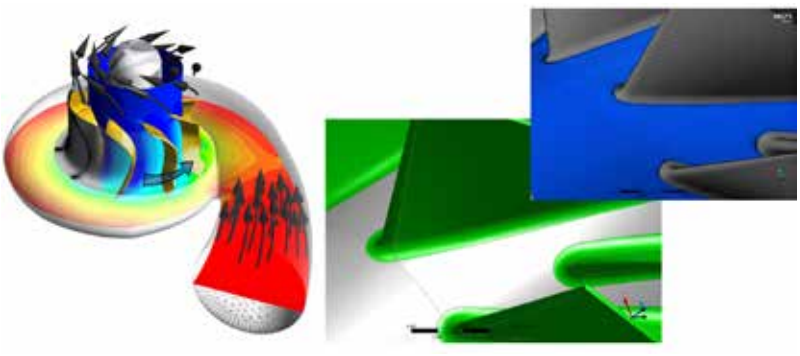

problem size and time to convergence for simulations of centrifugal compressors and other radial turbomachinery that have blades connected by a relatively thin hub at the outer radius. The newly added capability captures hub section movement that can complicate the movement of the blades. These problems can be solved using Fourier transform or harmonic analysis.

TurboSystem – BladeEditor and TurboGrid

ANSYS BladeModeler software is a specialized, easy-to-use tool for the rapid 3-D design of rotating machinery components. BladeModeler is used to design axial, mixed-flow and radial blade components in applications such as pumps, compressors, fans, blowers, turbines, expanders, turbochargers, inducers and more. With ANSYS 19.0 it is now possible to specify native rolling ball fillets at the hub and/or shroud directly in the blade features of BladeEditor, enhancing the parameterized geometry generation and robustness. The geometry is then passed to TurboGrid which generates a high quality structured hexahedral mesh of the blade passage, taking into account the fillets.

For more information:
Alessandro Arcidiacono, EnginSoft
a.arcidiacono@enginsoft.com

ANSYS ICEPAK

Overview

Icepak is a CFD code developed specifically for the thermo-fluid dynamics on electronic devices.
It has many advanced capabilities to model laminar and turbulent flows, in steady and transient state, and provides a vast library of fans, heat sinks and materials, allowing to solve complex physical problems with a three-dimensional level of detail; nowadays conjugate heat transfer and thermal radiation are the most widespread study applications in the electronics industry and in this context Icepak's solver, ANSYS Fluent, guarantees reliable results.

Workbench Integration

In Workbench mode Icepak offers a robust geometric parameterization on CAD objects considered in the project model, furthermore through the coupling with the mechanical module it is possible to perform thermo-structural verifications on different electronic components.

Engineers can rely on Icepak for an integrated electronics cooling solution for electronic applications ranging in scale from individual integrated circuits to packages and PCBs, up to computer housings and entire data centers.
Regarding the post processing of the results, Icepak software contains a full suite of qualitative and quantitative post-processing tools to generate meaningful graphics, animations and customized reports; in Workbench mode Icepak includes also ANSYS CFD-Post for advanced post-processing and animation tools.

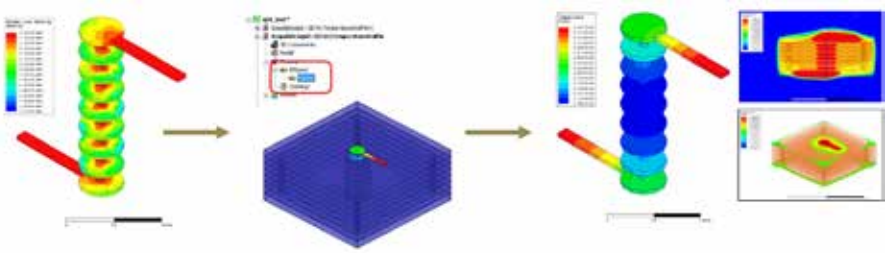

News at R19

In the new release ANSYS R19.0, Icepak is integrated in the ANSYS Electronics Desktop (AEDT) graphical user interface; this provides a CAD-centric solution for engineers who can leverage the easy-to-use ribbon interface to manage thermal issues within the same unified framework as ANSYS HFSS, ANSYS Maxwell and ANSYS Q3D Extractor.
Electrical and mechanical engineers working in this environment will enjoy a completely automated design flow with a highly versatile coupling from HFSS, Maxwell and Q3D Extractor into Icepak for thermal analysis.

In conclusion, in ANSYS Electronics Desktop, the redesigned user interface allows an intuitive user experience, improving the management of the multi-physical analyses; in this integrated environment it is possible also to run Iron Python scripts to create automatic advanced post-processing.

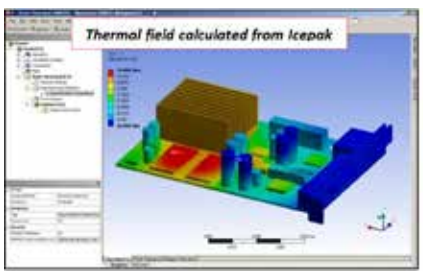

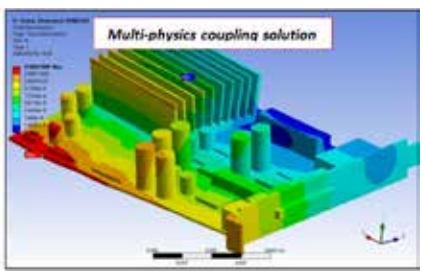

For more information:
Luca Padovan, EnginSoft
l.padovan@enginsoft.com

MultipleRun: an APP developed by EnginSoft for ANSYS Workbench

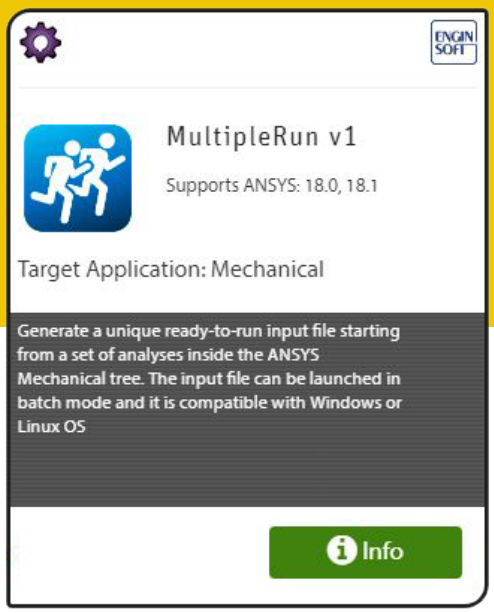

Not only does the ANSYS platform support the industry's most comprehensive set of tools for engineering simulation, but it also supports applications that extend its solutions to address specific customers' needs.
From the ANSYS App Store, a catalog of applications can be downloaded developed by ANSYS and other trusted partners that enhance the capabilities of the ANSYS Suite and make virtual prototyping experience easier and more effective than ever before.

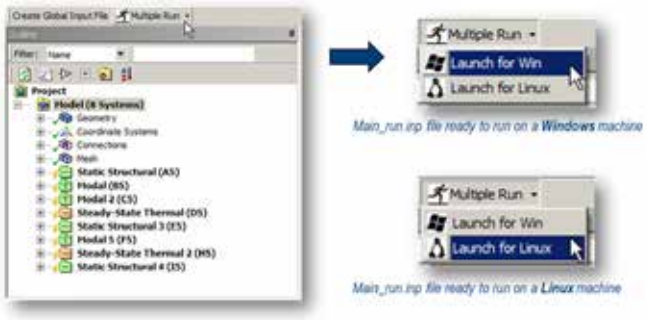

EnginSoft released the following apps for the Ansys App Store:

MultiStep Parametric loads, which exposes new parametric structural loads as Force, Pressure, Moment, and Displacement for multistep analyses;

Results2ASCII, which exports results into ASCII format including all wanted results organized in columns.

In particular the latest EnginSoft app uploaded to the ANSYS App Store will be described in this article: MultipleRun. This app generates a unique ready-to-run input file starting from a set of analyses inside the ANSYS Mechanical tree. The input file can be launched in batch mode and it is compatible with Windows or Linux OS.

The sequence "Tools>Write Input File" in Workbench allows to write an input file for each analysis in the Mechanical tree. This is a limit when a quite long tree is built and the user wants to launch the whole tree in one step in batch mode. This necessity has been identified in our customers, which usually work with long and complex analysis tree.

Consider the example in Figure 1.
In the Fig. 1 example, the APP creates a group of properly linked input files, connected to a unique main file, which is the only one to be submitted to the analyses queue. The customer will have the whole tree solved just launching one batch run (Fig. 2).

The following files have to be copied in a new working directory for the batch run (Fig. 3):

- Main_run.inp
- Group_1.inp
- …
- Group_n.inp

The user has to run the file Main_run.inp

According to Fig. 2:

- Group_1.inp merges the input files SYS.dat + SYS-1.dat + SYS-2.dat
- Group_2.inp merges the input files SYS-7.dat + SYS-8.dat
- Group_3.inp has only the input files SYS-12.dat

Figure 1 - Example

The input file created Main_run.inp launches Group_1.inp + Group_2.inp + Group_3.inp sequentially, so it can be run in batch mode on local or remote machine (e.g. cluster). Once the "Main_run.inp" input file is run, all the results files (i.e. *.rst, *.rth) are stored on subfolders located in the batch run main directory. The results files will be copied on the proper Workbench project's working directories to continue model post-processing in Workbench.

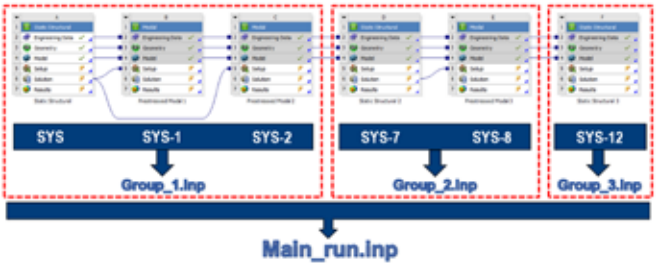

Figure 2 -Main Run

The extension allows to write a unique input file for all the Steady-State Thermal, Static Structural and Modal analyses (w or w/o Pre-stress) located inside the ANSYS Mechanical tree. All the analyses have to share Engineering Data, Geometry and Model cells in the Workbench project schematic. MultipleRun also supports the presence of «Imported Loads», coming from previous analyses..

MultipleRun is available at:
https://appstore.ansys.com/search?q=MultipleRun

For further information: act.support@enginsoft.it

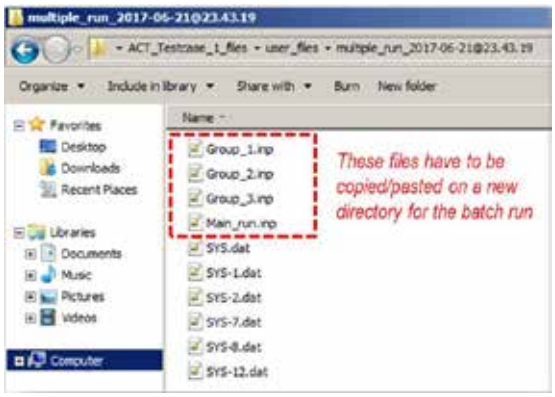

Figure 3 - Batch Run

ANSYS nCode DesignLife

Advanced Tool for Fatigue Assessment

ANSYS nCode DesignLife is the industry-leading tool for durability analysis. It calculates stresses, strains and cumulate damage using finite element analysis results. It can be used integrated into ANSYS Workbench or standalone. You can quickly create complex loading histories (duty cycles), pre and post processing signals. All the calculation engines are available for fatigue:

- stress-life
- strain-life
- spot welds
- seam welds
- vibration fatigue analysis
- accelerated testing
- virtual strain gauges
- high temperature fatigue

A wide database is also provided for materials and for vibration loads (DEF STAN, MIL, RTCA, USABC).

For further information:
a.taurisano@enginsoft.com

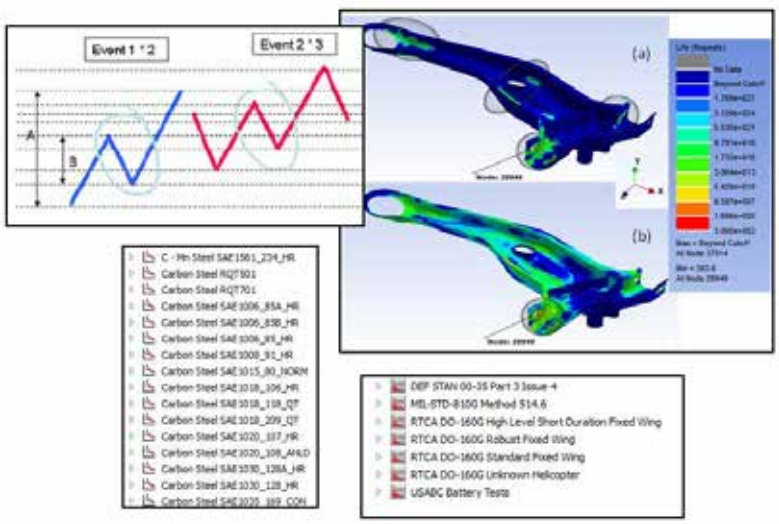

RecurDyn Europe is born!

As announced at the 2017 International CAE Conference, EnginSoft S.p.A and FunctionBay Germany GmbH have merged their power into a new company, which aims to dramatically increase the presence of RecurDyn software in the European CAE market. RecurDyn Europe GmbH, which got a strong endorsement from FunctionBay, Inc. (the Korean headquarter) is now ready to operate and reach its ambitious targets.

With several exceptions, Multi-Body-Dynamics (MBD) is still an under-exploited approach in industry. There are practical and theoretical reasons behind such a picture. First, the applied mechanics, which is the science behind Multi-Body-Dynamics, is a wide and really complex topic, that requires specifically trained users. Second, the Multi-Body method does not follow standardized processes: in order to achieve reliable results, both human insight and expertise play a crucial role. Finally, a relevant barrier can be identified in the obsolescence or low-usability of the MBD tools available in the market, which further increase the time for a new user to become productive.

RecurDyn Europe GmbH is more than a regular CAE company. It's mission is to make the Multi-Body-Dynamics the systematic (and correct) approach that designers choose any time they deal with moving devices. We deeply analyzed the current scenario and we see a great potential of growth.

Our initiative is built around RecurDyn, which is an innovative software for MBD simulation. Being much younger of all competitors, RecurDyn has been developed to meet higher specifications. Its interface is modern and intuitive, so that even unexperienced users reach a good level in a short time. The power comes from unique algorithms for handling contacts, flexible bodies, and, of course, from the optimized solver. Moreover, RecurDyn is the most open and most customizable software in its category. It is natively connectable with particles-based external software for co-simulation of mechanics and fluid dynamics tightly coupled. At the same time, it can be connected with 1D modelers for control design and system integration study. Customization is practically unlimited, since RecurDyn gives access to its interface and its objects through an internal programming environment.

RecurDyn Europe GmbH is a team of passionate and visionary engineers, who have been managing Multi-Body-Dynamics for decades. We have solved issues in any industrial sector at any level of complexity, so that we can quickly identify the best possible solutions. It must be remarked that "solution", in this specific context, means the synergic combination of know-how, software, and working method. We provide the whole package and we will support our future customers in all phases of the implementation.

The business model of RecurDyn Europe GmbH is innovative as well. We believe that our growth is possible only through a network of partners, which can be involved at different levels. The alliance will set in a way that each member has access to both competences and support from either the core team or other members. We very welcome new distributors who take a real commitment in this project: RecurDyn Europe GmbH is the key to open doors they were never able to open before.

RecurDyn Europe GmbH
Central Tower
Landsberger Strasse 110
80339 Munich, Germany
+49 89 32209823
www.recurdyn-europe.com

RecurDyn meets the Italian University

At the last CAE conference, prof. Jin Hwuan Choi gave a detailed speech about the trends and the power of multi-body simulation. Although this discipline is around for many decades, it has been always relegated to highly specialized niches of industry, making it less known than FEA, CFD and other simulation approach. Today, thanks to the boost given by the Industry 4.0 program, the multi-body approach is retrieving a leading role on the scene. Indeed, it is the method that better combines versatility, connectivity, speed, and accuracy, as set by the Digital Twin paradigm. The above concept is spreading within industry, as well as throughout the academic world. That's why the organizers of the 2017 CAE conference have registered a strong interest about RecurDyn from professors, researchers, and students that participated at the event.

Collaborating with universities is a distinctive hallmark of EnginSoft, that frequently lends its resources for research projects, graduation thesis and other dissemination initiatives. In this context, and, more in general, as part of the RecurDyn University Program, EnginSoft offered a free training course on RecurDyn, which was hold in Padova on last 23rd and 24th of January. The program includes a number of free or close-to-free solutions for those institutions that want to use RecurDyn for either didactic or research purposes.

The initiative has been on the whole really successful (above our expectations). We got fourteen representatives from six important universities, seating in our training room for two whole days. As usual, the expert engineers from EnginSoft gave, first, a general introduction about RecurDyn, and, then, moved to the hands-on sessions, where all participants built their fully featured models with RecurDyn.

The training course introduced the brand new V9R1 version of RecurDyn, with a fully renewed interface, improved solver and new important functionalities. There was not enough time to test all of them, but professors and students had anyway the chance to understand how easy, yet effective, the technology is. The characteristics of

Figure 1 – RecurDyn introduction course

RecurDyn perfectly fit with the typical needs of any didactic activity, where students are asked to develop models from scratch in a limited amount of time. On the other hand, the power of RecurDyn effectively and efficiently covers the most demanding applications that normally occur in a research context.

The course also gave the opportunity to exchange ideas about the current status of multi-body simulation in industry. In a certain sense, this initiative gave birth to a community of high-profile, academic users. This network represents an asset for both EnginSoft and FunctionBay. Indeed, the feedbacks coming from highly qualified users are transformed into valuable inputs for the continuous development of the technology.

The RecurDyn University Program is moving its first steps in Italy, but the first results we got are more than encouraging. In about six months a new training course for universities will be offered, to keep the network growing and to make RecurDyn a reference language in multi-flexible-body-simulation.

For more information:
f.maggio@enginsoft.com

TRUE LOAD
Measured Strain Data into Meaningful Load Time Histories

True-Load is a first to market to solution that leverages FEA models to place strain gauges on unmodified physical parts and then back calculate loading. Output directly feeds into True-QSE events, a powerful post processing tool that supports rapid virtual iteration. True-Load directly interfaces to FEA fatigue software to make FEA based fatigue with correlated loading events a natural part of the design cycle.

One of the most challenging tasks for an analyst is to develop load cases for their FEA model that match measured strain values. Typically, it will take weeks to develop the right load cases that match just one or two strain gauges at a single point in time. True Load is a calculation software for product engineering.

True-Load makes that situation a thing of the past. True-Load will determine optimal gauge placement based on the FEA model. Once strains are collected at these optimal gauge locations, the strain data is read into True-Load to calculate load time histories that will typically match the measured strain to within 2% at every point in time. When combined with True-QSE, interrogating any point in the model for strain, stress or displacement is easy and interactive. Typically, it takes a few minutes to determine the strain gauge placement and a few minutes to back calculate the loading profiles.

WHAT IS TRUE LOAD?

True Load software answers to some practical needs that are typical in many industries

- get the design loads (peak & time history) from strain gauge measurements, avoiding installation of load cells
- tell the user where the strain gauges have to be attached to minimize error in load estimation

True-Load provides

- Strain correlated loading
- Full field knowledge from a handful of strain gauges
- Easy interface to FEA durability

The only condition behind the approach is the linearity of the mechanical system, meaning that:

- components must not undergo large deformations
- contacts must be approximable with ideal constraints

The numerical technique behind True Load is robust. It is based on some fair assumptions and validated algorithms: results are reliable. Conditions 1 and 2 are not so restrictive. Most applications in automotive (suspensions, chassis, steering mechanism) and in machinery meet the requirements. This means that the method is applicable in a wide range of situations.

TRUE LOAD MAIN ADVANTAGES & STRENGTHS

Load cells are very expensive and can influence the system response. True Loads required strain gauges (that are less expensive and don't influence the system response)

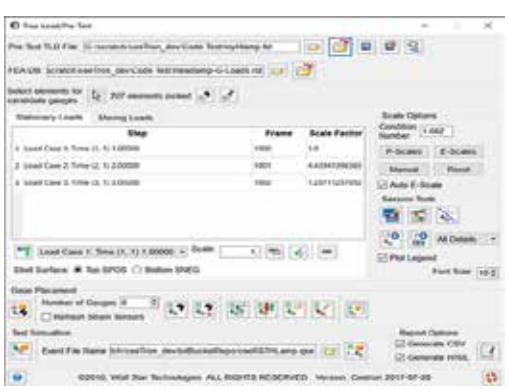

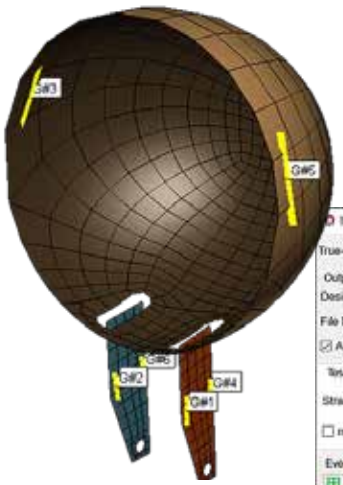

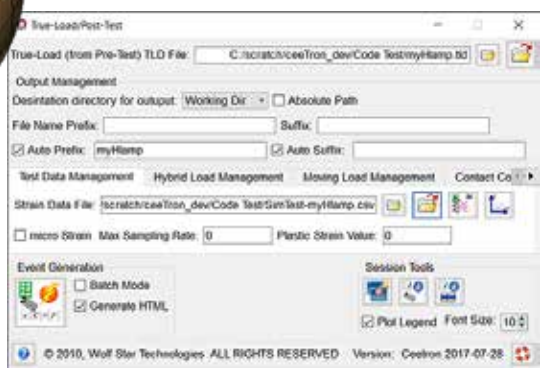

Placing strain gauges is always a challenge. It is very difficult to establish design loads from measurements taken in wrong places: True load drives the user to choose the correct position for correct load identification
True Load avoids time consuming post-processing for load identification.

INTERFACE WITH OTHER SOFTWARE

True Load has proper interfaces for the FE code typically in use in these environments as ANSYS Workbench, NASTRAN and ABAQUS. WolfStarTechnologies established development partnerships with: MSC / ANSYS / Dassault System's / Ceetron

As a leading European solution provider, EnginSoft signed a distribution agreement for Europe with Wolf Star Technologies who develops True Load since 2010.

For more information:
Danilo Col, EnginSoft
d.col@enginsoft.com

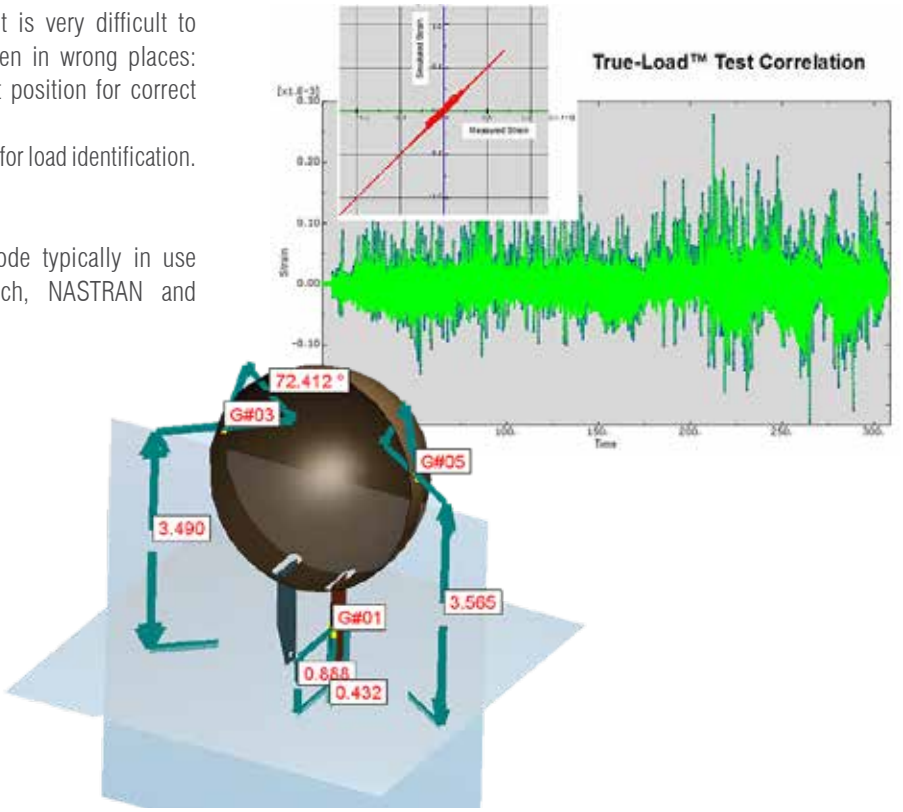

ProRegio project – Final Review Meeting

The final review meeting of the ProRegio EU co-financed project, which has seen EnginSoft as a partner among other key SMEs and Research Institutes of the manufacturing field, was held on the 11th and 12th of October last year in Athens.
The ProRegio project has been focused on the development of manufacturing intelligence based products-services with the aim to change the way customer requirements are addressed by manufacturing companies.
On the first day of the meeting, final results of the project were shown and demonstrated to the EU Officer, Dr. Erastos Filos, who reviewed them giving a very positive feedback to the project manager, Dr. Gisela Lanza, and the whole consortium.
On the 12th, a discussion roundtable was held hosting representatives of the consortium along with representatives

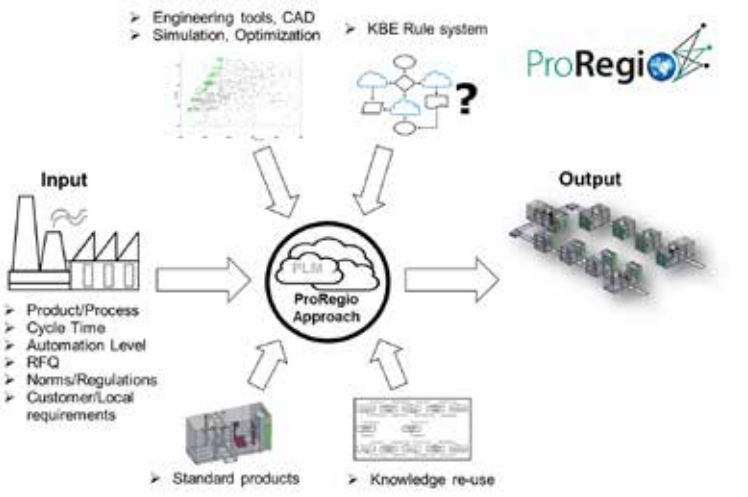

of external industries and universities, who were invited to the final meeting venue in order to verify the project reception from external parties. Also on this occasion, the audience feedback was extremely positive and many interesting ideas for further developments were raised.

Contact: g.borzi@enginsoft.com
References: http://www.h2020-proregio.eu/

FEMFAT Software
Unlimited fatigue simulation

FEMFAT is a universally applicable software program for the fatigue analysis of statically and/or dynamically loaded components and complete systems. Based on stresses from finite element analysis (compatible with the most used FEM software like Ansys, Abaqus,..,), FEMFAT delivers analysis results such as fatigue life or damage as well as safety factors. This enables the identification of lightweight design potentials as well as potential weak spots already at an early product development phase.

The methods used are a combination of classical nominal-stress or stress-strain concepts and calculation standards such as TGL and FKM as well as methods that have been developed at Engineering Center Steyr GmbH & Co KG ("ECS"). These include the support effect concept by means of relative stress gradients and mean stress influence in combination with the critical cutting plane method as well as new methods for the determination of equivalent stresses.
Moreover, there is the fact that FEMFAT has proven itself at ECS for many years in our everyday work of engineering services. This means that the wealth of experience gained from more than 1,000 successful projects dealing with fatigue is incorporated in FEMFAT – an advantage of inestimable value.

The advantages at a glance

- Reliable fatigue software for determining damage, fatigue life and safety factors
- "Software for engineers from engineers"
- Technologically advanced software
- Analysis options for metallic and non-metallic components
- Simultaneous analysis of base material and weld and/or spot joints
- Integrated material database
- A modular design allows a tailored solution for your particular set of challenges
- Flexible licensing options optimized for several usage patterns

FEMFAT is supported by EnginSoft. For more information:
Dario D'Agostino - d.dagostino@enginsoft.com

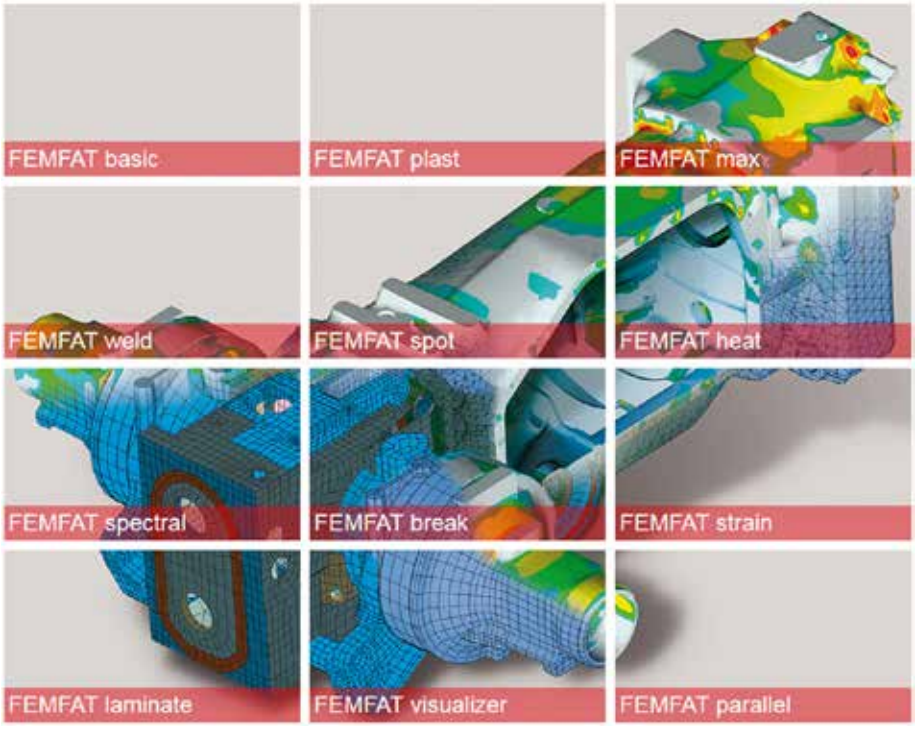

Joint Workshop on Exascale HPC at HiPEAC in Manchester

The HiPEAC conference is the premier European forum for experts in computer architecture, programming models, compilers and operating systems for embedded and general-purpose systems

The 13th HiPEAC conference took place in Manchester, UK, from January 22 to January 24, 2018. Associated workshops, tutorials, special sessions, several large poster session and an industrial exhibition run in parallel with the conference.
Counting on the participation of about 530 experts in the HPC sector, the ExaNeSt project consortium, together with the connected projects ExaNoDe, EcoScale and EuroEXA, actively promoted and presented a joint workshop within the HiPEAC conference: ExascaleHPC: the ExaNoDe, ExaNeSt, EcoScale, and EuroEXA projects

The successful acceptance of this kind of topic is proved by the numerous audience attending the full day workshop, whose main focus was related to the mentioned FET-HPC project results, together with the newly-started follow-up FET-HPC project, EuroEXA.

The four projects collectively cover the following areas, whose main achievements were highlighted during the workshop:

- High Performance Computing and Architectures, and their Evaluation
- 2.5D Integration, Packaging, and Cooling Technologies
- Novel, Unified, and Reconfigurable Accelerators and Tools to use them
- Low-power Processors and die-to-die Communication
- Low latency, Unified and Resilient Interconnects
- Task-based Programming Models and Runtime Systems
- Virtualization for HPC
- Fast Communication & Systems Software: MPI, PGAS, VM's, Libraries, Management
- HPC Extreme Scale Demonstrators
- Storage for HPC
- Exascale-class Applications and Mini-apps enabling System Co-design.

The organizing committee, representing the different project, guided the workshop through its three main sectors of application, namely:

- Memory, Communication, and Accelerator Virtualization
- Technology and Architecture
- Programming Environment, Applications and Evaluation

For further information and the detailed program:
https://www.hipeac.net/events/activities/7521/exascalehpc/
and stay tuned on http://www.exanest.eu/ to know about the next ExaNeSt workshop.

EVOLVING ENGINEERING SIMULATION: THE AGE OF THE DIGITAL TWIN

34th INTERNATIONAL CAE CONFERENCE AND EXHIBITION

INTERNATIONAL CAE CONFERENCE

2018

8 - 9 OCTOBER

Vicenza Convention Centre
@Fiera di Vicenza

Vicenza, ITALY

WWW.CAECONFERENCE.COM